ABSTRACT

XUE, ZUO. A Source-to-Sink Study of the Mekong River Delta: Hydrology, Delta Evolution, and Sediment Transport Modeling. (Under the direction of Jingpu Liu and Dave DeMaster).

The Mekong River is the third largest river in the Western Pacific. As the population and economy of the area booms, more and more dams are built in the Mekong basin. Concerns about negative impacts on downstream and the delta plain from upstream damming have been raised ever since the completion of the Manwan Dam, the first of the 13 major dams designed on the Upper Mekong, in 1993. The runoff of the Lower Mekong has a closer connection with the regional precipitation and El Niño Southern Oscillation during the post-dam period (1994-2005) than the pre-dam period (1950-1993). With ~ 200 new dams to be added to the basin in the next couples of decades, changes are expected in both hydrological regime and delta dynamics.

The Mekong River delivers ~160 million tons of sediment per year to the South China Sea (SCS). The Mekong River Delta (MRD) has the third largest delta plain in the world. High-resolution seismic profiling and coring during 2006 and 2007 cruises reveals a low gradient, subaqueous delta system, up to 20 m thick, surrounding the modern MRD in the west of the SCS. A late Holocene sediment budget for the MRD has been determined, based on the area and thickness of deltaic sediment. Approximately 80% of Mekong delivered sediment has been trapped within the delta area, which, together with a falling sea-level, resulted in a rapidly prograding MRD over the past 3000 yr.

The late Holocene evolution of the MRD has shown a morphological asymmetry indicated by a large down-drift area and a rapid progradation around Cape Camau, ~200 km

downstream from the river mouth. The coupled hydrodynamic-sediment transport modeling using the Regional Ocean Modeling System (ROMS) and Community Sediment Transport Model System (CSTMS) showed that wind is a most important factor influencing the along-shelf sediment transport. This associates MRD's asymmetric evolution with an increased wave influence during the Neoglaciation. Coastal currents formed by the geostrophically balanced Mekong plume are strengthened by intensified winter monsoons. Wave and tidal mixing re-suspends previously deposited Mekong sediments, which are then transported southwestward to the Gulf of Thailand. These results link sediment dynamics and delta evolution with variations in monsoonal activities during the late Holocene.

A Source-to-Sink Study of the Mekong River Delta: Hydrology, Delta Evolution, and Sediment Transport Modeling

by
Zuo Xue

A dissertation submitted to the Graduate Faculty of
North Carolina State University
in partial fulfillment of the
requirements for the degree of
Doctor of Philosophy

Marine Science

Raleigh, North Carolina

2010

APPROVED BY:

Jingpu Liu Committee Chair/Advisor	Dave DeMaster Committee Co-Chair/Advisor
Elana L Leithold	Ruoying He

Wenbin Lu
Minor Representative

DEDICATION

To my wife, Yaming Shao:

with you, I am a happy man!

BIOGRAPHY

Zuo Xue was born and grew up in the City of Qingdao, the most beautiful coastal city in east China. He graduated from Qingdao No.19 Middle School in 1998, where he met his wife. After that he began his undergraduate study in Ocean University of China, majored in Hydro and Engineering Geology. He was very active in social activities and used to be the president of the student board of the College of Geosciences. Upon graduation, he began his master's degree study in the First Institute of Oceanography, State Oceanic Administration of China, in Qingdao, majored in Environmental Science. His master's thesis research focused on coastal erosion induced by human activities. After he earned master's degree in 2005, he left his beloved hometown, Qingdao, and came to the United States to begin his doctoral study in North Carolina State University. To accomplish his Ph.D. study, he attended two geophysical cruises surveying the Mekong subaqueous delta in 2006 and 2007.

ACKNOWLEDGEMENTS

I would like to thank my advisor, Drs. Jingpu (Paul) Liu and Dave DeMaster, and my committee, Drs. Elana Leithold, Ruoying He, and Wenbin Lu. Without their invaluable insight and help I would not have been able to complete my Ph.D. study. I would especially like to thank Dr. Paul Liu for leading me into my current research field five years ago, and has always tried his best to provide me the most ideal study and research environment. I am extremely grateful to Dr. Dave DeMaster, who has given me detailed comments and suggests on my publications and dissertations as well. I also sincerely thank Dr. Ruoying He for spending a lot of time with me on the numerical modeling.

This study would not been possible without support from our Vietnamese colleagues, Drs. Van Lap Nguyen and Thi Kim Oanh Ta from Vietnam Academy of Science and Technology. I would also like to acknowledge my colleagues and friends at North Carolina State University. Dr. Huiqing Liu helped me a lot on the SWAN wave modeling part. Ke Chen and Yizhen Li gave me very detailed instructions on the ROMS modeling part. Laurel Childress and Benjamin Brulet helped me a lot on the organic carbon and grain size analysis. I extend many thanks to those people who have helped me in my work, and made this study possible, including Peggy Schexnayder, John Milliman, Kehui Xu, Courtney Harris, Liviu Giosan, Shiming Wan, Christopher Sherwood, and John Warner.

Finally, many thanks to my family- my wife who companied my study at North Carolina for five years, and my parents and brother back in China. I would not have been successful without their support.

TABLE OF CONTENTS

LIST OF TABLES

CHAPTER 2

CHAPTER 3

CHAPTER 4

LIST OF FIGURES

CHAPTER 1

CHAPTER 2

CHAPTER 3

CHAPTER 4

CHAPTER 5

CHAPTER 1: INTRODUCTION

As the main source of terrestrial sediments to the world oceans, rivers deliver approximately 12.6 billion tons of sediments to estuarine and coastal areas annually (Syvitski et al., 2005). The world's 25 largest rivers account for approximately 40% of all river derived sediments and 50% of the freshwater discharged into the ocean (McKee et al., 2004). A large part of these sediments are trapped in rivers' low reaches and contribute to extensive flood plain and delta plain development. Nowadays, approximate half a billion people are living on or near deltas (Syvitski et al., 2009). The population and economic growth, especially during the twentieth-century, have had a profound impact on deltas. The global surveys conducted by Syvitski et al. (2005 and 2009) indicate that soil erosion is accelerating (e.g., deforestation, agriculture, and mining), while at the same time, sediment flux to the coastal zone is decelerating (e.g. channel bank hardening, water diversion, and reservoir storage). 85% of the 33 major deltas all over the world have experienced severe flooding in the past decade, making the importance of understanding the delivery of fluvial sediment to the coastal ocean beyond question.

After being transported into the estuarine and coastal area, fluvial sediments experience a series of complicated dynamic processes controlled by physical (waves, currents, etc.), morphological, and biogeochemical conditions (flocculation, diagenesis, bioturbation, etc.). In low energy environments, the majority of fluvial sediments are deposited around the river mouth, whereas in high energy environments, which are typical for most large river estuaries, a large fraction of the sediments are transported out of the estuary by either across-margin advection/diffusion or along-shore advection/diffusion (Driscoll and Karner, 1999).

The purpose of the recent Source-to-Sink study in marine geology is to examine linked, terrestrial and marine sediment dispersal systems over the range of time scales for which sedimentary processes operate. In the past two decades, studies have been conducted on both large river systems such as the Amazon (Nittrouer et al., 1986; Nittrouer and DeMaster, 1996), Yellow (Alexander et al., 1991; Liu et al., 2004), Yangtze (Chen et al., 2000; Liu et al., 2007), Ganges-Brahmaputra (Michels et al., 1998; Goodbred and Kuehl, 1999), Fly (Harris et al., 2003), Po (Frignani and Langone, 1991; Cattaneo et al., 2003); and small mountainous river systems, such as Waipaoa (Forster and Carter, 1997; Gomez et al., 1998), Eel (Nittrouer, 1999; Leithold and Blair, 2001), Taiwanese Rivers (Milliman and Kao, 2005; Liu et al., 2008), and others. Fluvial sediment budgets have been updated compared to past estimates based on gauge stations that are usually several hundreds of kilometers inland of the coast.

Based on high-resolution seismic profiling, a series of subaqueous deltas or clinoform structures were examined in fluvial systems around world such as the Amazon, Yellow, Yangtze, Ganges-Brahmaputra, and others. Although historically the term “clinoform” referred to the foreset part of a delta system, now it actually includes the topset-foreset-bottomset morphology of delta systems (Walsh et al., 2004). These prograding depositional features are controlled by the interaction among sediment supply, coastal hydrodynamics, and local sea-level (Walsh et al., 2004). A common across-shelf clinoform structure was found in most offshore deltaic environments. The term “compound-clinoform” has been proposed to describe a subaerial/subaqueous delta couplet (Nittrouer et al., 1996; Swenson et al., 2005). At the same time, previous studies also showed strong along-shelf transport of

sediments off large river mouths, which connects sedimentary processes in deltas, subaqueous deltas and mid-shelf deposits (Yang and Liu, 2007; Liu et al., 2009). For example, distal delta lobes have been observed in coastal areas several hundreds of kilometers away from the river mouth of both the Yellow and Yangtze Rivers (Liu et al., 2004; Liu et al., 2007).

1. Delta Stratigraphy and Sediment Dispersal

A river delta is a landform that is created at the mouth of a river where it flows into an ocean. It is formed from the deposition of the riverine sediments carried by the river as the flow leaves the river mouth. The majority of the world's deltaic systems began their formation between 7,400 and 9,500 cal yr BP as a result of decelerating sea-level rise (Stanley and Warne, 1994). The architecture of a deltaic system is controlled by the interaction between boundary conditions and forcing factors, mainly including: (1) sediment supplied from rivers; (2) accommodation space; (3) coastal energy; and (4) the dynamics of discharge plumes (Syvitski and Saito, 2007). According to the dominant process, components of prograding deltas can be identified as: (1) delta plain, the large subaerial zone dominated by rivers, (2) delta front, the zone of interaction between fluvial and oceanographic processes, and (3) prodelta, the zone of quiet sedimentation from suspension disturbed only by gravity sliding and mass flow deposition (Reading, 1996). Conceptual process-based models for deltaic deposition emphasize the relative importance of fluvial input and basin reworking. This resulted in the tripartite system, in which deltas were classified as river/fluvial-

dominated, wave-dominated, or tide-dominated (Galloway, 1975).

The deposits of river-dominated deltas have well-developed delta top facies with characteristics the same as those of a fluvial system. The river channels build out to form the 'bird's foot'. Between these channels there are large interdistributary bays, the filling of which results in small scale coarsening-upward successions. For wave-dominated delta deposits the stratigraphic record displays well-developed mouth bar and beach sediments. Delta slope and prodelta deposits may not significantly differ from the river-dominated delta deposits. The deposits of tide-influenced deltas can be distinguished from other deltas by the presence of sedimentary structures and facies associations, such as oppositely directed paleoflow indicators and mud drapes, which indicate that tidal processes were active (Nichols, 1999).

Delta stratigraphy displays regional patterns of facies distribution, which are controlled by the relative dominance of eustatic, tectonic, and fluvial processes. On delta plains, sequence stratigraphy studies are mainly based on borehole core analyses. The depositional facies are determined from the sediment properties, including grain size, the sedimentary structure, fauna, and so on. For the subaqueous part, the combination of seismic profiling and coring demonstrates the presence of clinoform structures, the source and flux of sediment, and sedimentation processes involved in the delta development. From the view of sequence stratigraphy and sediment dispersal, here, I briefly review several well-studied river-deltaic systems around the world.

1.1 The Amazon Delta

The Amazon River has the largest drainage basin and water discharge in the world (Gibbs, 1967). The Amazon shelf is a coastal setting actively accumulating sediment and is presently forming a well defined clinoform structure dominated by muddy sediments (Nittrouer et al., 1996). Tides are the dominant physical forcing mechanism on the Amazon shelf, with a maximum range of ~ 6 m (Kuehl et al., 1996). About 50% of the sediment annually discharged from the Amazon accumulates within the inner-shelf mud-deposit (Kuehl et al., 1986). Sediment accumulated on the Amazon shelf is in the form of a prograding clinoform structure, with characteristic topset, foreset, and bottomset (Nittrouer et al., 1986). The overall succession of strata displays the characteristic coarsening upward of deltas.

On seismic profiles, the topset, foreset, and bottomset strata were defined by the dip of stratal surfaces (Alexander et al., 1986): the topset strata were those strata lying shoreward of foreset strata (gradients < 1:1500), where interbedding of sand and mud characterized the shelf strata near the river mouth (Nittrouer et al., 1996); the foreset strata were defined as those strata having gradients >1:1500, where the ^{210}Pb accumulation rates reached their highest value; the bottomset strata were defined as those lying seaward of the foreset (gradients < 1:1500) and downlap onto the transgressive sand layer.

The enormous Amazon sediment input along the Guianas-Amapa coast is reworked by tidal- and wave-induced currents. The shelf sediment dynamics is highly sensitive to the strength of the trade winds. Along the northern Amapa inner shelf and coast, modern Amazon sediment accumulation is limited to an offshore (> 30 m water depth) depocenter. The

mudbanks, which mainly consisted of Amazon-derived sediment, is present over a 1,400 km length of the coast, substantiating the along-shelf migration of a series of mudcapes (Allison et al., 2000).

1.2 The Mississippi Delta

The Mississippi Delta is classified as a typical river-dominated delta. Quaternary sediments deposited by the Mississippi River accumulated mainly in the deltaic system and the submarine fan (Boyd et al., 1989). The depositional sequences of the Mississippi Delta plain consist of a regressive and a transgressive component (Penland et al., 1988). Previous studies on the Mississippi Delta have verified that the present delta plain and associated nearshore barrier islands and submarine shoals are either direct or indirect products of cyclic delta-building events that have operated on a variety of temporal and spatial scales (Roberts, 1997). Major delta-building events occurred at a frequency of 1,000-2,000 yrs with sedimentary deposits ranging in thickness from 10 to 100 m (Roberts, 1997).

Characteristics of sedimentary facies of the Mississippi River delta were determined from grain-size analyses, examination of bedding and other structure seen in cores, and identification of associated fauna (Fisk et al., 1954). The sedimentary facies included 1) bar facies, which were deposits on the surface of the bulges at the mouths of distributaries, 2) prodelta facies, which were a belt of fine-grained deposits covering the delta front and the surrounding seafloor, 3) channel fill, natural levee, and marsh facies, and 4) interdistributary trough facies, which were layered sandy silts and clayey silts sections of the bay bottoms and

massive, poorly sorted, silty clays floor deeper parts of the bays (Fisk et al., 1954).

Repeated delta switching has been the fundamental process by which the Mississippi Delta has been built (Roberts, 1998). An early-stage subaqueous delta was found on the shallow (< 25 m water depth) continental shelf seaward of the Atchafalaya River mouths, which is also the most recent deltaic lobes of the Mississippi River (Neill and Allison, 2005). The muddy subaqueous clinoform extends ~ 21-26 km seaward of the shell reef. The clinoform structure consists of a topset surface (gradients between 1:2500 and 1:1600), a foreset (gradients < 1: 550), and a limited bottomset bed (< 0.5 km wide) (Neill and Allison, 2005).

1.3 The Yangtze Delta

The Yangtze River delta is classified as a typical tide-dominated mud delta with a funnel-shaped topography and several wide distributary channels or estuaries (Orton and Reading, 1993). The delta has an area of ~ 52,000 km^2 (23,000 km^2 subaerial and 29,000 km^2 subaqueous) (Li, 1986). The subaqueous delta can be further divided into three parts, which are subtidal flats (5 to 10 m water depth), delta front (from 5-10 to 15-30 m water depth), and prodelta (water depth greater than 15 to 20m) (Chen et al., 1987).

The Holocene depositional units consisted of: (1) tidal sand ridge, which consisted mainly of several sets of an upward-fining succession composed of poorly sorted very fine to medium sand, overlain by thickly interlaminated to thinly interbedded sand and mud; (2) prodelta, which was composed of dark-gray silty clay with thin shell beds and coarse-silt

layers. Its sediment had the finest grain size of all units with mud contents greater than 95%; (3) delta front, which was characterized by an upward-coarsening succession with relatively high sand contents; (4) lower intertidal to subtidal flat, which was characterized by thickly interlaminated to thinly interbedded dark-gray sand and mud with few shell fragments; (5) upper intertidal flat, which was composed of sediment similar to muddy intertidal flat deposits, and (6) surface soil, which was characterized by dull reddish brown to brown clayey silt with abundant plant rootlets and snail shell contents (Hori et al., 2001).

Although a large part of Yangtze-derived sediments have been trapped in the estuary and deltaic system, an elongated (~ 800 km) distal subaqueous mud wedge was found extending from the river mouth southward into the Taiwan Strait, substantiating the southward transport of Yangtze-derived sediment by the Zhejiang-Fujian Coastal Currents. The calculated volume of the distal mud wedge represented ~ 32% of the total Yangtze-derived sediment during the middle to late Holocene (Liu et al., 2007).

.

1.4 The Po Delta

The Po Delta was formed after the present sea level highstand was attained, representing a major component of the late Holocene high sea-level stand (Correggiari et al., 2005). The late Holocene high sea-level stand in the Adriatic Sea includes three depo-centers: 1) the Po delta and prodelta; 2) the central Adriatic prodelta wedge; and 3) the Gargano subaqueous delta, 600 km south of the Po delta. The Po delta wedge started to prograde in 5,500 yr BP and was characterized by alternating phases of rapid advance, switch and

abandonment of coastal and deltaic apparatuses (Correggiari et al., 2003).

The coastal area of the Po River delta was characterized by vertical superposition of: (1) a prodelta, which had an average thickness of 15-16 m and displays a transitional boundary to the underlying inner-shelf deposits; (2) a delta front, which was an up to 5 m thick fine to medium sand layer with a gradational lower boundary covering the fine-grained prodelta deposits; and (3) delta plain deposits, which were composed of fine-grained deposits and showed a sharp boundary with the underlying delta front deposit (Amorosi et al., 2008).

Inner shelf and lower prodelta deposits overlying the maximum flooding surface display strong condensation, and have similar geochemical features to late transgressive shelf deposits. This suggested that between 5,000 and 600 cal yr BP the Po River delta was sediment-starved (Amorosi et al., 2008). The modern Po Delta is the result of river-dominated growth. The increased sediment flux was derived from climatic change and by human impact both on the catchment and on the delta (Correggiari et al., 2005).

1.5 The Ganges-Brahmaputra Delta

The Ganges-Brahmaputra (G-B) Rivers has a sediment flux of ~ 1200 million tons/yr. Growth of the G-B Delta in the late Quaternary began 10,000-11,000 cal yr BP, which was ~ 2,000 to 3,000 yrs earlier than the global average and was demonstrated as the result of immense sediment discharge from the G-B Rivers (Goodbred and Kuehl, 2000). Stratigraphy of the G-B Delta displayed regional patterns of facies distribution, controlled by the relative dominance of eustatic, tectonic, and fluvial controls. In the tectonically active northeast delta,

fine-grained floodplain deposits were the dominant facies. In the western delta, sandy alluvial deposits were the dominant sedimentary feature. In the southern delta coastal plain, the dominance of eustasy and variations in the rate of sea-level rise resulted in a mix of fine- and coarse-grained facies (Goodbred et al., 2003). On the Gulf of Bengal seaward of G-B River, seismic profiling revealed a typical subaqueous delta system similar to that of the Amazon and Yellow. The progradation of the subaerial delta forced suspended sediment onto the shelf, forming the muddy subaqueous delta ~ 7,500 cal yr BP (Goodbred and Kuehl, 2000). The topset beds dipped gently (gradients 36:1000) and diverged offshore, more steeply dipping foreset beds (gradients 190:1000) converged further seaward, and relatively thin, gently dipping bottomset (gradients 22:1000) extend across the outer shelf. The erosional surface underlying the bottomset bed was presumed to be of late Pleistocene age (Kuehl et al., 1997).

Sediment budget estimation by Goodbred and Kuehl (2000) indicated that about one third of the G-B sediments have been deposited within the flood plain and delta plain. The remaining sediments appeared to be apportioned between the subaqueous delta and transport to the deep-sea Bengal fan via a nearshore canyon.

2. The Western Pacific and South China Sea

The Himalayas are among the youngest and most active mountain ranges on the planet, with high relief, steep gradients, frequent tectonic activity, intensive monsoon rainfall, and highly erodible rocks (Clift et al., 2008). The Himalayas and the Tibetan Plateau give rise to seven of the world's largest river systems, which are the Yellow (Huanghe), Yangtze

(Changjiang), Pearl (Zhujiang), Red (Songhong), Mekong (Lancang), Irrawaddy and Salween, and the G-B Rivers (Fig. 1). Five of these river systems drain into the Western Pacific. If sediments delivered by Taiwanese mountainous rivers are included, the sediment flux to the Western Pacific is approximate 2.2 billion tons/yr. These sediments account for approximate 17% of the terrestrial sediment flux to the global coastal ocean (12.6 billion tons/yr, Syvitski et al., 2005).

More than 75% of the marginal basins in the modern global ocean are concentrated in the Western Pacific continental margin (Tamaki and Honza, 1991). Among the marginal seas in the Western Pacific, the South China Sea (SCS) has the largest basin volume ($4{,}242\times10^5$ km^3, Wang 1999). The SCS has an area of 3,500,000 km^2 and its average depth is 1,212 m (Su, 2004). About 52% of the SCS is less than 200 m in depth and is covered mostly by sandy sediments, except for the mud zones on the inner shelf near large river mouths (Wang et al., 1992) (Fig. 2).

The SCS is under the influence of the East Asian Monsoon and is characterized by seasonal switches in wind direction, precipitation and runoff (Webster, 1987). The northeasterly winds prevail over the whole region with an average magnitude of 9 m/s in winter. In contrast, weak southwesterly winds of 6 m/s dominate over most parts of the SCS in summer (Hu et al., 2000). Surface currents of the SCS undergo a seasonal reversal of direction in the absence of major oceanic inflow.

The Mekong River is the largest river draining into the SCS in terms of freshwater and sediment load (160 million tons/yr, Milliman and Syvitski, 1992), followed by the Red River (Song Hong) (130 million tons/yr) and Pearl River (Zhu Jiang) (69 million tons/yr).

Another major source of sediment inputs are from the small mountainous rivers in Taiwan, which deliver ~ 300 million tons of sediments into the coastal sea annually (Liu et al., 2008).

Until the end of last century, the majority of sedimentation studies of the SCS were confined within the northern region. Result from the southwest SCS, especially the Vietnam Shelf, where the Mekong River Delta is located, was very limited. These previous studies showed the sedimentation rate on the continental slope ranges from 0.7 to 15 cm/kyr for the Holocene and 1.3-31 cm/kyr for the last glaciations (Wang et al., 1992). Maximum sedimentation rates were reported seaward of the Pearl River mouth and in areas around the paleo-rivers on the Sunda Shelf (Wang et al., 1992). A recent study on the Sunda Shelf showed the averaged sedimentation rates for the Holocene sediments ranges from 5 to 135 cm/kyr (Schimanski and Stattegger, 2005).

3. The Mekong River and Delta

3.1 Geological and Physical Setting

Originating from the Tibetan Plateau, the Mekong River runs through China (Yunnan province), Myanmar, Thailand, Lao PDR, and Cambodia and finally enters the SCS in southern Vietnam (Fig. 3). The total length of the Mekong River is about 4,750 km and approximately half of it is in China's Yunnan province (named locally the Lancang River). The Lower Mekong area (Cambodia, Lao PDR, Thailand and Vietnam) has a population of 60 million, the majority of which depends on the aquatic resources provided by the Mekong basin.

The climate of the Lower Mekong is humid and tropical. Mean annual rainfall ranges from 1,000 mm in Thailand to 3,200 mm in the mountainous region of Laos (Kite, 2001). The Lower Mekong is dominated by two distinct monsoon seasons: the rainy SW monsoon season and the dry NE monsoon season. The rainy season, which accounts for more than 80% of the annual rainfall, occurs between mid-May and early October. However, Gupta and Liew (2007) suggest that the summer snowmelt from the Tibetan plateau is the reason for the small water discharge rise in May.

The Mekong River flows over rocks for about 80% of its length and then across alluvium in Cambodia and Vietnam. Bedrock within China and Lao PDR is mainly sedimentary and metamorphic rocks. When the Mekong River reaches northern Cambodia, alluvial channel deposits with exposures of Triassic sedimentary rocks and Neogene basalts become the primary riverbed material. The river ultimately runs into the Mekong River Delta (MRD), which is composed of Holocene alluvial sediments, initially formed around 8,000 yr BP (Tamura et al., 2009).

3.2 Oceanographic Conditions and Sea Level Change

The coastal area in Southeast Asia is strongly influenced by the NE monsoon (December to February) and the SW monsoon (June to August). The coasts are exposed to seasonal high waves during these monsoon regimes. The northeast monsoon influences the eastern margin of the Philippines, Vietnam, and the east coast of the Malaysia Peninsula. The NE monsoons influence the coast of Myanmar, the east coast of southern Thailand, and

Indonesia (Wang, 2005). In general, the coastal currents in Southeast Asia are driven by prevailing monsoon winds. For the coast of the MRD, wave and currents (generated by strong NE monsoons) dominate the net alongshore sediment transport (Gagliano and McIntire, 1968).

Coasts in Southeast Asia experience low to moderate tidal ranges and a variety of tidal types influenced by conditions in the Pacific and Indian Oceans. Characteristic semi-diurnal tides of the Indian Ocean prevail in the west. Mixed tides of the Pacific occur in the eastern Indonesian archipelago and the Philippine waters. Almost pure diurnal tides predominate in the Gulf of Thailand and the Java Sea (Wang, 2005). The southern Vietnam shelf is controlled by two tidal sources: one the regular 3.5 m semidiurnal tides from the South China Sea in the east of MRD, and the other an irregular 0.8-1.0 m diurnal tide from the Gulf of Thailand in the west (Le et al., 2007).

Sea level research on the Sunda shelf revealed that the sea level was about -120 m around 19,000 cal yr BP (Hanebuth et al, 2009). For the MRD area, a sea level curve for the last 15,000 yr was rebuilt based on inland boreholes (Ta et al., 2002a). Both of the two curves show a rapid sea level rise since the last glacial episode. After reaching its maximum height around 6,000 yr BP, sea level has remained relatively steady until now (Fig. 4).

3.3 Delta Evolution

The MRD is located down stream of Kompong Cham, Cambodia. Its total area is 4.95×10^4 km^2 (Le et al., 2007). Detailed sedimentation studies have been conducted on its

subaerial deposits. Based on borehole cores collected on the delta plain, previous studies shows that the subaerial part of the MRD has continuously prograded more than 250 km from Cambodia toward the South China Sea since the Holocene sea-level highstand (Nguyen et al., 2000; Fig. 5).

As described above, sea level at the Last Glacial Maximum (LGM) has been estimated as about -120 m in Southeast Asia. In the MRD area, the shoreline was probably located far to the east and southeast near the shelf edge. The drop in sea level led to the downcutting of river channels and thus formed an incised-valley in the area of modern delta plain, passing the position of core BT2. As the sea level rose, the incised valley was gradually filled with a transgressive succession of fluvial/estuarine facies, followed by an open-bay facies. The sea-level was inferred at -60 m around 13,200 yr BP (Fig. 5a).

The global sea-level rise slowed down after 8,000 yrs BP, when most of the world's delta systems began their progradation. A coarsening-upward deltaic succession was formed on the MRD as a result of combined enormous fluvial sediment supply and accommodation created by decelerated sea-level rise (Figs. 5b and 5c). Local sea-level reached its maximum around 6,000 yrs BP, after which the MRD began its rapid progradation until now.

A phase shift from tide-dominated to an intermediated type tide-wave-dominated delta around 3,000 yrs BP has been proposed (Ta et al., 2002b). The tide-dominated delta was characterized by a well-developed mangrove forest on the subaerial delta plain, cross-shore sediment dispersal, and tide-influenced sedimentary facies. In contrast, the tide and wave-dominated delta exhibited a beach-ridge system in the subaerial delta plain, longshore sediment dispersal, and a steep delta-front topography, on which the proximal river-mouth

sediments were coarse grained and those more distal were fine grained (Figs. 5e and 5f; Ta et al., 2001a, 2001b, 2002a, and 2002b).

Although previous studies successfully examined the evolution of the subaerial part of the MRD in late Quaternary and its relationship with the sediment input from the Mekong system, geological evidence for shelf sediment dispersal and depositional processes is rather limited. In addition, neither the morphology nor the evolution of its subaqueous part has ever been documented.

3.4 Human Activity

Dams, in general, have major impacts on river hydrology, primarily through changes in the timing, magnitude, and frequency of low and high flows, ultimately producing a hydrologic regime differing significantly from the pre-impoundment natural flow regime (Magilligan and Nislow, 2005). Dams and reservoirs hold not only waters but also, maybe more important, a large quantity of sediment because of the reduced carrying capacity. It has been estimated that over 70% of the world's rivers are intercepted by large reservoirs, and half of them have a local sediment trapping efficiency of more than 80% (Kummu and Varis, 2007).

A strong correlation between water discharge and suspended sediment concentration (SSC) in both large/small and gauged/ungauged river systems has been studied extensively (Milliman and Syvitski, 1992; Meybeck et al., 2003; Morehead et al., 2003). As for the large river systems in Asia, such a relationship has been well documented in the Yangtze (Chen et

al., 2001), Yellow (Wang et al., 2006), Brahmaputra (Sarma, 2005), and Ganges rivers (Singh et al., 2006).

As the home of more than 70 million people, the Mekong River basin is experiencing a fast economic and population expansion. Needs for hydropower and freshwater bring construction of more and more dams and reservoirs along the main stream, which inevitably change the water/sediment discharge downstream and in the delta area in two ways: (1) flow regulation by dams shifts the original rhythm of water/sediment discharge controlled by monsoon forcing; and (2) large amount of sediments will be held behind the dams which will dramatically decrease the sediment flux in downstream. At the same time, a large number of engineering constructions, mainly dykes and weirs, are being built on the MRD plain to control floods and saltwater intrusion (Le et al., 2007). Dramatic changes are expected in sediment delivery to the SCS.

4. Dissertation Objectives and Hypotheses

Compared to other large river delta systems, a unique and intriguing feature of the MRD is its asymmetric feature, both temporally and spatially. Controlled by the Southeast Asian monsoon, both the hydrological regime and estuarine/nearshore hydrodynamic systems of the Mekong River show two contrasting scenarios annually within the watershed. The first scenario occurs when the SW monsoon brings more than 80% of the annual precipitation during the rainy season, which is usually between May and October (Debenay and Luan, 2006). Water discharge at Phnom Penh, Cambodia reaches a maximum in October (Gagliano

and McIntire, 1968; Milliman and Meade, 1983; Wolanski et al., 1998). The majority of suspended sediment in this dispersal system is exported to coastal waters (Wolanski et al., 1996).

The second scenario occurs during the dry season when both precipitation and water discharge are restricted. The limited fresh water supply, together with tidal asymmetry, generates a salt water intrusion that can reach 50 km upstream. In the estuarine area, wave and currents, generated by strong NE monsoon during the winter time, are the dominant factors controlling the net longshore sediment transport (Gagliano and McIntire, 1968). Previously deposited Mekong River sediments are re-suspended. The fine sediment can be transported and deposited several hundred kilometers downstream to the southwest coast of the Camau Peninsula (Nguyen et al., 2000).

Spatially the MRD exhibits an asymmetric evolution trend. The coastal area from the river mouth to the Camau Peninsula (east shore) is dominated by a regular 3.5 m semidiurnal tide from the SCS. This part of the MRD is experiencing fast erosion with an approximate rate of 1.1 km^2 / yr since 1885 (Saito, 2000), despite the large fluvial input. As part of the Gulf of Thailand, the west shore of the MRD is dominated by an irregular diurnal tide with 0.8-1.0 m tidal range (Le et al., 2007). The coast here has a nearly straight shoreline oriented north-southward. According to Saito (2000), this part of the peninsula experienced a rapid progradation at a rate of 1.2 km^2/ yr between 1885 and 1985.

As described above, detailed sedimentation studies have been conducted on the subaerial part of MRD. However, studies of the sedimentation processes on the continental shelf are still limited. Seismic and sediment core studies only have been conducted either

along the continental shelf edge (Schimanski and Stattegger, 2005) or to the south around the Sunda Shelf, where the paleo-shoreline was located during the LGM (Hanebuth et al., 2000, 2002, 2003, 2004, and 2009). To fully understand the asymmetric feature exhibited by the MRD, its relationship with the monsoon system and the potential influence brought by upstream water/sediment discharge alternation need to be addressed, the primary objectives of my Ph.D. dissertation research are:

1) Perform high resolution seismic surveys on the MRD's subaqueous deposits and correlate its stratigraphic architecture with inland boreholes; combine seismic data with grain size and accumulation rate data revealed by radioactive isotope dating techniques (^{210}Pb for 100-yr-scale and AMS ^{14}C for 5000-yr-scale). As part of this study I will estimate the volume of the deltaic deposit during the late Holocene;

2) Use mineralogy (X-ray Diffraction), stable isotope tracer (δ^{13}C) and C/N ratios to study the source of the sediments and bulk organic carbon deposited in the coastal area; explore differences in sedimentary processes for different hydrodynamic environments around the delta plain;

3) Perform numerical modeling of the sediment transport and dispersal on the Mekong shelf, so as to build a sediment dispersal/delta evolution model based on the combination of seismic surveying, cored sediment analyses, and numerical modeling;

4) Understand the dominant factors contributing to the MRD's asymmetric progradation during the late Holocene, with special focus on the influence from monsoon dynamics and climatic changes;

5) Use statistical methods (linear regression and time series analysis) to evaluate the

impact of anthropogenic processes (mainly constructions of dams and reservoirs), monsoon, and climatic changes, if there is any, on the water discharge and sediment delivery within the watershed over the last 50 years.

5. Outline of the Dissertation

In this dissertation, Chapter Two focuses on the changes in the hydrological regime of the Mekong River in the last 50 yrs, as it relates to the monsoon dynamics, climatic changes, and human activities (e.g. dams and reservoirs). A Geographic Information System (GIS)-based hydropower database for the Mekong basin is presented. The Mann-Kendall analysis is applied to the precipitation and runoff time series data collected from eight gauge stations along the main channel of the Lower Mekong (south of the Chinese Border) to detect a possible trend over the last 50 yrs. An emphasis is placed on the correlation among the runoff, local precipitation, Monsoon, and the El Niño Southern Oscillation (ENSO) during different time periods concerning the completion of major dams in the Upper Mekong.

Chapter Three presents the seismic profiling collected during two research cruises in 2006 and 2007 together with radioactive dating results from several gravity cores. This chapter aims to correlate the stratigraphic architecture of the subaqueous delta with the sedimentary facies revealed by borehole studies on the delta plain. A late Holocene sediment budget is established, based on the volume of the subaqueous delta. The subaqueous delta is further divided into four zones defined by different sedimentary processes and depositional features. The morphology asymmetry of the MRD over the past 3,000 yrs is explained as a

result of alongshore sediment transport strengthened by the NE monsoon.

Chapter Four extends the sediment dynamics study for the subaqueous delta by incorporating a numerical model of the sediment transport and dispersal on the Mekong shelf. The Regional Ocean Modeling System (ROMS) and the Community Sediment Transport Model System (CSTMS) are adapted to the study area. Together with an examination of source materials for the subaqueous delta and the sedimentation processes revealed by radioactive isotope tracers, this model simulates the sediment dynamics on the shelf as they relate to local hydrodynamics and fluvial sediment inputs. Wind driven currents and resuspension of sediments are indicated as key factors affecting local sediment transport and delta evolution.

Chapter Five includes the conclusions and future works.

This dissertation is the first study to present both a field survey and a numerical modeling study of the MRD, which has the third largest delta plain in the world, yet whose sediment dynamics have not been examined. It reproduces the late Holocene evolution of the MRD with an intriguing morphological asymmetry. The investigation will extend our knowledge of a large tropical deltaic system's sedimentation response to changes in the monsoon systems.

References

Alexander, C.R., DeMaster, D.J. and Nittrouer, C.A., 1991. Sediment accumulation in a modern epicontinental-shelf setting: The Yellow Sea. Marine Geology, 98: 51-72.

Alexander, C.R., Nittrouer, C.A. and DeMaster, D.J., 1986. High-resolution seismic stratigraphy and its sedimentological interpretation on the Amazon continental shelf. Continental Shelf Research, 6: 337-357.

Allison, M.A., Lee, M.T., Ogston, A.S. and Aller, R.C., 2000. Origin of Amazon mudbanks along the northeastern coast of South America. Marine Geology, 163(1-4): 241-256.

Amorosi, A., Dinelli, E., Rossi, V., Vaiani, S.C. and Sacchetto, M., 2008. Late Quaternary palaeoenvironmental evolution of the Adriatic coastal plain and the onset of Po River Delta. Palaeogeography, Palaeoclimatology, Palaeoecology, 268(1-2): 80-90.

Boyd, R., Suter, J.R. and Penland, S., 1989. Relation of sequence stratigraphy to modern sedimentary environments. Geology, 17(10): 926-929.

Cattaneo, A., Correggiari, A., Langone, L. and Trincardi, F., 2003. The late-Holocene Gargano subaqueous delta, Adriatic shelf: Sediment pathways and supply fluctuations. Marine Geology, 193(1-2): 61-91.

Chen, Z., Li, J., Shen, H. and Wang, Z., 2001. Yangtze River of China: historical analysis of discharge variability and sediment flux. Geomorphology, 41(2-3): 77-91.

Chen, Z., Song, B., Wang, Z. and Cai, Y., 2000. Late Quaternary evolution of the sub-aqueous Yangtze Delta, China: Sedimentation, stratigraphy, palynology, and deformation. Marine Geology, 162(2-4): 423-441.

Chen, Z., Zhou, C., Dong, Y. and Sun, J., 1987. Subaqueous topography and sediments off modern Changjiang Estuary. In: Q. Yan and S. Xu (Editors), Recent Yangtze Delta Deposit. East China Normal University Press, Shanghai, pp. 238-245.

Clift, P.D. et al., 2008. Correlation of Himalayan exhumation rates and Asian monsoon intensity. Nature Geosicence, 1(12): 875-880.

Correggiari, A., Cattaneo, A. and Trincardi, F., 2005. The modern Po Delta system: Lobe switching and asymmetric prodelta growth. Marine Geology, 222-223: 49-74.

Debenay, J.-P. and Luan, B.T., 2006. Foraminiferal assemblages and the confinement index as tools for assessment of saline intrusion and human impact in the Mekong Delta and neighbouring areas (Vietnam). Revue de Micropaleontologie, 49(2): 74-85.

Driscoll, N.W. and Karner, G.D., 1999. Three-dimensional quantitative modeling of clinoform development. Marine Geology, 154(1-4): 383-398.

Fisk, H.N., McFarlan, E.J., Kolb, C.R. and Wilbert, L.J.J., 1954. Sedimentary Framework of the Modern Mississippi Delta. Journal of Sedimentary Petrology, 24(2): 76-99.

Foster, G. and Carter, L., 1997. Mud sedimentation on the continental shelf at an accretionary margin-Poverty Bay, New Zealand. New Zealand Journal of Geology and Geophysics, 40: 157-173.

Frignani, M. and Langone, L., 1991. Accumulation rates and 137Cs distribution In sediments off the Po River delta and the Emilia-Romagna coast (Northwestern Adriatic Sea, Italy). Continental Shelf Research, 11(6): 525-542.

Gagliano, S.M. and Mcintire, W.G., 1968. Reports on the Mekong River Delta, Louisiana State University.

Galloway, W.E., 1975. Process framework for describing the morphologic and stratigraphic evolution of deltaic depositional systems. In: M.L. Broussard (Editor), Deltas, Models for Exploration. Houston geological Society, Houston, pp. 87-98.

Gibbs, R.J., 1967. The Geochemistry of the Amazon River system: part I, The factors that control the salinity and the composition and concentration of the suspended solids. Geological Society of America Bulletin, 78: 1203-1232.

Gomez, B., Eden, D.N., Peacock, D.H. and Pinkney, E.J., 1998. Floodplain construction by recent, rapid vertical accretion: Waipaoa River, New Zealand. Earth Surface Processes and Landforms, 23(5): 405-413.

Goodbred, S.L. and Kuehl, S.A., 1999. Holocene and modern sediment budgets for the Ganges-Brahmaputra river system: evidence for highstand dispersal to flood-plain, shelf, and deep-sea depocenters. Geology, 27(6): 559-562.

Goodbred, S.L. and Kuehl, S.A., 2000. The significance of large sediment supply, active tectonism, and eustasy on margin sequence development: Late Quaternary stratigraphy and evolution of the Ganges-Brahmaputra delta. Sedimentary Geology, 133(3-4): 227-248.

Goodbred, S.L., Kuehl, S.A., Steckler, M.S. and Sarker, M.H., 2003. Controls on facies distribution and stratigraphic preservation in the Ganges-Brahmaputra delta sequence. Sedimentary Geology, 155(3-4): 301-316.

Gupta, A. and Liew, S.C., 2007. The Mekong from satellite imagery: A quick look at a large river. Geomorphology, 85(3-4): 259-274.

Hanebuth, T., Stattegger, K. and Grootes, P.M., 2000. Rapid flooding of the Sunda Shelf: A

late-glacial sea-Level record. Science, 288(5468): 1033-1035.

Hanebuth, T., Stattegger, K. and Saito, Y., 2002. The stratigraphic architecture of the central Sunda Shelf (SE Asia) recorded by shallow-seismic surveying. Geo-Marine Letters, 22(2): 86-94.

Hanebuth, T.J.J. and Stattegger, K., 2004. Depositional sequences on a late Pleistocene-Holocene tropical siliciclastic shelf (Sunda Shelf, southeast Asia). Journal of Asian Earth Sciences, 23(1): 113-126.

Hanebuth, T.J.J., Stattegger, K. and Bojanowski, A., 2009. Termination of the Last Glacial Maximum sea-level lowstand: The Sunda-Shelf data revisited. Global and Planetary Change, 66(1-2): 76-84.

Hanebuth, T.J.J., Stattegger, K., Schimanski, A., Ludmann, T. and Wong, H.K., 2003. Late Pleistocene forced-regressive deposits on the Sunda Shelf (Southeast Asia). Marine Geology, 199(1-2): 139-157.

Harris, P.T., Baker, E.K., Core, A.R. and Short, S.A., 2003. A preliminary study of sedimentation in the tidally dominated Fly River delta, Gulf of Papua. Continental Shelf Research, 13(4): 441-472.

Hori, K. et al., 2001. Sedimentary facies and Holocene progradation rates of the Changjiang (Yangtze) delta, China. Geomorphology, 41(2-3): 233-248.

Hu, J., Kawamura, H., Hong, H. and Qi, Y., 2004. A review on the currents in the South China Sea: seasonal circulation, South China Sea warm current and Kuroshio Intrusion. Journal of Oceanography, 56(6): 607-624.

Kite, G., 2001. Modelling the Mekong: hydrological simulation for environmental impact

studies. Journal of Hydrology, 253(1-4): 1-13.

Kuehl, S.A. et al., 1996. Sediment deposition, accumulation, and seabed dynamics in an energetic fine-grained coastal environment. Continental Shelf Research, 16(5-6): 787-815.

Kummu, M. and Varis, O., 2007. Sediment-related impacts due to upstream reservoir trapping, the Lower Mekong River. Geomorphology, 85(3-4): 275-293.

Le, T.V.H., Nguyen, H.N., Wolanski, E., Tran, T.C. and Haruyama, S., 2007. The combined impact on the flooding in Vietnam's Mekong River delta of local man-made structures, sea level rise, and dams upstream in the river catchment. Estuarine, Coastal and Shelf Science, 71(1-2): 110-116.

Leithold, E.L. and Blair, N.E., 2001. Watershed control on the carbon loading of marine sedimentary particles. Geochimica et Cosmochimica Acta, 65(14): 2231-2240.

Li, C., 1986. Delta sedimentation. In: M. Ren (Editor), Modern sedimentation in coastal and nearshore zone of China. China Ocean Press, Beijing and Springer Verlag, Berlin, pp. 253-378.

Liu, J.P. et al., 2008. Flux and fate of small mountainous rivers derived sediments into the Taiwan Strait. Marine Geology, 256(1-4): 65-76.

Liu, J.P., Milliman, J.D., Gao, S. and Cheng, P., 2004. Holocene development of the Yellow River's subaqueous delta, North Yellow Sea. Marine Geology, 209(1-4): 45-67.

Liu, J.P. et al., 2007. Flux and fate of Yangtze River sediment delivered to the East China Sea. Geomorphology, 85(3-4): 208-224.

Liu, J.P. et al., 2009. Fate of sediment delivered to the sea by Asian large rivers, Long-distance transport and formation of remote alongshore clinothems. SEPM-The

Sedimentary Record, 7(4): 4-9.

Magilligan, F.J. and Nislow, K.H., 2005. Changes in hydrologic regime by dams. Geomorphology, 71(1-2): 61-78.

McKee, B.A., Aller, R.C., Allison, M.A., Bianchi, T.S. and Kineke, G.C., 2004. Transport and transformation of dissolved and particulate materials on continental margins influenced by major rivers: benthic boundary layer and seabed processes. Continental Shelf Research, 24(7-8): 899-926.

Meybeck, M., Laroche, L., Durr, H.H. and Syvitski, J.P.M., 2003. Global variability of daily total suspended solids and their fluxes in rivers. Global and Planetary Change, 39(1-2): 65-93.

Michels, K.H., Kudrass, H.R., Hubscher, C., Suckow, A. and Wiedicke, M., 1998. The submarine delta of the Ganges-Brahmaputra: cyclone-dominated sedimentation patterns. Marine Geology, 149(1-4): 133-154.

Milliman, J.D. and Kao, S.J., 2005. Hyperpycnal discharge of fluvial sediment to the ocean: Impact of super typhoon Herb (1996) on Taiwanese rivers

doi:10.1086/431906. The Journal of Geology, 113(5): 503-516.

Milliman, J.D. and Meade, R.H., 1983. World-wide delivery of river sediment to the oceans. Journal of Geology, 91: 1-21.

Milliman, J.D. and Syvitski, J.P.M., 1992. Geomorphic/tectonic control of sediment discharge to the ocean: the importance of small mountainous rivers. Journal of Geology, 100: 525-544.

Morehead, M.D., Syvitski, J.P., Hutton, E.W.H. and Peckham, S.D., 2003. Modeling the

temporal variability in the flux of sediment from ungauged river basins. Global and Planetary Change, 39(1-2): 95-110.

Neill, C.F. and Allison, M.A., 2005. Subaqueous deltaic formation on the Atchafalaya Shelf, Louisiana. Marine Geology, 214(4): 411-430.

Nguyen, L.V., Ta, T.K.O. and Tateishi, M., 2000. Late Holocene depositional environments and coastal evolution of the Mekong River Delta, Southern Vietnam. Journal of Asian Earth Sciences, 18(4): 427-439.

Nichols, G., 1999. Sedimentology and Stratigraphy. Blackwell Science, Oxford, 273 pp.

Nittrouer, C.A., 1999. STRATAFORM: overview of its design and synthesis of its results. Marine Geology, 154(1-4): 3-12.

Nittrouer, C.A. and DeMaster, D.J., 1996. The Amazon shelf setting: tropical, energetic, and influenced by a large river. Continental Shelf Research, 16(5-6): 553-573.

Nittrouer, C.A., Kuehl, S.A., DeMaster, D.J. and Kowsmann, R.O., 1986. The deltaic nature of Amazon shelf sedimentation. GSA Bulletin, 97(4): 444-458.

Nittrouer, C.A. et al., 1996. The geological record preserved by Amazon shelf sedimentation. Continental Shelf Research, 16(5-6): 817-841.

Orton, G.J. and Reading, H.G., 1993. Variability of deltaic processes in terms of sediment supply, with particular emphasis on grain size. Sedimentology, 40: 475-512.

Penland, S., Boyd, R. and Suter, J.R., 1988. Transgressive depositional systems of the Mississippi Delta plain; a model for barrier shoreline and shelf sand development. Journal of Sedimentary Research, 58(6): 932-949.

Reading, H.G., 1996. Sedimentary environments: processes, facies and stratigraphy.

Blackwell Science, Cambridge, MA, 25 pp.

Roberts, H.H., 1997. Dynamic changes of the Holocene Mississippi River delta plain : The delta cycle. Journal of Coastal Research, 13(3): 691-710.

Roberts, H.H., 1998. Delta switching: early responses to the Atchafalaya River diversion. Journal of Coastal Research, 14(3): 882.

Saito, Y., 2000. Deltas in Southeast and East Asia: their evolution and current problems. In: N. Mimura and H. Yokoki (Editors), APN/SURVAS/LOICZ Joint Conference on Coastal Impact of Climate Change and Adaption in the Asia-Pacific Region, Kobe, Japan, pp. 185-191.

Sarma, J.N., 2005. Fluvial process and morphology of the Brahmaputra River in Assam, India. Geomorphology, 70(3-4): 226-256.

Schimanski, A. and Stattegger, K., 2005. Deglacial and Holocene evolution of the Vietnam shelf: stratigraphy, sediments and sea-level change. Marine Geology, 214(4): 365-387.

Singh, M., Singh, I.B. and Muller, G., 2006. Sediment characteristics and transportation dynamics of the Ganga River. Geomorphology, I86(1-2): 144-175.

Stanley, D.J. and Warne, A.G., 1994. Worldwide initiation of Holocene Marine Deltas by deceleration of sea-Level rise. Science, 265(5169): 228-231.

Su, J., 2004. Overview of the South China Sea circulation and its influence on the coastal physical oceanography outside the Pearl River Estuary. Continental Shelf Research, 24(16): 1745-1760.

Swenson, J.B., 2005. Fluviodeltaic response to sea-level perturbations: amplitude and timing of shoreline translation and coastal onlap. Journal of Geophysical Research, 110:

doi:10.1029/2004JF000208.

Syvitski, J.P.M. et al., 2009. Sinking deltas due to human activities. 2(10): 681-686.

Syvitski, J.P.M. and Saito, Y., 2007. Morphodynamics of deltas under the influence of humans. Global and Planetary Change, 57(3-4): 261-282.

Syvitski, J.P.M., Vorosmarty, C.J., Kettner, A.J. and Green, P., 2005. Impact of humans on the flux of terrestrial sediment to the global coastal ocean. Science, 308(5720): 376-380.

Ta, T.K.O., Nguyen, V.L., Kobayashi, I., Tateishi, M. and Saito, Y., 2001. Late Pleistocene-Holocene stratigraphy and delta progradation, the Mekong River Delta, South Vietnam. Gondwana Research, 4(4): 799-800.

Ta, T.K.O., Nguyen, V.L., Tateishi, M., Kobayashi, I. and Saito, I., 2005. Holocene delta evolution and depositional models of the Mekong River Delta, Southern Vietnam. In: L. Giosan and J.P. Bhattacharya (Editors), River Deltas-Concepts, Models, and Examples. SEPM, Tulsa.

Ta, T.K.O., Nguyen, V.L., Tateishi, M., Kobayashi, I. and Saito, Y., 2001. Sedimentary facies, diatom and foraminifer assemblages in a late Pleistocene-Holocene incised-valley sequence from the Mekong River Delta, Bentre Province, southern Vietnam: the BT2 core. Journal of Asian Earth Sciences, 20(1): 83-94.

Ta, T.K.O. et al., 2002. Sediment facies and Late Holocene progradation of the Mekong River Delta in Bentre Province, southern Vietnam: an example of evolution from a tide-dominated to a tide- and wave-dominated delta. Sedimentary Geology, 152(3-4): 313-325.

Ta, T.K.O. et al., 2002. Holocene delta evolution and sediment discharge of the Mekong River, southern Vietnam. Quaternary Science Reviews, 21(16-17): 1807-1819.

Tamaki, K. and Honze, E., 1991. Global tectonics and formation of marginal basins: role of the western Pacific. Episodes 14, 224-2230 pp.

Tamura, T. et al., 2009. Initiation of the Mekong River delta at 8 ka: evidence from the sedimentary succession in the Cambodian lowland. Quaternary Science Reviews, 28(3-4): 327-344.

Walsh, J.P. et al., 2004. Clinoform mechanics in the Gulf of Papua, New Guinea. Continental Shelf Research, 24(19): 2487-2510.

Wang, H., Yang, Z., Saito, Y., Liu, J.P. and Sun, X., 2006. Interannual and seasonal variation of the Huanghe (Yellow River) water discharge over the past 50 years: connections to impacts from ENSO events and dams. Global and Planetary Change, 50(3-4): 212-225.

Wang, P., 1999. Response of Western Pacific maringal seas to glacial cycles: paleoceanographic and sedimentological features. Marine Geology, 156: 5-39.

Wang, P., Jian, Z. and Liu, Z., 1992. Late Quaternary sedimentation rate in the South China Sea. In: Z. Ye and P. Wang (Editors), Contributions to Late Quaternary Paleoceanography of the South China Sea. Qingdao Ocean Univ. Press, Qingdao, pp. 23-41.

Wang, P.P., 2005. The coastal environment of Southeast Asia. In: A. Gupta (Editor), The Physical Geography of Southeast Asia. Oxford, New York, pp. 179-180.

Webster, P.J., 1987. The Elementary Monsoon. Wiley, New York.

Wolanski, E., Ngoc Huan, N., Trong Dao, L., Huu Nhan, N. and Ngoc Thuy, N., 1996. Fine-sediment dynamics in the Mekong River Estuary, Vietnam. Estuarine, Coastal and Shelf Science, 43(5): 565-582.

Wolanski, E., Nguyen, H.N. and Spagnol, S., 1998. Sediment dynamics during low flow

conditions in the Mekong River Estuary, Vietnam. Journal of Coastal Research, 14: 472-482.

Yang, Z.S. and Liu, J.P., 2007. A unique Yellow River-derived distal subaqueous delta in the Yellow Sea. Marine Geology, 240(1-4): 169-176.

Figures

Fig. 1. River systems originating from the Tibetan Plateau

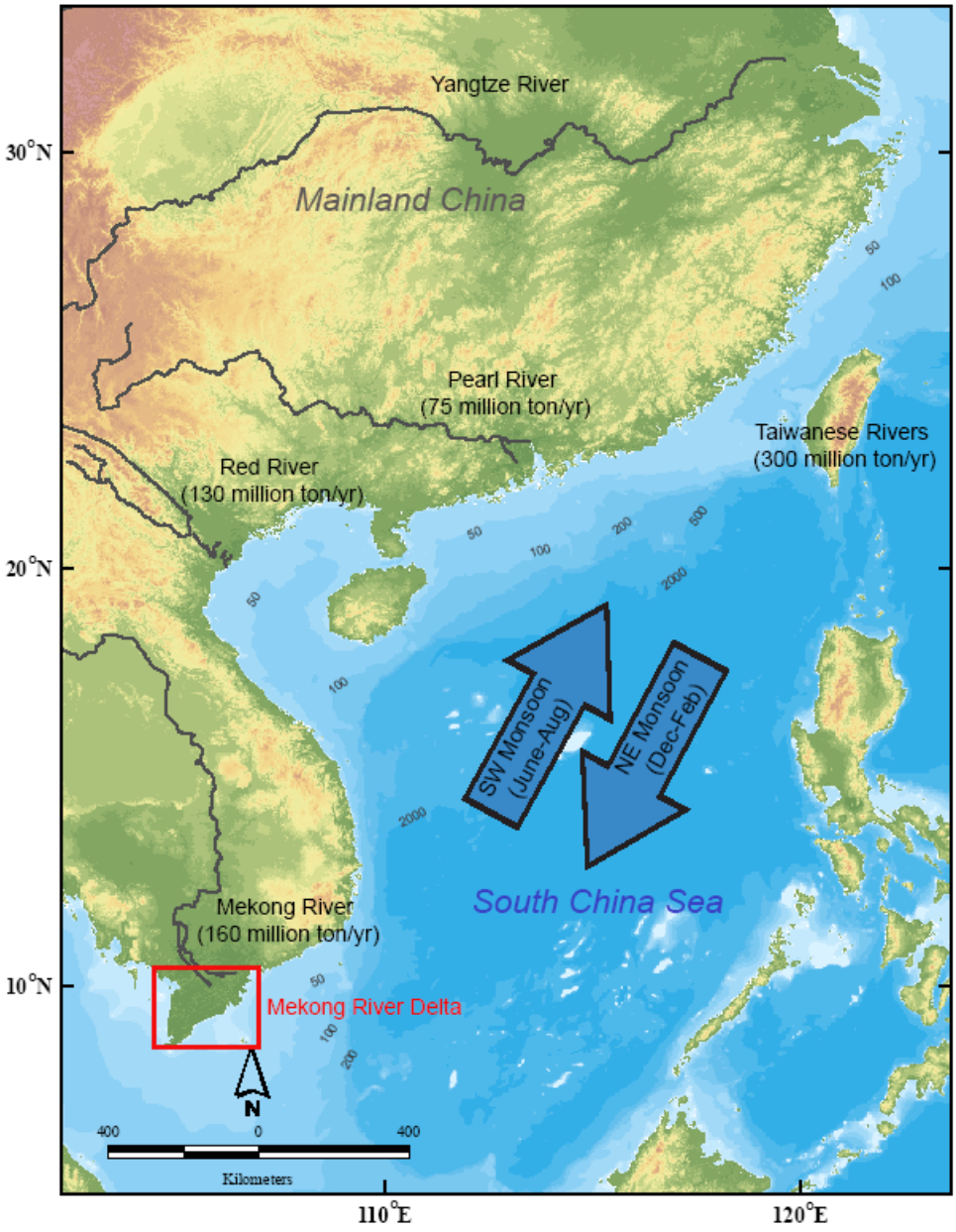

Fig. 2. A bathymetric map of the South China Sea with major fluvial sediment inputs and Southeast Asian Monsoon system

Fig. 3. The Mekong River and basin

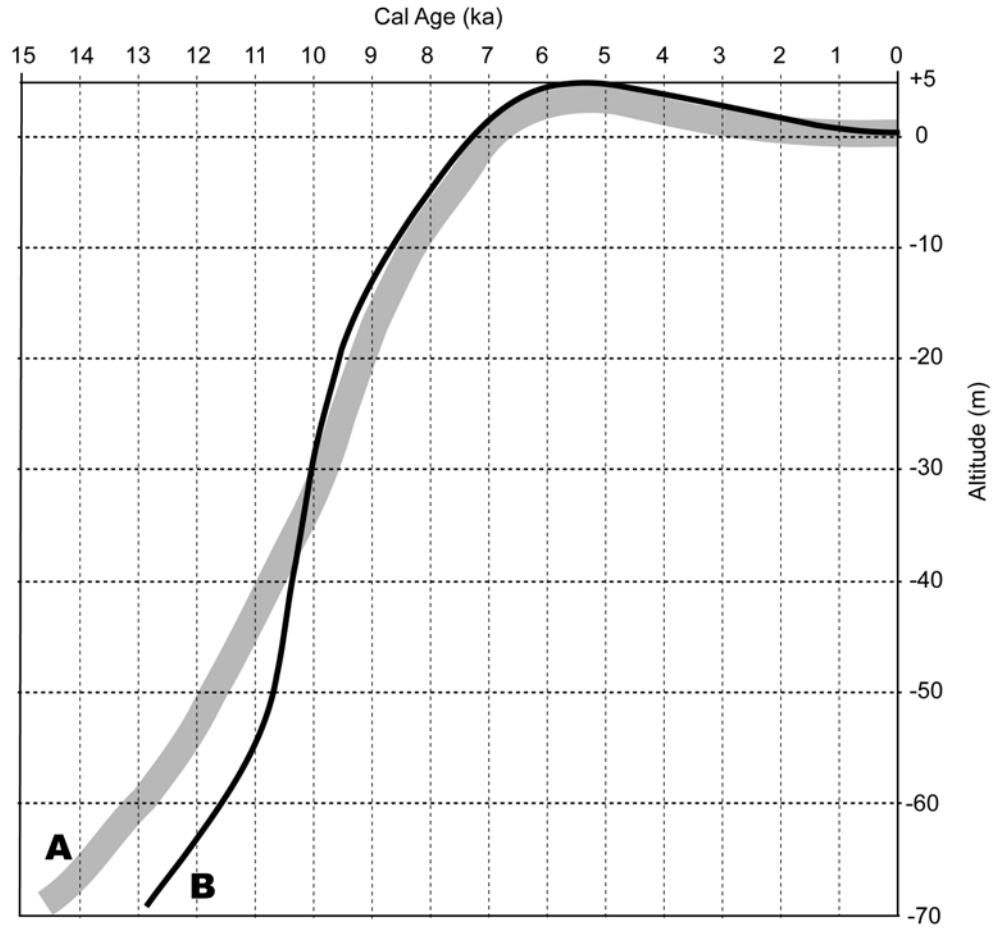

Fig. 4. Sea-level curve for the Sunda Shelf and the Mekong River Delta.
Line A for the Mekong River Delta and Line B for the Sunda Shelfafter Hanebuth et al., 2000 and Ta et al., 2002a.

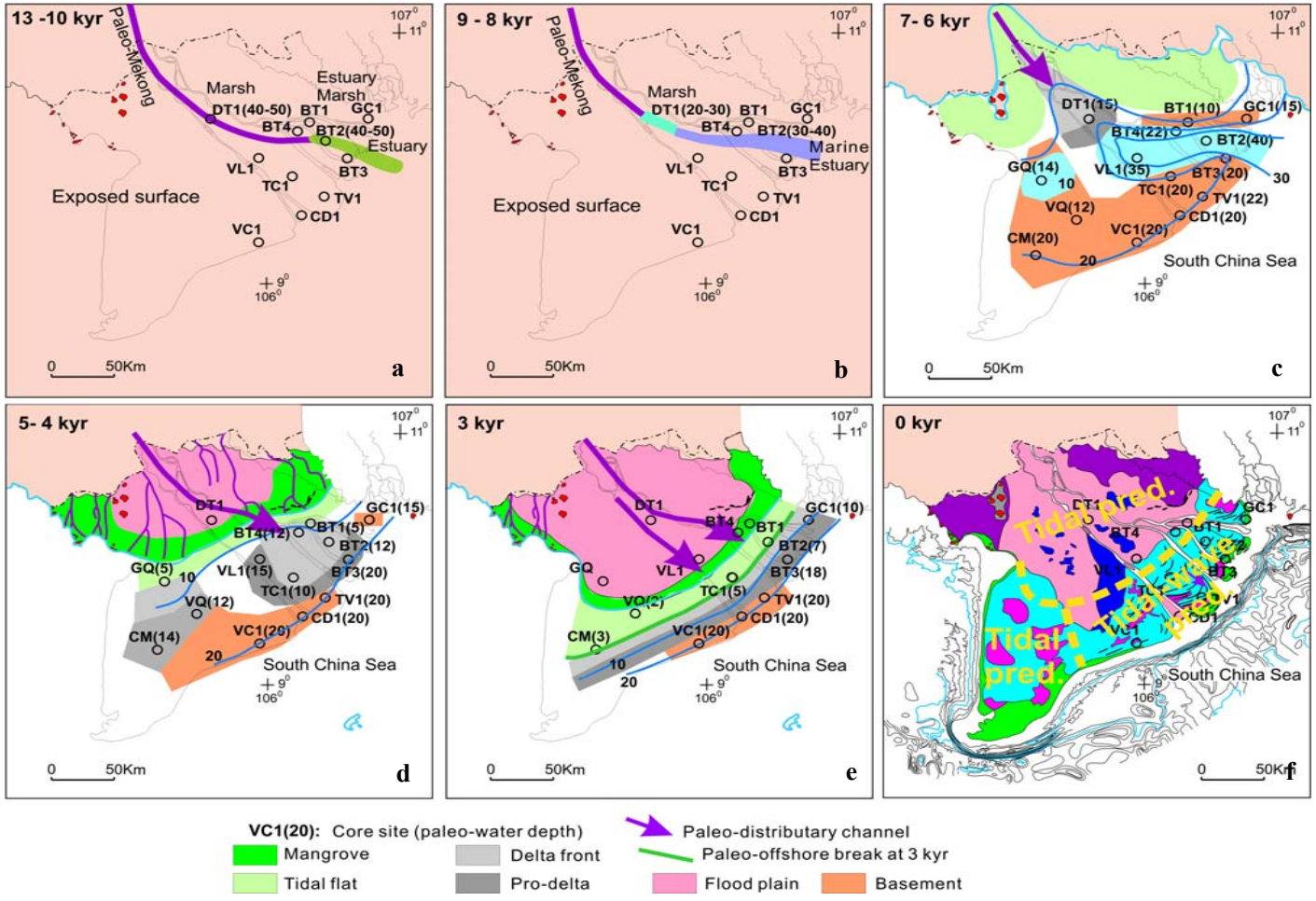

Fig. 5. Evolution of the Mekong River Delta since 13,000 yr BP. courtesy of Dr. Thi Kim Oanh Ta.

CHAPTER 2: CHANGES IN HYDROLOGY AND SEDIMENT DELIVERY OF THE MEKONG RIVER IN THE LAST 50 YEARS: CONNECTION TO DAMING, MONSOON, AND ENSO[1]

Zuo Xue, J. Paul Liu and Qian Ge

[1] This chapter is based on a manuscript accepted by *Earth Surface Processes and Landforms*

Abstract

The Mekong River is the third largest river in the Western Pacific. As the population and economy booms, more and more dams are built in the Mekong basin. Concerns about negative impacts on downstream and the delta plain from upstream damming have been raised ever since the completion of the Manwan Dam in 1993. Although numbers of study were made focused on runoff and sediment flux characters of the Mekong River, little is known at present on the relationship among monsoons, El Niño Southern Oscillation (ENSO), precipitation, runoff, and impact of dams on the delta dynamics.

A comprehensive hydropower GIS database covering the entire Mekong basin is presented in this study. With another 200 new dams to be added to the basin in the next couples of decades, changes are expected in both hydrological regime and delta dynamics. On one hand, the runoff of the Lower Mekong River showed a closer connection with the regional precipitation and ENSO in the post-dam period (1993-2005) than in the pre-dam period (1950-1993). Such relationship is expected to be even closer when more dams are completed. On the other hand, both daily maximum and minimum water levels on the delta plain showed abrupt drop since the end of 1994. This reduced water-level gradient between the river and sea inevitably weakens the sediment discharge to the coast, which might intensify the on-going coastal erosion on the east shore of the delta plain.

KEYWORDS: Mekong River; Hydrological Regime; Monsoon; Impact of Dams; delta dynamics

1. Introduction and Background

Dams have major impacts on river hydrology, primarily through changes in the timing, magnitude, and frequency of low and high flows, ultimately producing a hydrologic regime differing significantly from the pre-impoundment natural flow regime (Magilligan and Nislow, 2005; Syvitski et al., 2009). Dams and reservoirs hold not only water but also large quantities of sediments because of the reduced riverine carrying capacity. It has been estimated that over 70% of the world's rivers are intercepted by large reservoirs, and half of them have a local sediment trapping efficiency of more than 80% (Kummu and Varis, 2007).

A number of studies have indicated a strong correlation between water discharge and suspended sediment concentration (SSC) in both large/small and gauged/ungauged river systems (eg. Milliman and Syvitski, 1992; Meybeck et al., 2003; Morehead et al., 2003). The rating curve, based on the power regression between water discharge and SSC, is generally expressed as:

$$Cs=aQ^b \quad (1)$$

or a natural logarithm transformed linearized equation :

$$lnCs= ln(a) + blnQ \quad (2)$$

where *Cs* stands for the SSC (kg/m^3), *Q* stands for the water discharge (m^3/s), and *a* and *b* are unitless coefficients. Although *a* and *b* may have no particular physical meaning, the negative correlation between *ln(a)* and *b* has been demonstrated to be an index of soil erodibility and erosivity (Asselman, 2000). For large river systems in Asia, such a relationship has been well documented in the Yangtze (Chen et al., 2001), Yellow (Wang et al., 2006), Brahmaputra (Sarma, 2005), and Ganges Rivers (Singh et al., 2007).

Yang et al. (2007) analyzed 234 pairs of *ln(a)* and *b* coefficients from ten gauge stations along the Yangtze River and derived a strong negative parameter correlation (r^2=0.988). Wang et al. (2008a) further examined the negative correlation from one of these stations over different time periods and demonstrated that such correlation indicated an increased erosive power and decreased sediment supply. They also concluded that such changes were the results of extensive human activities along the Yangtze River, especially from upstream damming.

The Mekong River is Asia's third largest river in terms of length and sediment load. It delivers approximately 160 million tons of sediment and 475 km^3 of fresh water per year into the South China Sea (Milliman and Meade, 1983). Originating from the Tibetan Plateau, the 4,750 km long Mekong River runs through China (Yunnan province), Myanmar, Thailand, Lao PDR, and Cambodia before it finally enters the South China Sea in southern Vietnam. The river has a watershed of 832,000 km^2 (river basin generated and calculated by HYDROSHEDS, World Wildlife Fund-US, Fig. 1). The climate of the Lower Mekong (from China border to the south) is humid and tropical. Mean annual rainfall ranges from 1,000 mm in Thailand to 3,200 mm in the mountainous region of Laos PDR (Kite, 2001). The Lower Mekong River Basin is dominated by two distinct monsoon seasons: the rainy southwest monsoon season and the dry northeast monsoon season. While most researchers agree that the rainy season accounts for more than 80% of the annual rainfall between mid-May and early October, Gupta and Liew (2007) suggests that the summer snowmelt from the Tibetan plateau is the reason for the small rise in water discharge rise during May and that the period from June to November accounts for the 80% of the yearly discharge.

The Mekong River flows over rocks for about 80% of its length before it enter the alluvial plain of Cambodia and Vietnam. Bedrock within China and Lao PDR are mainly sedimentary and metamorphic rocks. When the Mekong River reaches northern Cambodia, alluvial channel deposits with exposures of Triassic sedimentary rocks and Neogene basalts become the primary riverbed material. The river ultimately runs into the Mekong River Delta (MRD), which is composed of Holocene alluvial sediments and has experienced a rapid progradation since 8,000 yr BP (Tamura et al., 2009; Xue et al., 2010).

As the home of more than 70 million people, the Mekong River basin is experiencing a rapid economic and population growth. Increasing demand for hydropower and freshwater leads to the construction of more and more dams and reservoirs along the main stream, which will inevitably change the water/sediment discharge downstream in two ways: (1) flow regulation from upstream dams will shift the original rhythm of water/sediment discharge controlled by monsoon forcing; and (2) large amounts of sediments are held behind the dams, which dramatically decreases the sediment flux downstream. Le et al. (2007) points out that if the riverine sediment inflow to the sea is decreased by the construction of upstream dams, extensive estuarine siltation and increased flooding, together with increased coastal erosion and the loss of coastal wetlands, are likely to occur in the MRD.

The most controversial hydropower project on the Mekong River so far is the Lancang Cascade within China's Yunnan Province in the upstream area. Since the completion of the Manwan Dam (the first of the 14 dams in total) in 1993, arguments have been raised about its positive and, especially, negative impact on the Lower Mekong River basin. Nguyen (2003) observed increased monthly-averaged water discharge in both the dry (November to

April) and wet (May to October) seasons at Chiang Sean station (746 km downstream of the dam, position see Fig. 1) after the completion of the dam. An detailed analysis of the runoff trend at six gauge stations in the middle-downstream indicated that the frequency and magnitude of water level fluctuations increased in the post-dam period (1993-2000) (Lu and Siew, 2006). A general consensus is that the operation of the Manwan Dam has considerably increased downstream discharges during dry seasons (Nguyen, 2003; Lu and Siew, 2006; Kummu and Varis, 2007). A correlation analysis of river runoff and SSC in the middle-downstream showed that the SSC was positively correlated with water discharge with R^2 values ranging from 0.52 to 0.77 (Kummu and Varis, 2007). Although there was a sharp decrease of sediment flux at Chiang Sean shortly after the completion of the dam, other stations downstream did not show abrupt changes (Lu and Siew, 2006; Kummu and Varis, 2007). Because of the sporadic SSC measurements and inconsistent observation standards, comprehensive analysis of the dams' impact on Lower Mekong's sediment flux is still not available.

The determination of the overall downstream impact of the Lancang Cascade is complicated. Changes of river runoff and sediment flux are not solely caused by dam construction/operation. Analysis of other environmental factors, such as monsoons, precipitation, solar activities, El Niño Southern Oscillation (ENSO), and human activities other than damming, are also needed to reasonably evaluate Mekong's hydrological trend including the dam impact. For example, Campbell (2007) showed that the low flows between 2003 and 2004 were caused by low precipitation in the Lowe Mekong basin. Cogels (2007) pointed out that the downstream impact from the Lancang Cascade has been exaggerated. Li

and He (2008) demonstrated that large scale climate change could influence the water levels of the gauge stations around the Lancang Cascade. A recent examination of SSC variations in the Upper Mekong showed that the Manwan Dam's impact was very limited even at gauge stations 401 km downstream (Fu et al., 2008). Another detailed review by Lu et al. (2008) confirmed that monthly-averaged water levels and the river runoff averaged for the pre- and post-dam periods were similar.

Although there have been a number of studies on the hydrological response of the Mekong River to the impact of the Lancang Cascade, contemporary changes of environmental factors, such as precipitation and monsoon systems, however, were not considered in such studies. The purpose of this paper are: (1) to present a comprehensive hydropower GIS database covering the entire Mekong River basin; (2) to use time series techniques to re-analyze Mekong's hydrological trends, including use of local precipitation information; and (3) to examine the correlation between the Mekong River flow and monsoons as well as the Mekong's possible connection with ENSO activities.

2. Data and Methods

Hydropower development data (dams and reservoirs) were collected through various sources, including the World Wildlife Fund (US) and field offices, other non-governmental organizations, published reports and literature, and personal communications. The hydropower information from all the six countries sharing the Mekong River was clipped by the watershed, generated by HydroSHEDS (WWFUS), using GIS software ArcGIS™ 9.2 by ESRI®.

We re-examined the hydrological data (runoff and SSC, Kummu and Varis, 2007; Walling, 2008) together with the precipitation rates from eight gauge stations along the mainstream (data source: Mekong River Commission based in Vien Tiane, Lao PDR; geographic locations of gauge stations are shown in Fig. 2, data details are listed in Table 1). We also collected the daily maximum and minimum water levels at two stations on the delta plain, namely, Can Tho and My Thuan (locations see Fig. 1). The Mann-Kendall analysis (Mann, 1945; Kendall, 1975) was used to analyze the trends of precipitation and runoff time series. Before Fourier spectral analysis, the runoff time series were deseasonalized using the normal quantile transform proposed by Montanari (2005). Considering the gap in SSC data, spectral analysis of periodicities was carried out only on runoff data following the method described in Bloomfield, 1976, Brockwell and Davis, 1991, and Venables and Ripley, 2002, using statistical software 'R'.

We used the Indian monsoon (IM) index developed by Wang and Fan (1999) and Wang et al. (2001) (http://apdrc.soest.hawaii.edu), the East Asian monsoon (EAM) index and South China Sea monsoon (SCSM) index developed by Li and Zeng (2005) (http://www.lasg.ac.cn/staff/ljp), and the Nino3.4 index developed by Rayner et al. (2003) (http://www.cdc.noaa.gov/gcos_wgsp/Timeseries/Nino34/) to study Mekong's possible connection with monsoons and ENSO activities.

3. Results

3.1 Hydropower Development

The hydropower GIS database contains the information on 297 dams in total, among which, 6 are in Myanmar, 34 are in Cambodia, 29 are in China, 71 are in Laos, 16 are in Thailand, and 141 are in Vietnam (geographical inequality is partially caused by skewed data source). Based on their development status, dams are grouped into three categories, which are: (1) in operation, (2) under construction, and (3) under feasibility study and planned (Fig. 2a). The majority of the hydropower data collected in this study falls into the 'Feasibility Study and Planned' category (200 in total, capacity of approximate 25,700 MW, Fig. 2b).

The largest hydropower project in the Upper Mekong River is no doubt the Lancang Cascade, which has a total capacity of 18,000 MW (six on the Upper Lancang and eight on the Lower Lancang, Magee, 2006a, Fig. 2c), about 80% of that of the Three Gorges Dam on the Yangtze River (22,500 MW). According to Magee (2006a, 2006b), the Lancang River's hydropower potential is over 25,500 MW. The initial plan of the Lancang Cascade was made in early 1980s, referred to as a stair-step series, of which 14 dams are to be constructed on the Lancang River in Yunnan Province, China. So far, the attention has been mainly focused on the eight dams designed on the Lower Lancang River, of which two are already completed (Manwan and Dachaoshan); another two are under construction (Xiaowan and Jinghong); while the remaining four (Nuozhadu, Gongguoqiao, Ganlanba and Mengsong) are still in the planning or preparatory stages. The status of the six dams planned in the Upper Lancang Rive with a designed capacity of approximate 7,700 MW and a reservoir volume of 11.39

billion m^3 in total (Li et al., 2001) still remains unknown. However, they are likely to be built eventually (Magee 2006a).

For the Lower Mekong River, extensive hydropower projects have been planned in the Sekong, Sesan, and Sre Pok River basins, i.e. the 3Ss basin (Fig. 2d), through various funding sources such as the Asian Development Bank. The 3Ss basin has an approximate area of 78,650 km^2, covering parts of Cambodia (33% of total basin area), Lao PDR (29%), and Vietnam (38%). The combined runoff from 3Ss subbasins accounts for about 17% of the Mekong's annual discharge, making 3Ss the largest subbasin of the Mekong River (ADB report, 2006). There are 65 dams (16 on Sekong, 30 on Sre Pok, and 19 on Sesan) in our database within the 3Ss basin with a total capacity of 9,500 MW. Ever since the completion of the Yali Falls (900 MW, completed in 1999), the largest dam in this area so far, concerns have been raised about its impact on downstream water quality, fisheries, irregular water level fluctuations, and other characteristics (The Fisheries Office of Ratanakiri Province, 2000; Wangpattana, 2007). However, its impact on downstream sediment transport is still not known.

3.2 Spatial and Temporal Variation of Water and Sediment

Fig. 3 is a box plot of the precipitation (Fig. 3a, this study) and runoff/SSC data (Figs. 3b and 3c, Kummu and Varis, 2007; Walling, 2008) at the eight stations (from left to right in the downstream direction). The precipitation rates vary considerably at different stations during the last 50 years. High precipitation rate is documented at the three downstream

stations (Nakhon Phanom, Khong Chiam, and Pakse). The maximum precipitation rate is documented at Nakhon Phanom with a mean precipitation rate of 2298.7 mm/yr (1953-2005) and the minimum rate is documented at Luang Prabang with a mean precipitation rate of 1293.9 mm/yr (1950-2006).

A large part of the sediments in the Lower Mekong River is sand and fine pebbles transported as bedload (Plinston and He, 2000). Confined by the river channel, most of these sediments are stored inside the main channel (Gupta and Liew, 2007). The bed material of the Mekong River is complicated and varies throughout the main channel. Gupta and Liew (2007) divided the Lower Mekong River into eight units based on different channel characters. Among the stations in this study, Chiang Sean and Luang Prabang are located on the 'Upper rock-cut channel'; Vien Tiane, Nong Khai, Nakhon Phanom, and Mukdahan are located on the 'alluvial channel'; Khong Chiam is located on 'Lower rock-cut channel'; and Pakse is located on the 'composite channel' (Fig. 3c).

As documented by Kummu and Varis (2007) and Walling (2008), the river runoff showed an increasing trend downstream while the SSC shows no steady trend along the main channel (Figs. 3b and 3c). Walling (2008) explained this phenomenon as a 'conveyance losses' associated with sediment storage starting from Jinghong (~50 km upstream of Chiang Sean). Wood et al. (2008) reported a 2-5 km wide floodplain deposited around the Chiang Sean area and a 0.5-2 m thick sandy silt layer that was mainly the result of levee and near channel deposits.

Non-parametric Mann-Kendall analysis of the annual precipitation shows no significant trend in most of the stations except for Luang Prabang (p-value 0.015) and Pakse

(p-value 0.004, Fig.4c). For yearly averaged runoff data, no significant trend was found at any station during the period of 1950-2005. Fig.4 shows the trend of annual precipitation and average runoff at Chiang Sean and Pakse over the past 50 years. Trend analysis was not performed on SSC data because of data discontinuity. However, in spite of the sporadic SSC dataset, Walling (2005) suggested that sediment loads of the Mekong River were relatively stable in the past 40 years.

We examined the daily maximum and minimum water level of two gauge stations along the two main tributaries on the MRD, i.e. the Bassac and Mekong Rivers (position see Fig. 1). Both maximum and minimum water levels at these two stations showed a clear drop around the end of 1994 (Figs. 5a and 5b).

3.3 Correlation between Precipitation, Runoff, and SSC

Because basin-wide precipitation data were not available for the Mekong River, the linear regression analysis was performed between the sum of the precipitation in a month at the eight stations and the monthly averaged runoff at Pakse, the last station in this study. A time series plot of the 10-day-averaged precipitation (sum of eight stations) and runoff (Pakse) shows a 20-to-35-day lag (Fig. 6a), based on which linear regression analysis was performed with a one-month lag between the two time series, i.e. the total precipitation at the eight stations during a month and the mean runoff at Pakse of the following month. Fig. 6b shows that during both pre-dam (1950-1992) and post-dam (1993-2005) periods, runoff at Pakse is strongly correlated with the total precipitation at the eight stations. The hypothesis test using

general linear model indicated that the correlation is significantly different during the pre-dam and post-dam periods (p-value=0.03). The runoff is more dependent on regional precipitation during the post-dam period (slope 6.22) than during the pre-dam period (slope 5.51).

The correlation between SSC and runoff has been examined for both Upper Mekong (Fu et al., 2008) and Lower Mekong (Lu and Siew, 2006; Kummu and Varis, 2007). These studies show that on one hand, the runoff-SSC relationship varies from station to station; on the other hand, impoundment of the Manwan dam shows no apparent influences on such relationship. Fig. 7 shows the parameter rating curve of five stations (stations Vien Tiane, Nakhon Phanom and Pakse are not included because of limited SSC data). To reduce the bias brought by the discontinuous SSC data, correlation analysis for the rating parameter was performed on a monthly-averaged basis. Our results show that $ln(a)$ and b was negatively correlated (n=123, r^2=0.97), similar to the situation of the Yangtze River (Yang et al., 2007; Wang et al., 2008). In the downstream direction the parameter correlation shows a trend of decreased sediment supply and increased erosive power, which is consistent with the spatial distribution of the SSC discussed in the previous section. For any single station, changes of the parameter relationship are not obvious over the past 50 years.

3.4 Spectral and Coherence analysis of the Rainfall, Runoff, Monsoon, and ENSO

The discontinuity in SSC data prevented any comprehensive evaluations of Lower Mekong's sediment regime (Walling, 2005; Lu and Liew, 2006; Kummu and Varis, 2007;

Campbell, 2007; Walling, 2008). However, continuous runoff data since 1960 was available and could be retrieved from the Mekong River Commission. For example, Fig. 8a shows a time series plot of SSC/runoff data at Chiang Sean. Using the normal quantile transform method proposed by Montanari (2005), the autocorrelation function of the deseasonalized daily runoff shows no appreciable periodicity at lag 365, confirming the absence of significant seasonality at the yearly period (Fig. 8b).

The Fourier spectral analyses of the average annual runoff at all the eight stations show a dominant 4.8-yr peak during 1960-2005 (Figs. 9a and 9b). This 4.8-yr periodicity is strongly correlated with the IM index (Figs. 9c and 9d). Runoffs at the lower four stations (from station Nakhon Phanom to Pakse) are also characterized by a 3.0-yr periodicity (Fig. 9b). Although the correlation between the runoff at four upper stations (from Chiang Sean to Nong Khai) and the EAM is not clear (Fig. 9e), the coherence analysis shows the 3.0-yr periodicity of runoffs at the lower four stations is strongly correlated with the EAM (Fig. 9f).

Compared with the pre-dam period, the spectral analyses of deseasonalized daily runoff at all eight stations show a smoother periodgram during the post-dam period (Figs. 10a, 10b, 10c, and 10d). An intriguing 6.6-yr peak was detected in runoffs during the post-dam period (Figs. 10c and 10d). Together with the 7.2-yr peaks shown in the cross coherence between the runoff and Nino 3.4 index (Figs. 10e and 10f), this 6.6-yr periodicity may indicate a strengthened runoff-ENSO relationship.

4. Discussion

4.1 Dam's Influence on Sediment and Water Regime

Although the Mekong River basin is experiencing rapid hydropower development, the hydropower database presented in this study shows that the majority of these dams, 200 out of 297, fall into the 'Feasibility Study and Planned' category. Compared with the other two large rivers on the Western Pacific, i.e., the Yellow and the Yangtze Rivers, both the quantity and the capacity of the hydropower projects within the Mekong basin are very limited. At the current stage, influence of dams on downstream sediment regime is not apparent. Previous studies have revealed that Manwan Dam had little influence on runoff-SSC relationship (Kummu and Varis, 2007; Fu et al., 2008) and the sediment load was relatively stable over the past 40 years (Walling, 2005). In this study an intra-annual change in the rating parameter relationship is not apparent for any single station. This is different from the Yangtze River case, which shows significant changes in the rating parameter relationship during the last 50 years because of increased human interventions (Wang et al., 2008a).

Dams and reservoirs will minimize the variation of the upstream inflow, making local runoff more sensitive to local environmental settings, such as precipitation, evaporation, soil type, and human activities. The correlation between the runoff at the last station (Pakse) and the total precipitation at the eight stations was significantly different during the pre-dam and post-dam period. The runoff was more dependent on regional precipitation during the post-dam period (slope 6.22) than during the pre-dam period (slope 5.51). This indicates that as

the number of dams on the Mekong River increases, the regional precipitation rate plays an even more important role on river runoff. A similar case has been documented by Xu et al. (2007) for the extensively dammed Yangtze River, indicating a strong correlation between runoff and regional precipitation (R^2 value was up to 0.90 at the Datong station, the last station on the main channel of theYangtze).

4.2 Dam Construction and Delta Dynamics

The Mekong River delivers 160 million tons of sediment into the coastal area annually. A large part of Mekong sediment will be transported southwestward by the coastal currents strengthened by the strong northeast monsoon, resulting in the rapid progradation of the large down-drift delta plain (Liu et al. 2009; Xue et al. 2010). Over the past 3000 yr, the evolution of the MRD has shown a morphological asymmetry indicated by a limited progradation on the eastern part of the MRD. This asymmetric feature was explained by increased wave influence (Xue et al., 2010). On a relative short time scale, Saito (2000) documented that eastern part of the MRD has been under serious erosion at a rate of 1.1 km^2/yr since 1885. This erosion should be a result of combined natural processes, mainly the strong hydrodynamics and the sea-level rise, and human activities, which continuously decrease the sediment flux.

Both maximum and minimum water levels at the two stations on the delta plain showed a clear drop around the end of 1994 (Fig. 5). This will weaken the sediment discharge to the river mouth. Thus less source materials will be transported to eastern part of

the MRD. Although the water level drop happened one year after the completion of the Manwan Dam, further information of other human activities in the downstream area, specifically on the delta plain (e.g., construction of dykes and embankments, Le et al., 2007), are needed to evaluate upstream dam's contribution to these decreased water levels. Nevertheless, as more and more dams are being introduced to both upstream and downstream area, the water-level gradient between the river and sea will be further weakened. In addition, more sediment will be hold behind the dams. A reduced sediment delivery from the Mekong River mouth will further intensify the coastal erosion.

4.3 Connections between Hydrology and Monsoons

Originating from the Tibetan Plateau, the hydrology of the large rivers along the Western Pacific is inevitably affected by the IM, EAM, west Northern Pacific monsoon (WNPM), and ENSO activities. For example, Ding and Chan (2005) point out that the Upper Yangtze River is influenced by the IM, whereas the Lower Yangtze River is controlled by the EAM. Wang et al. (2008a) indicated that the sediment flux of the Upper Yangtze River is apparently influenced by the IM. Xu et al. (2008) demonstrated the correlation between Yellow River sediment flux and EAM intensity over the past 50 years.

In contrast with the Yangtze and Yellow Rivers which transport in an east-west direction, the Mekong runs in a north-south direction stretching from subtropical (33º N, Tibetan Plateau) to tropical area (9º N, South China Sea) and thus is more vulnerable to the changes of different climatic systems. Ice core studies from the southern Tibetan Plateau,

where the source of Mekong River is located, revealed that the variations in the accumulation rates within the ice cores are closely correlated with sea-surface and 500-mb air temperature over the North Indian Ocean and atmospheric circulation over Asia (Kang et al., 2007). The Indochina Peninsula, through which the Lower Mekong River runs, is in the intersection of the three monsoon systems, i.e. the IM, EAM, and WNPM, making the hydrology of the Lower Mekong River very complicated.

A basin-wide precipitation analysis by Costa-Cabral et al. (2008) revealed that the southeastern Mekong River basin, where the lower four stations in this study are located, had the highest rate of annual precipitation in the whole basin during 1979-2000. The bar chart in Fig. 3a also shows that the lower four stations generally have a higher precipitation rate than the upper ones. This can explain the strong correlation between the EAM and the runoffs in this area (Fig. 9f). Although studies on the Asia-Australia monsoon system indicate that the Indochina Peninsula can also be under the control of the SCSM system (a tropical monsoon system closely linked to the WNPM, Wang et al., 2009), the runoff data show no stronger correlation with the SCSM than with the EAM.

4.4 Connections between Hydrology and ENSO

Although initially it was speculated that the previously discussed 4.8-yr periodicity of the IM and runoff data could be related to ENSO activities, the cross coherence analysis between Nino 3.4 index and IM index does not show any peak around 4- to 7-yr periodicity during the period of 1950-2005 (Fig. 11). The relationship between IM and ENSO is very

complicated and has changed through the decades (Kumar et al., 1999; Gershunov et al., 2000; Wang et al., 2001; Maraun and Kurths, 2005). In contrast with a weakening relationship between the IM and ENSO, a strengthening relationship between the EAM and ENSO has been documented by Wang et al. (2001 and 2008b). These relationships along with the strong correlation between the EAM and the runoff of the lower four stations (Fig. 9f), will augment the flow adjustment brought by the Lancang Cascade, making the Lower Mekong River more sensative to the ENSO activities. As shown in Figs. 10c to 10f, the 6.6-yr periodicity of runoffs during the post-dam period may indicate a strengthened ENSO-runoff relationship.

5. Conclusions

Precipitation rates vary considerably along the middle and lower reaches of the Mekong River. Generally the lower four stations (Nakhon Phanom to Pakse), are more influenced by the EAM and have more rainfall than the upper four stations (Chiang Sean to Nong Khai). Mann-Kendall trend analysis showed no significant change in precipitation and runoff over a 50-yr period. Correlation between runoff at Pakse and total precipitation at eight stations changed significantly after the impoundment of the Manwan Dam. The parameter rating curve showed a trend of decreased SSC and increased erosive power downstream-ward. Impoundment of the Manwan dam showed no apparent influence on the runoff-SSC relationship.

Spectral analyses showed a 4.8-yr periodicity at all eight stations, which was strongly correlated with the IM. Additionally, the lower four stations, located in the southeast part of

the Mekong River basin, were also characterized by a 3.0-yr periodicity, which explained their close relationship with the EAM. While the relationship between IM and ENSO is complicated, river runoff showed a smooth periodgram that was significantly related with the ENSO after the impoundment of dam.

In the next couples of decades, approximate 200 dams with a total capacity of ~ 25,700 MW are likely to be built in the Mekong basin. Besides the Lancang Cascade in the Upper Mekong, the 3Ss basin in the Lower Mekong will be another hot-spot for dam construction. With more and more dams are likely to be built in the Mekong basin, river runoff will have an even closer connection with local precipitation, thus become more sensitive to ENSO impacts. On the delta plain, daily maximum and minimum water level records show an abrupt drop at the end of 1994. The reduced water-level gradient between the river and sea will inevitably weaken the alongshore sediment transport dominated by the southwest-ward coastal currents and thus enhance the coastal erosion along the east coast of the delta plain.

Acknowledgements

Financial support of this study is from the National Science Foundation and the Office of Naval Research, USA. We thank Dr. Zhongyuan Chen at East China Normal University for encouraging our submission of this paper. We would also like to thank Mr. Leo Bottrill at MPO office, World Wildlife Fund (USA) for giving us the permission of the Great Mekong Subregion hydropower database. The authors also wish to express their gratitude to Ms. Yaming Shao and Dr. Wenbin Lu (Dept. of Statistics, North Carolina State University)

for their support in the statistical analysis. We thank Mr. Ke Chen, Dr. Dave DeMaster, Dr. Elana Leithold (Dept. of Marine, Earth, and Atmospheric Sciences, North Carolina State University) and Ms. Yiyi Wong for their valuable suggestions during this work. Two anonymous reviewers significantly improved the manuscript.

References

ADB, 2006. Sesan, Sre Pok, and Sekong River Basins Development Study in Kingdom of Cambodia, Lao People's Democratic Republic, and Socialist Republic of Vietnam, Asian Development Bank.

Asselman, N.E.M., 2000. Fitting and interpretation of sediment rating curves. Journal of Hydrology, 234(3-4): 228-248.

Bloomfield, P., 1976. Fourier Analysis of Time Series: An Introduction. Wiley.

Brockwell, P.J. and Davis, R.A., 1991. Time Series: Theory and Methods. Second edition. Springer.

Campbell, I.C., 2007. Perceptions, data, and river management: Lessons from the Mekong River. Water Resources Research, 43: W020407, doi:10.1029/2006WR005130.

Chen, Z., Li, J., Shen, H. and Zhanghua, W., 2001. Yangtze River of China: historical analysis of discharge variability and sediment flux. Geomorphology, 41(2-3): 77-91.

Cogels, O., 2007. Mekong hydropower development is good, Bangkok Post.

Costa-Cabral, M.C. et al., 2008. Landscape structure and use, climate, and water movement in the Mekong River basin. Hydrologcial Process, 22: 1731-1746.

Ding, Y.H. and Chan, J.C.L., 2005. The East Asian summer monsoon: an overview. Meteorology and Atmospheric Physics, 89: 117-142.

Fu, K.D., He, D.M. and Lu, X.X., 2008. Sedimentation in the Manwan reservoir in the Upper Mekong and its downstream impacts. Quaternary International, 186(1): 91-99.

Gershunov, A., Schneider, N. and Barnett, T., 2000. Low-Frequency Modulation of the ENSO-Indian Monsoon Rainfall Relationship: Signal or Noise. Journal of Climate, 14:

2486-2491.

Gupta, A. and Liew, S.C., 2007. The Mekong from satellite imagery: A quick look at a large river. Geomorphology, 85(3-4): 259-274.

Kang, S. et al., 2007. Annual Accumulation in the Mt. Nyainqentanglha Ice Core, Southern Tibetan Plateau, China: Relationships to Atmospheric Circulation over Asia. Arctic, Antarctic, and Alpine Research, 39(4): 663-670.

Kendall, M.G., 1975. Rank Correlation Methods. Charles Griffin, London.

Kite, G., 2001. Modelling the Mekong: hydrological simulation for environmental impact studies. Journal of Hydrology, 253(1-4): 1-13.

Kumar, K.K., Rajagopalan, B. and Cane, M.A., 1999. On the Weakening Relationship Between the Indian Monsoon and ENSO. Science, 284(5423): 2156-2159.

Kummu, M. and Varis, O., 2007. Sediment-related impacts due to upstream reservoir trapping, the Lower Mekong River. Geomorphology, 85(3-4): 275-293.

Le, T.V.H., Nguyen, H.N., Wolanski, E., Tran, T.C. and Haruyama, S., 2007. The combined impact on the flooding in Vietnam's Mekong River delta of local man-made structures, sea level rise, and dams upstream in the river catchment. Estuarine, Coastal and Shelf Science, 71(1-2): 110-116.

Li, Y. et al. (Editors), 2001. Da xi'nan yu Lancang Jiang-Meigong He ciquyu hezuo kaifa (The Great Southwest and Lancang-Mekong Subregional Cooperative Development). Yunnan MinZu, Kunming.

Li, J. and Zeng, Q., 2005. A new monsoon index, its interannual variability and relation with monsoon precipitation. Climatic and Environmental Research, 10(3): 351-365.

Li, S. and He, D., 2008. Water Level Response to Hydropower Development in the Upper Mekong River. AMBIO: A Journal of the Human Environment, 37(3): 170-176.

Liu, J.P. et al., 2009. Fate of sediments delivered to the sea by Asian large rivers: Long-distance transport and formation of remote alongshore clinothems. SEPM-The Sedimentary Record, 7(4): 4-9.

Lu, X.X. and Siew, R.Y., 2006. Water discharge and sediment flux changes over the past decades in the Lower Mekong River: possible impact of the Chinese dams. Hydrology and Earth System Sciences, 10: 181-195.

Lu, X.X., Wang, J.J. and Grundy-Warr, C., 2008. Are the Chinese Dams to be Blamed for the Lower Water Level in the Lower Mekong? In: M. Kummu, M. Keskinen and O. Varis (Editors), Modern Myths of the Mekong. Helsinki University of Technology-TKK, pp. 39-51.

Magee, D., 2006a. New Energy Geographies: Powershed Politics and Hydropower Decision Making in Yunnan, China, University of Washington, Seattle.

Magee, D., 2006b. Powershed Politics: Yunnan Hydropower under Great Western Development. The China Quarterly, 185: 23-41.

Magilligan, F.J. and Nislow, K.H., 2005. Changes in hydrologic regime by dams. Geomorphology, 71(1-2): 61-78.

Mann, H.B., 1945. Non-parametric test against trend. Econometrica, 13: 245-259.

Maraun, D. and Kurths, J., 2005. Epochs of phase coherence between El Nino/Sourthern Oscillation and Indian monsoon. Geophysical Research Letters, 32(L15709): doi:10.1029/2005GL023225.

Meybeck, M., Laroche, L., Durr, H.H. and Syvitski, J.P.M., 2003. Global variability of daily total suspended solids and their fluxes in rivers. Global and Planetary Change, 39(1-2): 65-93.

Milliman, J.D. and Meade, R.H., 1983. World-wide delivery of river sediment to the oceans. Journal of Geology, 91: 1-21.

Milliman, J.D. and Syvitski, J.P.M., 1992. Geomorphic/tectonic control of sediment discharge to the ocean: the importance of small mountainous rivers. Journal of Geology, 100: 525-544.

Montanari, A., 2005. Deseasonalisation of hydrological time series through the normal quantile transform. Journal of Hydrology, 313(3-4): 274-282.

Morehead, M.D., Syvitski, J.P., Hutton, E.W.H. and Peckham, S.D., 2003. Modeling the temporal variability in the flux of sediment from ungauged river basins. Global and Planetary Change, 39(1-2): 95-110.

Nguyen, Q.M., 2003. Hydrologic Impacts of China's Upper Mekong Dams on the Lower Mekong River, [Online] http://mekongriver.org/publish/qghydrochdam.htm.

Plinston, D. and He, D.M., 2000. Water resources and hydropower in the Lancang River basin., Policies and Strategies for Sustainable Development in the Lancang River Basin. Asian Development Bank, pp. 234-266.

Rayner, N.A. et al., 2003. Global analyses of sea surface temperature, sea ice, and night marine air temperature since the late nineteenth century. J. Geophys. Res., 108.

Saito, Y., 2000. Deltas in Southeast and East Asia: Their evolution and current problems. In: N. Mimura and H. Yokoki (Editors), APN/SURVAS/LOICZ Joint Conference on Coastal

Impact of Climate Change and Adaption in the Asia-Pacific Region, Kobe, Japan, pp. 185-191.

Sarma, J.N., 2005. Fluvial process and morphology of the Brahmaputra River in Assam, India. Geomorphology, 70(3-4): 226-256.

Singh, M., Singh, I.B. and Muller, G., 2007. Sediment characteristics and transportation dynamics of the Ganga River. Geomorphology, 86(1-2): 144-175.

Syvitski, J.P.M. et al., 2009. Sinking deltas due to human activities. 2(10): 681-686.

Tamura, T. et al., 2009. Initiation of the Mekong River delta at 8 ka: evidence from the sedimentary succession in the Cambodian lowland. Quaternary Science Reviews, 28(3-4): 327-344.

The Fisheries Office, R.P., 2000. A study of the Downstream Imapcts of the Yali Falls Dam in the Se San River Basin in Ratanakiri Province, Northeast Camboida.

Venables, W.N. and Ripley, B.D., 2002. Modern Applied Statistics with S. Fourth edition. Springer, 392-397 pp.

Walling, D.E., 2005. Evaluation and analysis of sediment data from the lower Mekong River, Mekong River Commission, Vientiane.

Walling, D.E., 2008. The Changing Sediment Load of the Mekong River. Royal Swedish Academy of Sciences, 37(3): 150-157.

Wang, B. and Fan, Z., 1999. Choice of South Asian summer monsoon indices. Bull. Amer. Meteor. Soc, 80: 629-638.

Wang, B., Wu, R. and Lau, K.-M., 2001. Interannual Variability of the Asian Summer Monsoon: Contrasts between the Indian and the Western North Pacific-East Asian

Monsoons. Journal of Climate, 14(20): 4073-4090.

Wang, H., Yang, Z., Saito, Y., Liu, J.P. and Sun, X., 2006. Interannual and seasonal variation of the Huanghe (Yellow River) water discharge over the past 50 years: Connections to impacts from ENSO events and dams. Global and Planetary Change, 50(3-4): 212-225.

Wang, H., Yang, Z., Wang, Y., Saito, Y. and Liu, J.P., 2008a. Reconstruction of sediment flux from the Changjiang (Yangtze River) to the sea since the 1860s. Journal of Hydrology, 349(3-4): 318-332.

Wang, B., Yang, J., Zhou, T. and Wang, B., 2008b. Interdecadal Changes in the Major Modes of Asian-Australian Monsoon Variability: Strengthening Relationship with ENSO since the Late 1970s. Journal of Climate, 21: 1771-1789.

Wang, B. et al., 2009. Multi-scale climate variability of the South China Sea monsoon: A review. Dynamics of Atmospheres and Oceans, 47(1-3): 15-37.

Wangpattana, A., 2007. Dams in the Sekong Basin: Environmental overviews fail to see Cambodia, International Rivers Report.

Wood, S.H., Ziegler, A.D. and Bundarnsin, T., 2008. Floodplain deposits, channel changes and riverbank stratigraphy of the Mekong River area at the 14th-Century city of Chiang Saen, Northern Thailand. Geomorphology, 101(3): 510-523.

Xu, K., Milliman, J.D., Yang, Z. and Xu, H., 2007. Climatic and Anthropogenic Impacts on Water and Sediment Discharges from the Yangtze River (Changjiang), 1950-2005. In: A. Gupta (Editor), Large Rivers: Geomorphology and Management. John Wiley & Sons, Ltd.

Xu, J., 2008. Response of land accretion of the Yellow River delta to global climate change and human activity. Quaternary International, 186(1): 4-11.

Xue, Z., Liu, J.P., DeMaster, D., Nguyen, V.L. and Ta, T.K.O., 2010. Late Holocene evolution of the Mekong subaqueous delta, southern Vietnam. Marine Geology, 269(1-2): 46-60.

Yang, G. et al., 2007. Sediment rating parameters and their implications: Yangtze River, China. Geomorphology, 85(3-4): 166-175.

Tables

Table 1. Precipitation and Gauge station data details

Station	Precipitation		Water Discharge		Suspended Sediment Concentration	
	Data Points	Data Range	Data Points	Data Range	Data Points	Data Range
Chiang Sean	14609	1966-2005	16802	1960-2005	810	1962,1968-1975
Luang Prabang	20819	1950-2006	16802	1960-2005	330	1962;1985-1992;1997-2002
Vien Tiane	21184	1949-2006	16802	1960-2005	24	1962 & 1968
Nong Khai	19724	1952-2005	13424	1960-2005	956	1972-1978,1981-1992,1994-2003
Nakhon Phanom	19358	1953-2005	16802	1960-2005	118	1972-1975
Mukdahan	20454	1950-2005	16802	1960-2005	1432	1962-1982,1984-2003
Khong Chiam	10592	1977-2005	14610	1966-2005	348	1966-1969;1972-1980;1982-1986
Pakse	20819	1950-2006	16802	1960-2005	137	1962;1990;1997-2002

Figures

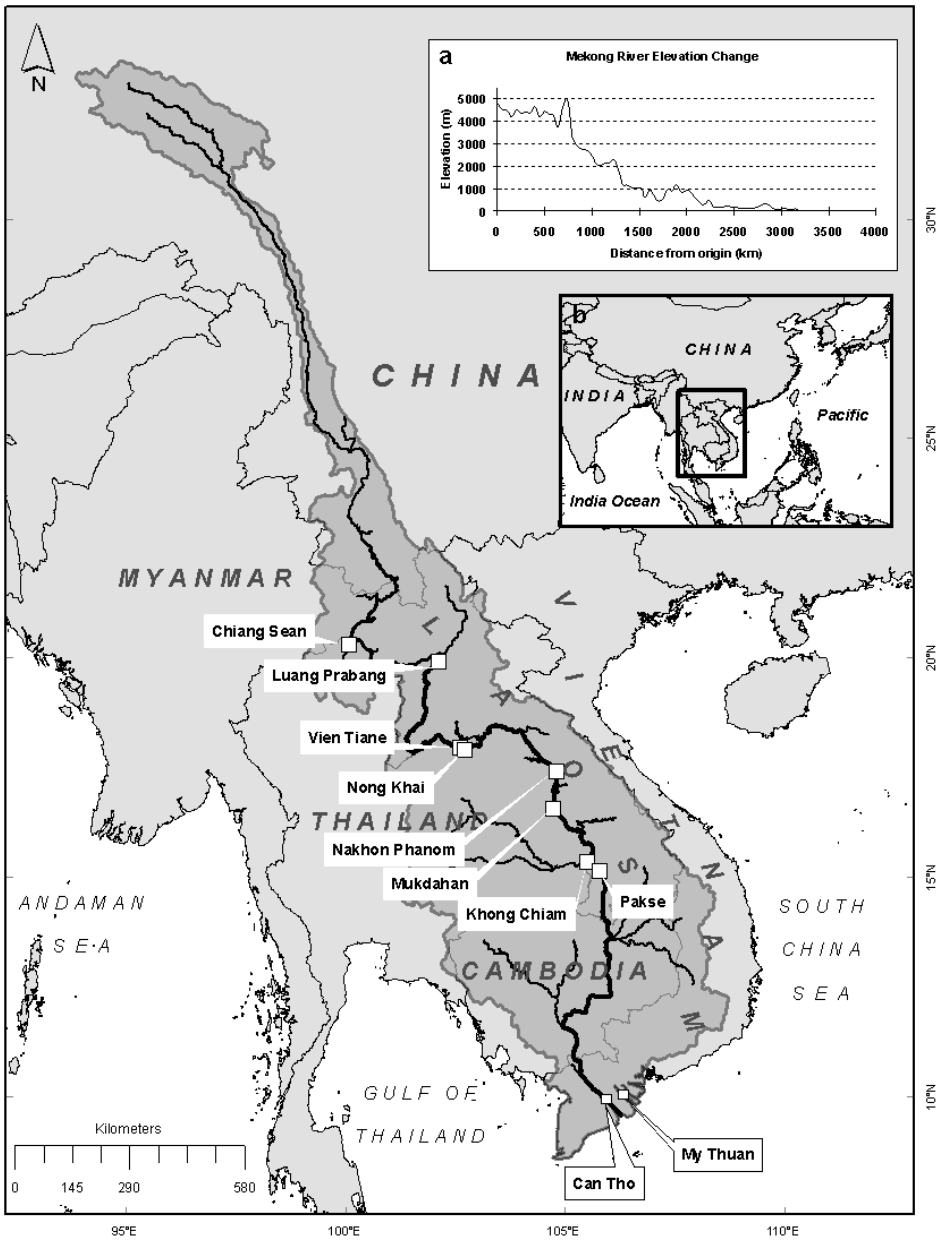

Fig. 1. The Mekong River basin and location of gauge stations. (a) elevation change of the main channel from the Tibetan Plateau to the South China Sea. (b) a location map of the study area.

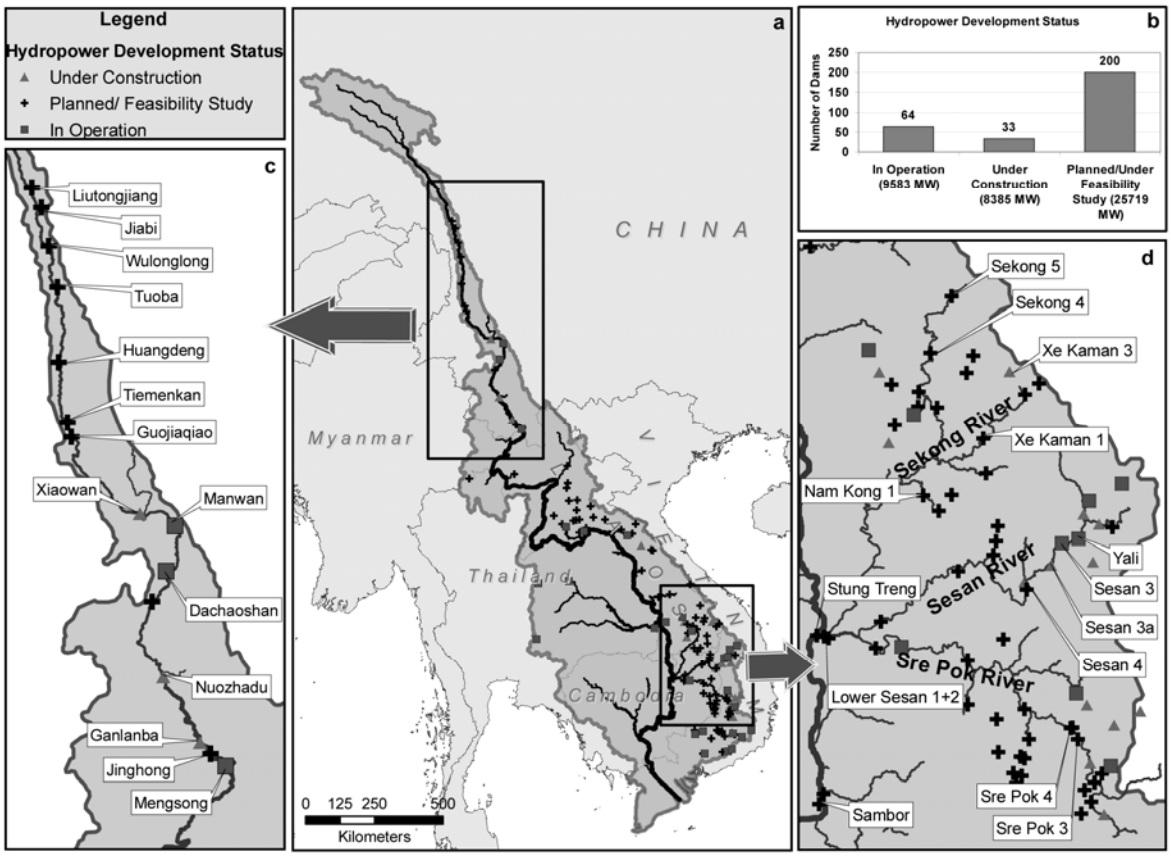

Fig. 2. Hydropower development within the Mekong River Basin. (a) Distribution of dams within the basin; (b) a bar chart of the hydropower development status; (c) Lancang Cascade; (d) the Sekong, Sesan, Sre Pok Rivers Basin area in Lower Mekong.

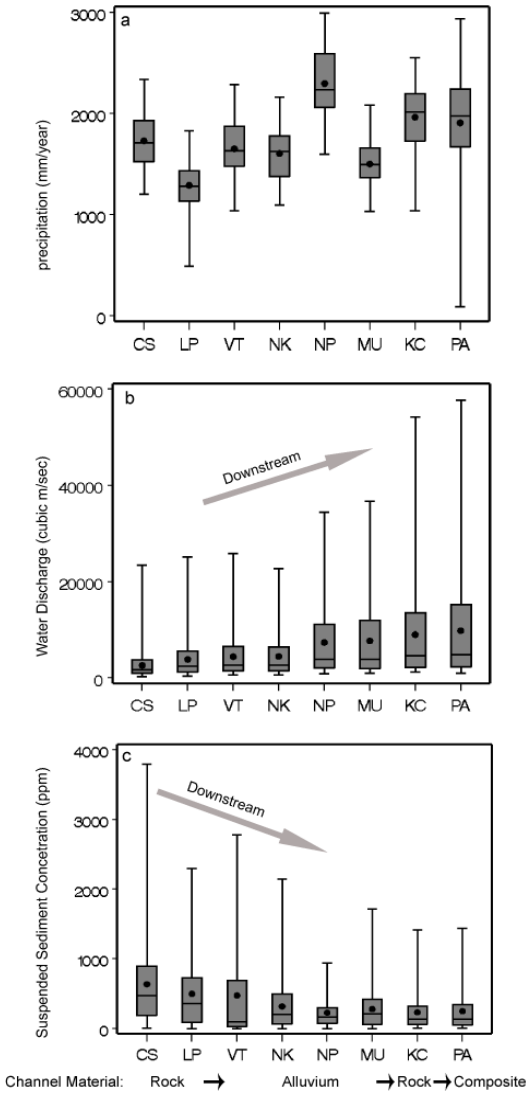

Fig. 3. Box-whisker plots of precipitation, runoff and suspended sediment concentration at the eight stations in this study. (a) precipitation, (b) runoff and (c) suspended sediment concentration. The mean (solid dot), median, 75th percentile, and maximum values show an increasing trend of water discharge while a decreasing trend of suspended sediment concentration in downstream direction. The precipitation rate varies at different station. (CS-Chiang Sean, LP- Luang Prabang, VT- Vien Tiane, NK-Nong Khai, NP-Nakhon Phanom, MU-Mukdahan, KC-Khong Chiam, and PA-Pakse. Channel material information is from Gupta and Liew, 2006).

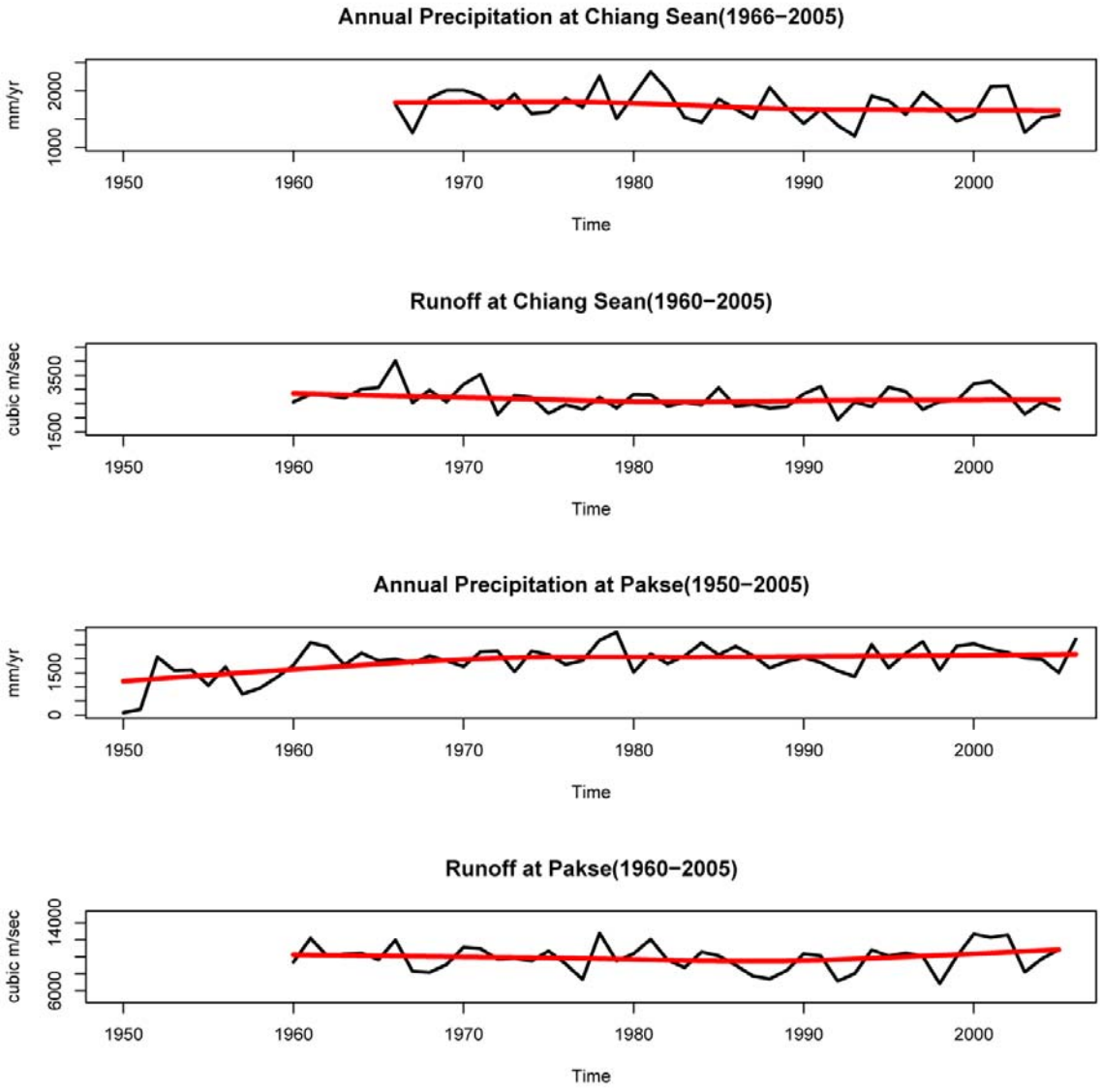

Fig. 4. Trends in precipitation and runoff at Chiang Sean and Pakse. Like Chiang Sean, the majority of the precipitation and runoff data show no significant trend by the Mann-Kendall analysis. Two exceptions are the precipitation series at Luang Prabang and Pakse stations.

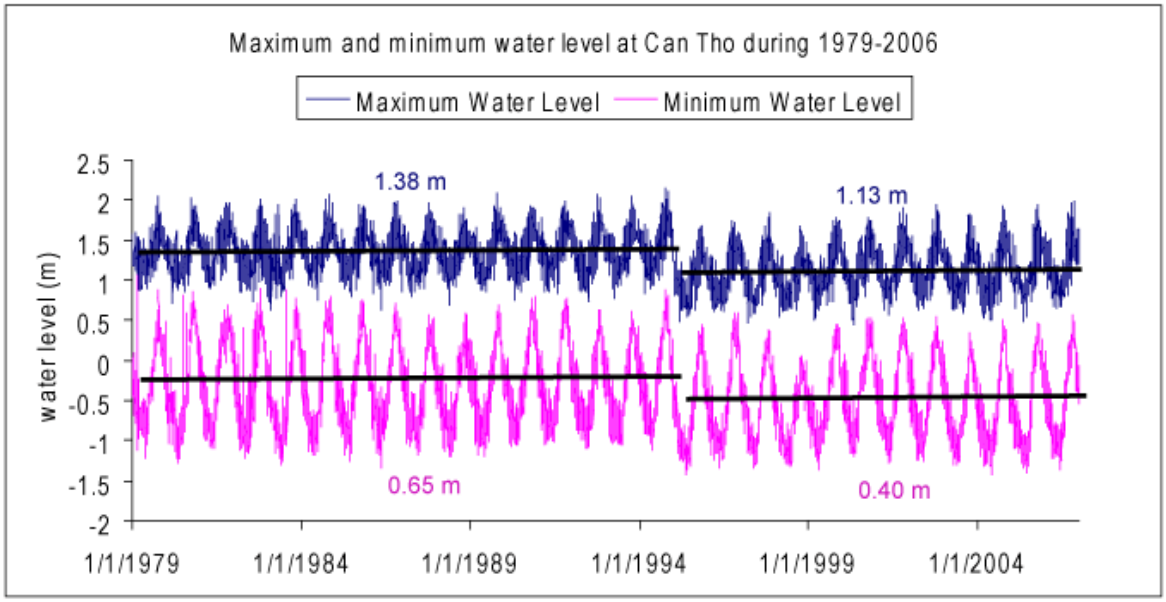

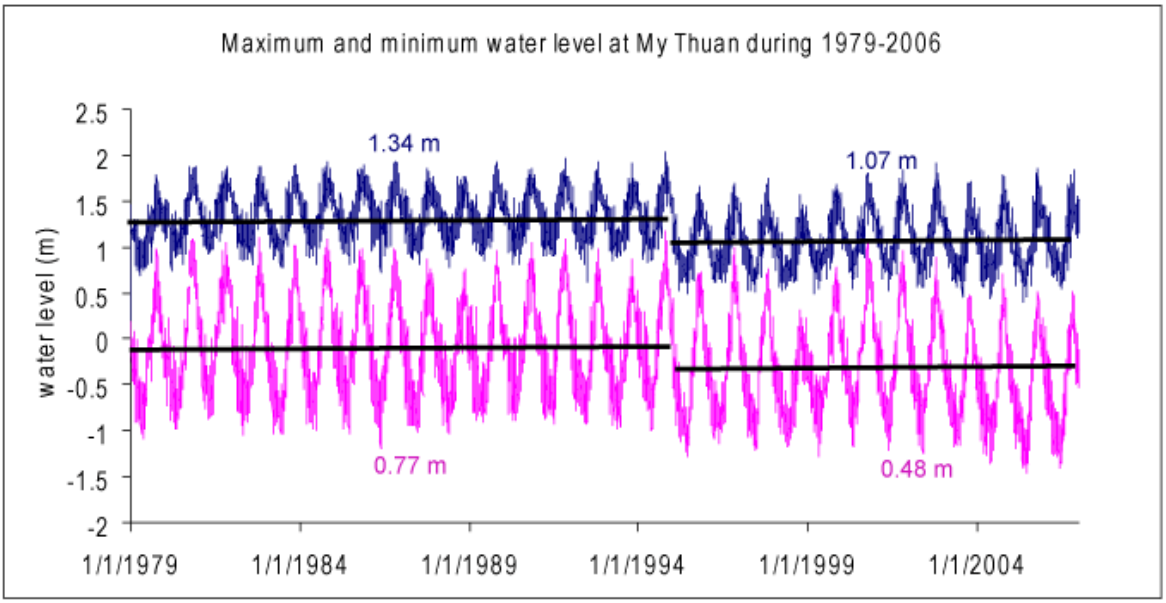

Fig. 5. The daily maximum and minimum water level at two stations on the Mekong River Delta plain. Both stations Can Tho and My Thuan show an abrupt decrease in the maximum and minimum water levels since the end of 1994.

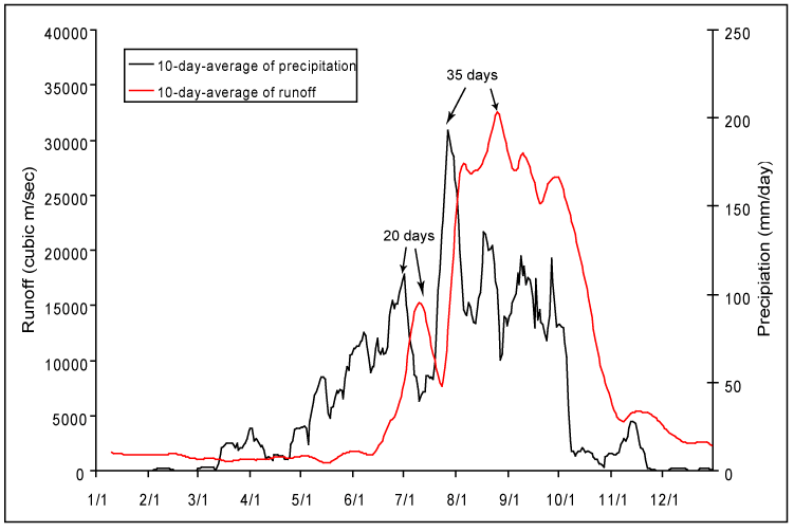

a. Time series plot of precipation (eight stations) and runoff (Pakse)

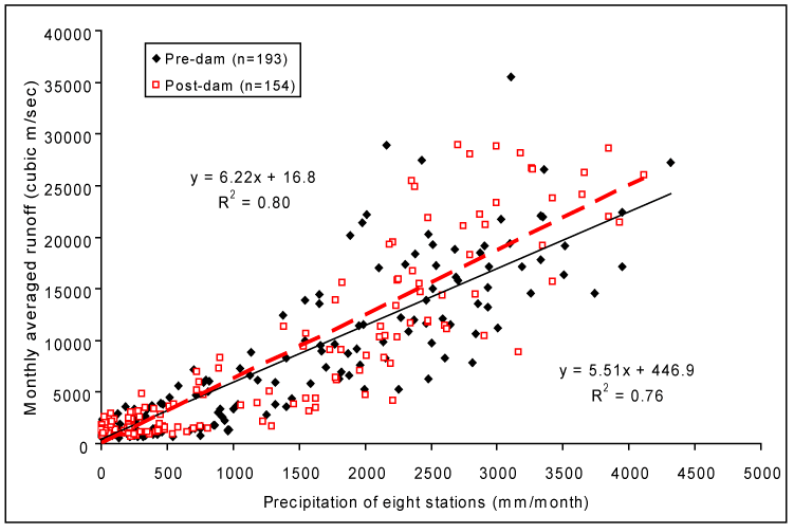

b. Correlation between precipation (eight stations) and runoff (Pakse)

Fig. 6. Correlation between the regional precipitation (annual sum of the eight stations) and the runoff at Pakse station (the last station in this study). (a) A one-year (2005) time series plot of the 10-day averaged precipitation (eight stations) and runoff (Pakse) shows a 20-to-35-day lag between the two time series. (b) Correlation between precipitation and runoff significantly changed after the impoundment of the Manwan Dam in 1993. The runoff in Lower Mekong River is more dependent on regional precipitation during the post-dam period (slope 6.22) than during the pre-dam period (slope 5.51) due to the flow adjustment from upstream dams.

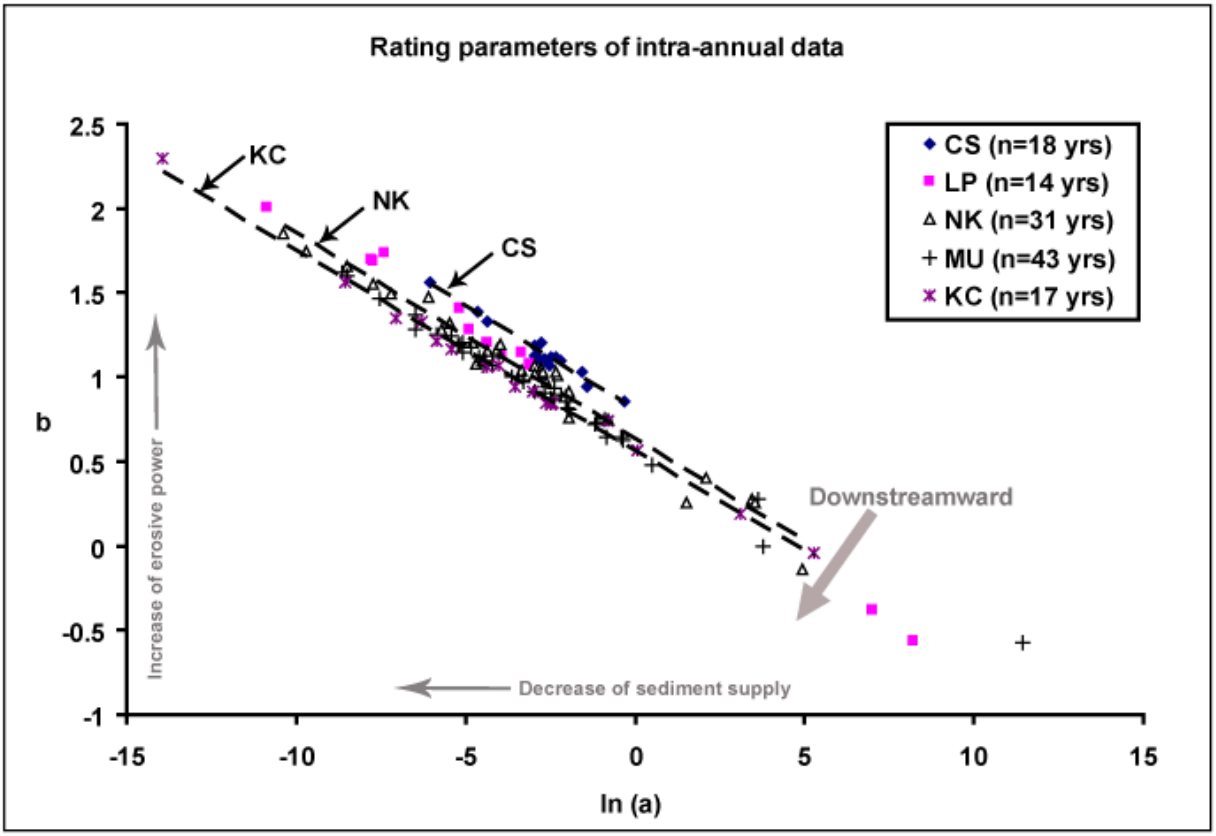

Fig. 7. Rating parameters obtained from intra-annual data at five of the eight stations. n=123, R^2=0.97. Three trend lines stands for stations CS, NK, and KC. The parameter correlation downstream shows a trend of decreasing sediment supply and increasing erosive power. Explanation of the physical meaning of *ln(a)* and *b* is from Wang et al. (2008).

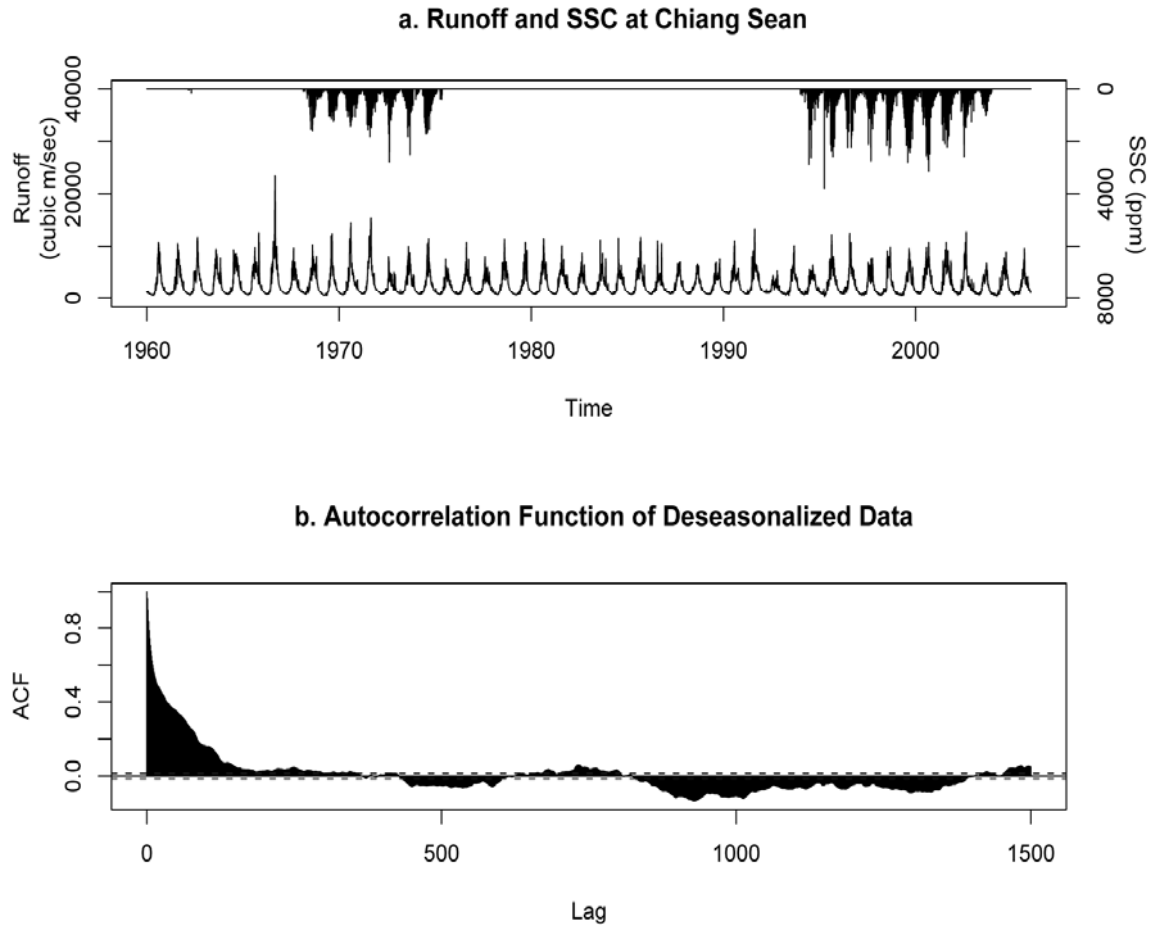

Fig. 8. Time series plot and autocorrelation function. (a) Time series plot of the runoff and SSC data at Chiang Sean and (b) Plot of the autocorrelation function of the deseasonalized daily runoff data.

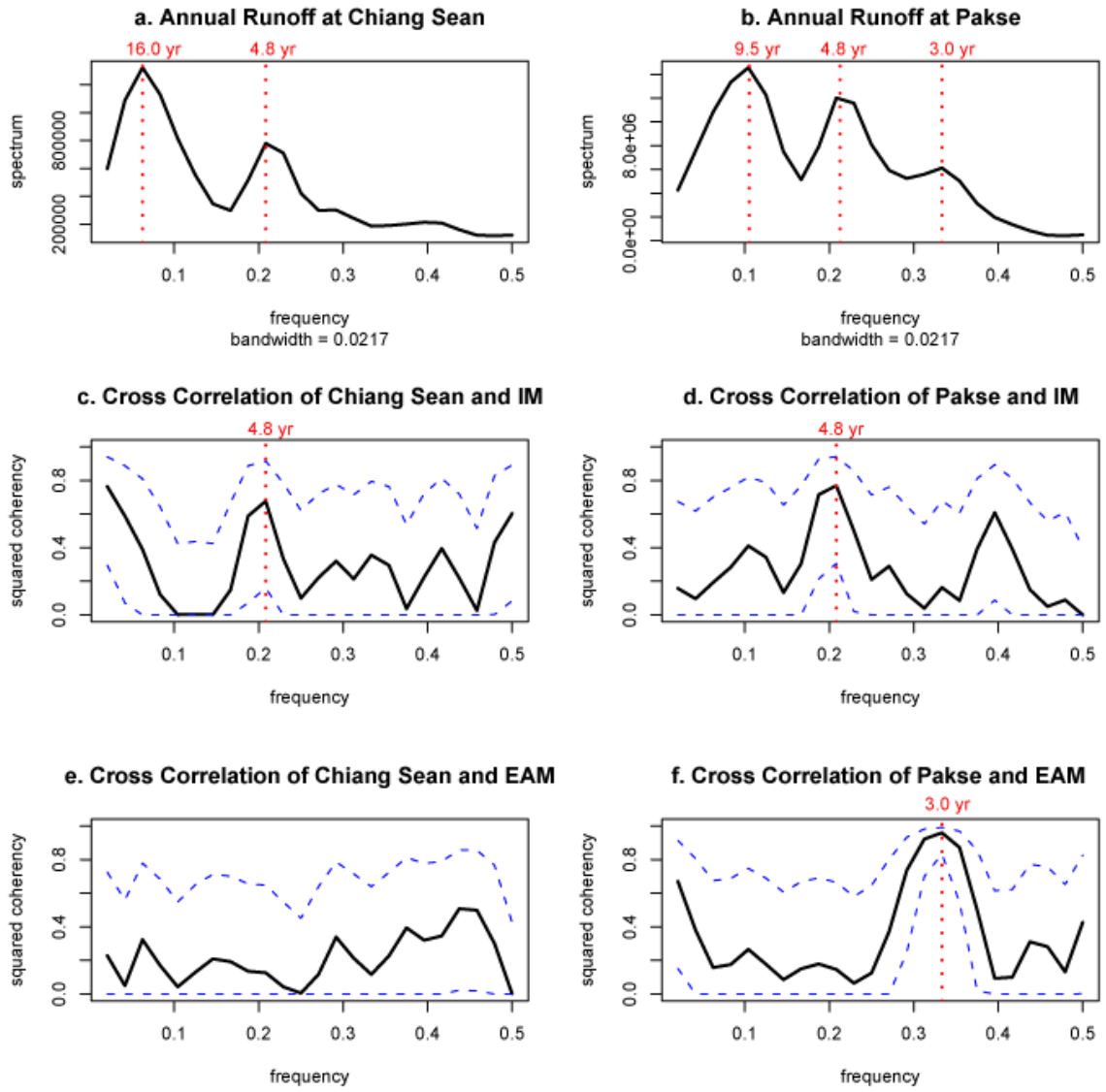

Fig. 9. Results of spectral and coherence analysis of runoff and monsoon indexes at Chiang Sean and Pakse. (a) Spectral analysis of yearly averaged runoff at Chiang Sean; (b) Spectral analysis of yearly averaged runoff at Pakse; (c) and (d) Cross correlation between runoff and Indian monsoon (IM) index at Chiang Sean and Pakse (dashed line is a 95% confidence interval, same in the following figures); (e) and (f) Cross correlation between runoff and East Asian Monsoon (EAM) index at Chiang Sean and Pakse.

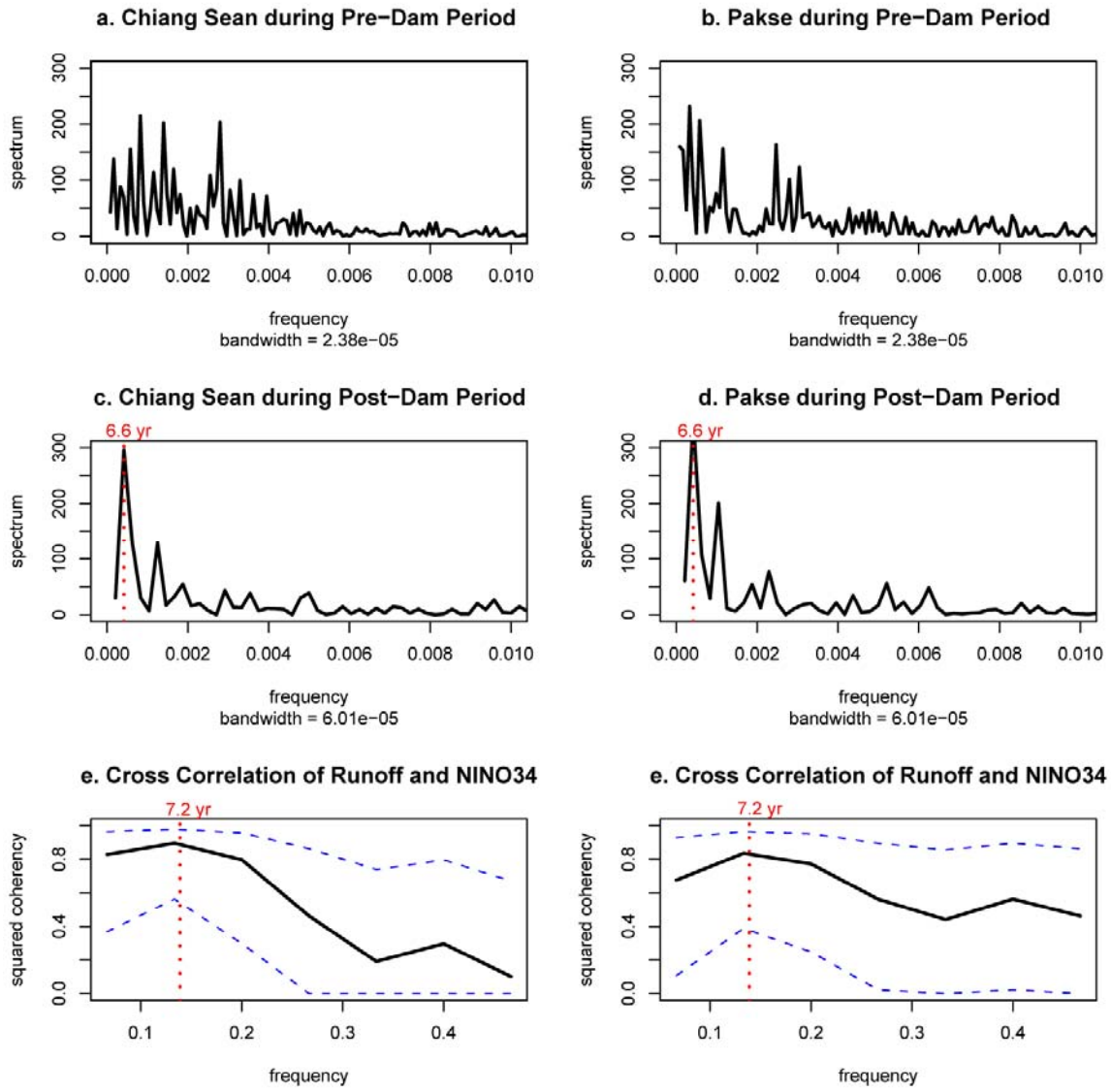

Fig. 10. Dam impact on Lower Mekong's runoff. (a) and (b) Spectral analysis of daily runoff at Chiang Sean and Pakse during pre-dam period (1960-1992); (c) and (d) Spectral analysis of daily runoff at Chiang Sean and Pakse during post-dam period (1993-2005); (e) and (f) Cross correlation between runoff and Nino 3.4 index at Chiang Sean and Pakse.

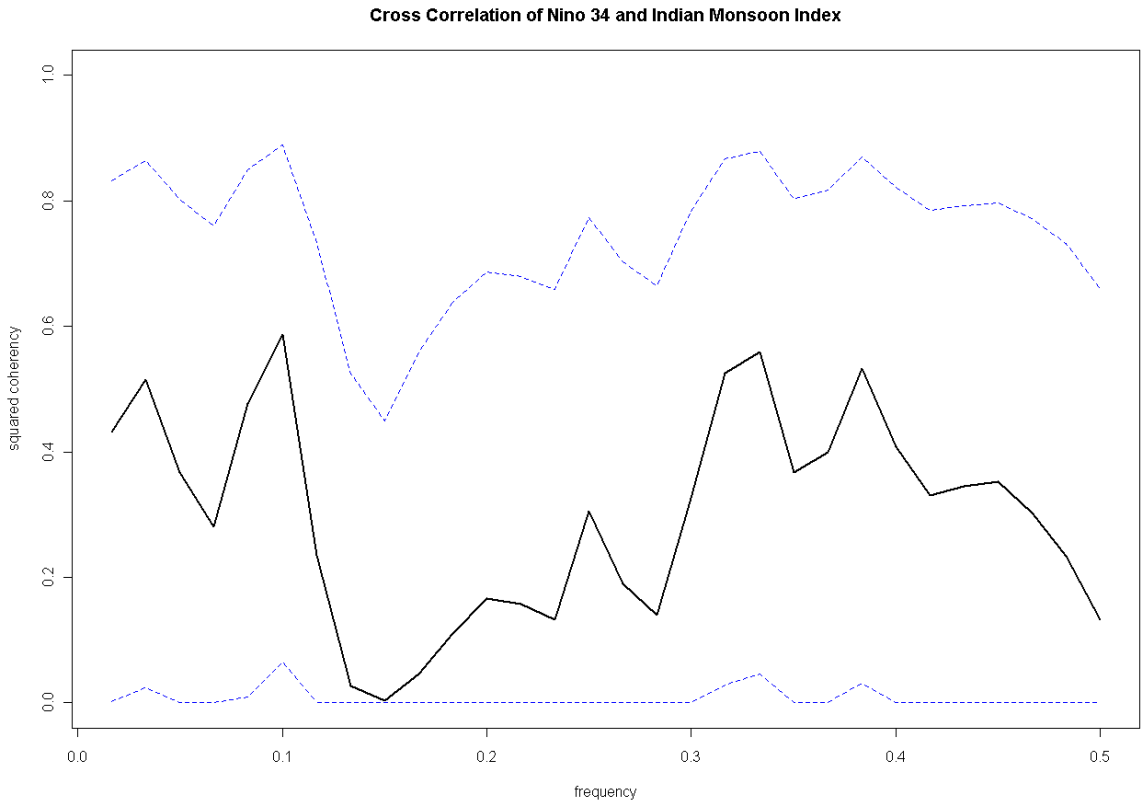

Fig. 11. Cross correlation between Nino 3.4 and Indian Monsoon indexes.

CHAPTER 3: LATE HOLOCENE EVOLUTION OF THE MEKONG SUBAQUEOUS DELTA, SOUTHERN VIETNAM[2]

Zuo Xue, J. Paul Liu, Dave DeMaster, Lap Van Nguyen, Thi Kim Oanh Ta

[2] This chapter was published in *Marine Geology*, 269(1-2)

Abstract

As Asia's third largest river, with regard to sediment load, the Mekong River delivers approximately 160 million tons of sediment per year to the South China Sea. High-resolution seismic profiling and coring during 2006 and 2007 cruises revealed a low gradient, subaqueous delta system, up to 20 m thick, surrounding the modern Mekong River Delta (MRD) in the west of the South China Sea. Based on clinoform structure, grain size, ^{210}Pb, AMS ^{14}C, and $\delta^{13}C$ results, the subaqueous delta is divided into four zones defined by different sedimentary processes and depositional features.

Over the past 3,000 yrs, the evolution of the MRD has shown a morphological asymmetry indicated by a large down-drift area and a rapid progradation around Cape Camau, ~ 200 km downstream from the river mouth. This asymmetric feature is consistent with increased wave influence. The strong southwestward coastal current, strengthened by the strong NE monsoon, plays an important role locally in longshore transport of resuspended sediments into the Gulf of Thailand.

A late Holocene sediment budget for the MRD has been determined, based on the area and thickness of deltaic sediment. Approximately 80% of Mekong delivered sediment has been trapped within the delta area, which, together with a falling sea-level, resulted in a rapidly prograding MRD over the past 3,000 yrs.

1. Introduction

Most of the world's deltaic systems began their formation between 7,400 and 9,500 cal yrs BP as a result of decelerating sea-level rise (Stanley and Warne, 1994). These deltaic systems are characterized by different stratigraphy controlled by variations in relative sea level, fluvial inputs, marine dynamics, morphology, and tectonics. Conceptual processes-based models for deltaic deposition include: 1) river-dominated/influenced, such as the Mississippi, Yellow, and Po deltas, 2) wave-dominated/influenced, such as the Nile and Danube deltas, 3) tide-dominated/influenced, such as the Amazon, Yangtze, and Fly deltas (Galloway, 1975), and 4) deltas dominated by the combination of the former three processes, such as the Mekong Delta (Ta et al., 2002a, 2002b). The evolution of a deltaic system is a non-steady process and is usually characterized by lobe switching, such as in the Mississippi (Roberts, 1997; and 1998) and Po deltas (Correggiari et al., 2005), and even changes of dominant process, such as in the Mekong delta (Ta et al., 2002a).

As part of the prograding depositional units of the deltaic systems, subaqueous deltas and clinoform structures have been documented in numerous deltaic systems including the Amazon (Nittrouer et al., 1986, 1996), Yellow (Liu et al., 2004; Liu et al., 2007a), Yangtze (Chen et al., 2000; Liu et al., 2007b), Po/Adriatic Sea (Cattaneo et al., 2003), Ganges-Brahmaputra (Kuehl et al., 1997; Goodbred and Kuehl, 1999, 2000), and Fly River/Gulf of Papua (Walsh et al., 2004; Slingerland et al., 2008). Late Quaternary sediment budgets have been established, based on the volume estimation of these subaqueous deltas and clinoform structures. Although historically the term "clinoform" has referred to the foreset part of a

deltaic system, recent usage of the term refers to the topset-foreset-bottomset morphology of deltaic systems. The term "compound-clinoform" has been proposed to describe a subaerial/subaqueous delta couplet (Nittrouer et al., 1996; Swenson et al., 2005). Determined by multiple factors such as marine hydrodynamics, fluvial sediment inputs, eustatic sea level, and subsidence, the development and character of subaqueous deltas vary among different locations. In general, energetic marine environments, such as the Amazon Shelf, Gulf of Bengal, or Gulf of Papua are ideal for subaqueous delta development, whereas low energy environments, such as the Gulf of Mexico are less suited for development of such a feature (Swenson et al., 2005).

Studies of the sedimentation processes on the continental shelf off the Mekong River Delta (MRD) are limited. Seismic and sediment core studies only have been conducted either along the continental shelf edge (Schimanski and Stattegger, 2005) or to the south around the Sunda Shelf, where the paleo-shoreline was located during the Last Glacial Maximum (LGM) (Hanebuth et al., 2000, 2002, 2003, 2004, and 2009). This paper will present the results of a seismic and sediment core field study of the MRD's coastal area between 2006 and 2007, with specific interests focused on the morphology and sedimentary processes of the subaqueous delta.

2. The Study Area

2.1 The Mekong River and Delta

The Mekong River originates in the Tibetan Plateau, runs through China, Myanmar, Thailand, Lao PDR, Cambodia, and finally enters the South China Sea in southern Vietnam (Fig. 1). The total length of the Mekong River is about 4,750 km and approximately half of it is in China's Yunnan province, locally known as the Lancang River. The Lower Mekong River region (Cambodia, Lao PDR, Thailand and Vietnam) has a population of 60 million, the majority of which depend on the aquatic resources provided by the river basin. The Mekong River watershed has an area of 832,000 km^2 (HYDROSHEDS v2.01, World Wildlife Fund, US). Annual water discharge of the Mekong River is ~ 470×10^9 m^3 and the estimated annual sediment flux is ~160 million tons (Milliman and Syvitski, 1992). Compared with other large rivers, the Mekong River has a smaller drainage area than the Yangtze, Mississippi, or Ganges-Brahmaputra Rivers, but its sediment yield is about twice that of the Mississippi and nearly equal to that of the Yangtze. The estuarine area of Mekong River exhibits a funnel-like shape and is dominated by large tides with a maximum range of 3.2 m and average tide of 2.2 m (Wolanski et al., 1996).

The MRD is a wide, low-lying delta with an area of 49,500 km^2 (Le et al., 2007). The delta plain is the third largest in the world (Coleman and Roberts, 1989), 50% greater than the Yangtze delta, and is only exceeded by the Amazon and the Ganges-Brahmaputra deltas. With fast economic development in the Lower Mekong region, infrastructure (mainly dams and reservoirs upstream and artificial dykes in the delta plain), deforestation, and shrimp

farms are dramatically changing the Mekong River's water and sediment discharge from source to sink.

There have been 47 typhoons that have hit southern Vietnam between 1954 and 1991. The highest monthly frequency of typhoons is documented in the flood season (Imamura and To, 1997). The most destructive typhoon in recent years was Typhoon Linda in November 1997, which introduced strong erosion along the eastern coast of the Mekong Delta. Modeled results show that the combination of the flood and Typhoon Linda can introduce up to 0.6-0.8 m of inundation along the MRD estuaries as far as 70 km inland (Le et al., 2007).

2.2 Southeast Asian Monsoon

Controlled by the Southeast Asian monsoon, both the hydrological regime and estuarine/nearshore hydrodynamic systems of the Mekong River exhibit two contrasting scenarios annually. The first scenario occurs when the southwest monsoon brings more than 80% of the annual precipitation during the rainy season, which is usually between May and October (Debenay and Luan, 2006). Water discharge at Phnom Penh, Cambodia, reaches a maximum in October and a minimum in May (Gagliano and McIntire, 1968; Milliman and Meade, 1983; Wolanski et al., 1998). The majority of suspended sediment is exported to coastal waters (Wolanski et al., 1996). The second scenario occurs during the dry season when both precipitation and water discharge are limited. Tidal asymmetry, together with limited fresh water supply, generates a salt water intrusion that can reach 50 km upstream, pumping the sediment upstream (Wolanski et al., 1998).

The hydrodynamics of the southern Vietnam shelf are strongly influenced by the Southeast Asian monsoon (Hu et al., 2000). Modeled results in the Mekong River mouth reveal that currents can reach 0.55 m/s with directions shifting between NE in winter and SW in summer (Kubicki, 2008). For the nearshore area of the MRD, a general consensus is that waves and currents generated by the strong NE monsoon during the dry season dominates the net alongshore sediment transport (Gagliano and McIntire, 1968; Nguyen et al., 2000). Previously deposited Mekong River sediments are resuspended from the seabed, with fine particles transported and deposited several hundreds kilometers away to the southwest coast of the Camau Peninsula (Nguyen et al., 2000).

2.3 Delta Plain Development

Sea-level research on the Sunda Shelf reveals that sea-level was about -120 m around 19,000 to 20,000 cal yrs BP (Hanebuth et al, 2009). For the MRD, a sea-level curve for the last 15,000 cal yrs was developed, based on inland boreholes (Ta et al., 2002a). Both the sea-level curve of the Sunda Shelf and that of the MRD show a rapid sea-level rise since the last glacial episode. After reaching its maximum height around 5,500 cal yrs BP, sea-level has been slightly falling until recently.

Sedimentological and stratigraphic analyses of boreholes on the lower delta plain indicate that postglacial sea-level rise and transgression have caused the infilling of an incised paleo-valley (Ta et al., 2005). The upcore sequence in deposits ranges from marsh and estuarine sediments to open-bay deposits to pro-delta and delta-front sediments, capped

by subtidal and intertidal deposits and beach ridges (Ta et al., 2005). ^{14}C measurements indicate that the initial development of the MRD was around 8,000 cal yrs BP after the mid-Holocene sea-level highstand (Tamura et al., 2009). Since then, the subaerial part of the MRD has continuously prograded more than 250 km from Cambodia border toward the South China Sea (Nguyen et al., 2000). Over the past 3,000 cal yrs, the modern delta plain and the sediment below (including paleo-subaqueous deltaic deposits) have accumulated about 360×10^9 m^3 of sediment, which is equal to 144 million tons of sediment per year (Ta et al., 2002a). At the same time, sequence stratigraphic analyses indicate that the last 3,000 cal yrs were characterized by delta progradation changing from tidal influenced to increasingly wave influenced southward sediment dispersal. During this period the rate of delta progradation decreased, and the facies of the delta front steepened (Ta et al., 2002a).

3. Data and Methods

Two research cruises were conducted in April 2006 and March 2007 by the Sea-level Change and Ocean Margin Evolution Laboratory at North Carolina State University (NCSU). The research is a joint study with the Institute of Geography, Vietnam National Center for Natural Science and Technology. Approximately 1,150 km of high-resolution seismic profiles were obtained using an EdgeTech 0512i Chirp Sonar Sub-bottom Profiler (frequency range: 0.5–12 k) together with a number of gravity cores (for seismic tracklines and core positions see Fig. 1; for details of gravity cores in this study see Table 1).

In the laboratory at NCSU, seismic and navigation data were processed using

EdgeTech Discover Sub-bottom software (Version 3.27). Grain size analysis (4-5 samples per core with 10 cm intervals) was done using a LS 13 320 Laser Diffraction Particle Size Analyzer (Beckman Coulter©, size range 0.04 μm ~ 2000 μm, Table 1). ^{210}Pb activities were determined following a procedure similar to that of DeMaster et al. (1994). Calculated ^{210}Pb activities were normalized to the sample's mud contents (grain size less than 63 μm).

The majority of the sediment cores recovered in this study consisted of brown-colored mud with few foraminifera. Foram shell samples were only found in cores located on the northwest shore of the Camau Peninsula. Because no continuous distribution of a particular species occurred down core with sufficient abundance, ^{14}C chronologies and organic carbon (C_{org}) stable isotope ratios ($\delta^{13}C$) were established on the C_{org} content of the bulk-sediment. The C_{org} samples were prepared following a method similar to that of Leithold et al. (2006). CO_2 produced from the combustion of the organic matter was analyzed for carbon isotopic ratios using a Delta V IRMS with a standard dual inlet. CO_2 from the C/N elemental analyzer (FLASH 1112 Series) was collected cryogenically and sent to the WHOI National Ocean Sciences AMS facility, where it was converted to graphite and analyzed for its ^{14}C content using accelerator mass spectrometry.

4. Results

High resolution seismic records (Fig.s 3, 4, 6, 7, and 8) revealed the stratigraphic structure of a subaqueous delta system (<30 m water depth), surrounding the modern MRD. Generally, seismic profiles showed a prominent subsurface reflector, overlain by a thick

clinoform that thinned offshore. Relatively high-gradient foreset strata occurred seaward of the Mekong River mouth and near Cape Camau. The boundary of the subaqueous delta front is shown in Fig. 2. Based on differences in the nature of the clinoform and associated sediment, this subaqueous delta was divided into four zones as described below (Table 3).

Between 1997 and 2000, a number of borehole cores were successively retrieved on the MRD plain. A schematic delta evolution model was developed covering sedimentation facies since the last sea-level low stand (Nguyen et al., 2000, 2005; Ta et al., 2001a, 2001b, 2002a, 2002b, 2005)(see core positions in Fig. 2). We refer to these boreholes to correlate the facies architecture within the subaqueous delta.

Six cores were analyzed for their ^{210}Pb activity. Supported levels were determined by averaging the total ^{210}Pb activities from the bottom of selected cores (primarily MKII14 and MKII07; the latter core had a raw ^{14}C age of 3,120 yrs in its deepest samples). Based on the counting statistics, the error in total ^{210}Pb activities is 3%-5%. This error range is negligible to that of the support level, which is 0.3 dpm/g mud as a most realistic assumption. A supported level of 1.44±0.3 dpm/g mud was used for cores located on the east shore (cores MKI01, MKI02, and MKII14) and 1.09±0.3 dpm/g mud for cores located on the west shore (cores MKII03, MKII07, and MKII09) to calculate excess ^{210}Pb activities in the seabed.

The ^{14}C data reported in this study for the Mekong shelf are given as "raw" ^{14}C ages, i.e., they have been normalized to a common δ^{13}C value, but not corrected for a reservoir age or atmospheric ^{14}C/^{12}C variations. These relative ages (reported in ^{14}C yrs) were used to assess the nature of sedimentation at a given coring site and were not used for age correlation with the ^{14}C data from the boreholes (which were reported in units of ^{14}C yrs BP).

4.1 Zone I. Mekong River mouth

Zone I is located seaward of the Mekong River mouth (Fig. 2). Water depth increases sharply seaward of the river mouth. Portions of two seismic profiles recovered from this area, i.e. Line 2006-1 (cross shore) and Line 2006-3 (parallel to shoreline), are shown in Fig.s 3 and 4.

Line 2006-1 (Fig. 3) shows a high-gradient foreset bed compared to the rest of the clinoform structures in the east shore and west shore of the Camau Peninsula. It has a smooth outline and the gradient of the foreset strata is approximately 2.5:1000. The delta front has a very limited bottomset bed and a foreset bed up to 15 m thick, which consists of a succession of sub-parallel strata. The foreset strata are correlated to the delta front facies in Cores BT2 and BT3, which was described as a 7 to 10 m intercalated greenish gray silt, sandy silt, and fine sand layer (see cross section BT2-BT3 in Fig.s 3a and 3c). Underlying the foreset strata is a ~ 5 m thick transparent layer that can be correlated to the pro-delta/shelf mud facies of Core BT2. The strata end at ~ 20 m depth with an uneven strong reflection, which reflects the sharply increased sand content documented in Core BT3 at the same depth. Although this sand layer in BT3 was initially regarded as a transgressive sand layer, its ^{14}C age is between 4,000 and 4,200 cal yr BP, indicating that it was formed by a regressive erosion episode instead of a transgressive one (Ta et al., 2002a).

Line 2006-3 (parallel to shoreline) reveals an incised valley fill (Fig. 4b). This seismic track is located ~ 20 km seaward of the modern river mouth (~ 20 m water depth). Its facies can be well correlated to the lower part of Core BT2 (Fig. 4a), which shows an incised valley

fill sequence recovered on the MRD plain (Ta et al., 2002a, 2005). On the top of the profile there is ~ 2 m thick weak lamination. Underneath, there is a 12-20 m thick weak reflection with a "ω" shape bottom deeply cutting into the underlying sediments. This weak reflection is correlated to the bay facies, which consists of homogenous greenish-grey mud with little grain size variation (Ta et al., 2002a). The deep cut was probably formed by a landward migrating tidal inlet during high sea-level stand, similar to the one documented outside the Gironde Estuary in France (Allen and Posamentier, 1993).

Beneath the homogeneous weak reflection unit there is a 15-25 m thick layer of subparallel strata, coinciding with the estuarine facies in Core BT2 between 37 and 55 m depth. This estuarine facies is characterized by intercalated yellowish-grey coarse sand and greenish-grey silty sand (Ta et al., 2001a). Further down, the seismic profile shows discontinuous strata, which is correlated to the marsh facies in BT2 dated at 13,258 ± 115 cal yr BP. The incised valley fill sequence is terminated by an uneven strong reflector at a depth of 60 m.

A shallow gravity core, MKI01 (position see Fig. 1), was recovered seaward of the Bassac River mouth (~ 4.5 m water depth). There is an excess ^{210}Pb-riched layer in the top 10 cm, which could be an ephemeral deposit or a seasonal surface layer (Fig. 5a). A clear drop in excess ^{210}Pb activity was observed at 11 cm depth. Another core, MKI02, located 40 km southwest along the coast, also showed a similar drop in excess ^{210}Pb activity at a similar depth (Fig. 5b). These sharp drops of ^{210}Pb activity may be caused by event sedimentation such as flooding. Because of their short length (< 40 cm), cores in this area were not analyzed for ^{14}C or δ^{13}C activity.

4.2 Zone II. East shore of the Camau Peninsula

Zone II is along the east shore of the Camau Peninsula (Fig. 2), where the coastline has been under serious erosion at a rate of 1.1 km^2/yr since 1885 (Saito, 2000). Clinoforms in this area are characterized by low-gradient foreset strata.

Fig. 6 shows parts of two cross-shore seismic profiles, i.e. Line 2006-7 (Fig. 6b) and Line 2007-11 (Fig. 6d). Both have a low-gradient foreset (< 5:1000). Line 2006-7 has up to 20 m thick foreset beds with sub-parallel strata, which are correlated to the delta front facies in Core VC1, 10 km northwest, at a depth between 5 m and 11 m. Underlying the foreset beds is an ~ 8 m thick transparent layer. An uneven surface with strong reflectivity was observed at a depth of ~ 25 m. Line 2007-11 has up to 8 m thick foreset beds directly overlying a strong reflector at ~20 m depth. There is a remarkable concave feature in the middle of the topset (Fig. 6d), which may be the result of coastal erosion as described above.

Core MKII14 (14.5 m water depth) was retrieved from the seaward limit of the clinoform shown on Line 2007-11 (Fig. 6d). The sediments are made up of a mixture of clay, silt, and sand dominated by silt (48.26 %, Table 1). Grain size shows little variation throughout the 50-cm-long core. MKII14 shows minimal excess ^{210}Pb activity (Fig. 5c). The excess ^{210}Pb activity profile suggests that the sediments may have deposited at a high accumulation rate. The radiocarbon data give "raw" ^{14}C ages on the order of 1,310 – 1,870 yrs (Table 2, Fig. 5c). δ^{13}C values of these samples vary between -23.2 and -23.6‰. These δ^{13}C data suggest a mixed terrestrial/marine source for the bulk C_{org}. The thousand year old bulk C_{org} ^{14}C ages are consistent with the preponderance of the organic matter coming from

the accumulation of old terrestrial soil organic matter from land.

4.3 Zone III. Cape Camau

In Zone III the strata exhibited a series of high-gradient foreset layers between 11 m and 25 m water depth. From the tip of Cape Camau to the northwest, reflectivity of the clinoforms is much weaker than in Zones I and II. Sediments varied from a mixed sand-silt-clay to a clayey silt (Table 1).

Line 2007-15 (Fig. 7a) showed relative steep foreset strata (~ 5:1000). The topset, overlying intensive gas-charged sediment, was flat and continuous to the shore. A strong reflector was located at ~ 30 m depth. Compared with Line 2007-15, the foreset strata shown by Line 2007-6 were weak in reflectivity and low in gradient (~1:1000, Fig. 7d). Both profiles show gas-charged sediment underling the topset.

Core MKII09 (10.0 m water depth) was located on the foreset of the clinoform on Line 2007-6 (Fig. 7d). This 100-cm-long gravity core primarily was composed of fluid mud. Grain size shows little variation throughout the core. All three bulk sediment samples from the top (2 cm), middle (40 cm), bottom (100 cm) have a ^{14}C age around 850 yr (Table 2, Fig. 5d). The $\delta^{13}C$ measurements indicate that the C_{org} at this site is a mixture of terrestrial/marine origin (-24.1 to -24. 4‰, Table 2). The ^{210}Pb activity profile from Core MKII09 shows no minimal excess activity throughout the core. The reason for the lower bulk organic matter ^{14}C ages in core MKII09 in Zone III (ages ~850 yr) relative to the core MKII14 in Zone II (ages 1310 – 1870 yr) is not known because the stable carbon isotopic data at core MKII09

indicated a more terrestrial (or old) C_{org} source ($\delta^{13}C$ ~ -24.2‰) compared to MKII14 ($\delta^{13}C$ ~ -23.2 to -23.6‰).

4.4 Zone IV. West shore of the Camau Peninsula

As part of the Gulf of Thailand, the west shore of the Camau Peninsula is dominated by an irregular diurnal tide with a range of 0.8-1.0 m (Le et al., 2007). This part of the peninsula experienced rapid progradation at a rate of 1.2 km^2/ yr between 1885 and 1985 (Saito, 2000). The lower part of the Camau Peninsula (roughly from Core CM1 to the south, Fig. 2) was not formed until 3,000 cal yrs BP (Nguyen et al., 2000). Here we refer to Borehole CM1 (Nguyen et al., 2005) for facies correlation.

Clinoforms in this zone generally have low gradients and low reflectivity. Two cross shore profiles, Line 2007-1 and Line 2007-5, are shown in Fig. 8. The clinoform in Line 2007-5 exhibited a very gentle foreset with a gradient of 0.6:1000. The majority of the foreset strata are transparent with weak laminae (Fig. 8a). Only a very limited delta front with strong reflectivity developed and ended at 10m water depth, leaving the majority of the shelf/pre-delta facies uncovered. A strong reflection was observed at ~ 20 m depth. The subaqueous delta front ended between the east end of Line 2007-2 and Line 2007-1. No distinct deltaic facies was observed on Line 2007-1, which exhibited a homogenous light reflector overlying on an uneven paleo-surface with strong reflectivity (Fig. 8d).

Core MKII07 (10 m water depth) was collected from the seaward limit of the delta front (on Line 2007-5, see Fig. 8a). It mainly consists of clayey silt with little vertical

variation. An oyster shell sample was observed at 12 cm depth. Calculated accumulation rate for the upper 30 cm of this core is ~ 0.57 cm/yr (Fig. 5e). ^{14}C measurements of the C_{org} from the top (1 cm), upper middle (15 cm), lower middle (31 cm), and bottom (47 cm) yield ages of 800±25, 1300±25, 2930±30, and 3120±35 yrs (Table 2). $\delta^{13}C$ values of these four samples indicate that the C_{org} is from a mixed terrestrial/marine source (-23.26 ~ -24.16 ‰, comparable with that of Cores MKII09 and MKII14). If the ^{14}C age of the organic matter at the surface seabed has remained constant over time, the radiocarbon data suggest an accumulation rate as low as 0.02 cm/yr for this core.

Although the majority of the cores collected in this study are made up of brown-colored muddy sediments with high porosity, core MKII03 along Line 2007-1 (6 m water depth, position see Fig. 8c) were made up of greenish silt. ^{210}Pb profiles of cores MKII03, located on the weak reflector on Line 2007-1 (Fig. 8d), are shown in Fig. 5f. Excess ^{210}Pb activity in the top 30 cm of MKII03 shows excess activities in the upper 5 cm, overlying a zone of uniform activity with minimal excess activity, depending on the supported ^{210}Pb activity chosen. Below the zone of uniform activity the total ^{210}Pb activity decreases, but this may be due to a change in sediment type (e.g., grain size, or organic matter content). Calculated accumulation rate below the zone of uniform activity is ~ 0.49 cm/yr (Fig. 5f).

Shell samples were found at 12 cm, 45 cm and 49 cm depth in this core. $\delta^{13}C$ values of three samples from the top (1 cm), middle (31 cm) and bottom (54 cm) of this core vary between ~ -20.65 and ~ -21.23 ‰, indicating a greater contribution of marine plankton to the bulk organic matter content of this core as compared to the other cores examined in this study. Bulk C_{org} ^{14}C measurements from the surface (1 cm), middle (31 cm), and bottom (54 cm) of

this core yielded ages of 50±25, 495±30, and 1570±30 yrs, respectively. The younger ^{14}C ages are consistent with the greater relative abundance of marine planktonic organic matter at this site (as indicated by the $\delta^{13}C$ data). If the ^{14}C age of the bulk organic matter at the sediment-water interface is assumed to remain constant over time, the radiocarbon data indicate an accumulation rate of ~ 0.03 cm/yr.

5. Discussion

5.1 Asymmetric delta evolution

Because of the large amount of fluvial sediment input and a decreasing sea-level, the MRD has prograded 250 km from the Cambodia border to the South China Sea in the last 6,000 yrs (Nguyen et al., 2000). However, the progradation process is not constant throughout the late Holocene. After the delta body refilled the former bight, the delta edge began to be exposed to longshore currents. A phase shift from "tidal dominated" to "wave and tidal dominated" around 3,000 cal yrs BP has been reported, based on facies changes in inland boreholes (Ta et al., 2002a). In contrast, to the "tidal dominated" regime, a "wave and tidal dominated" MRD is characterized by a large subaerial delta plain, longshore sediment dispersal, and steep delta-front topography in the proximal delta (Ta et al., 2005). Although the subaqueous delta front has had a high progradation rate over the past 3,000 yrs, on a smaller time scale its development is a non-linear process with cycles of deposition and erosion. In Zone II where both tide and wave energy is strong, the MRD is suffering serious

erosion (Saito, 2000). The seismic profile also shows scour/erosion of the clinoform structure (see Line 2007-11 in Fig. 6d).

An 'asymmetric delta model' was first proposed by Bhattacharya and Giosan (2003) to describe the morphological and facies difference between the updrift and downdrift of a wave-influenced deltaic system. For the first time, high resolution seismic profiles reveal a subaqueous delta surrounding the MRD with a morphological asymmetry. The fastest delta progradation rate (~ 26 m/yr, Fig. 2) is found around Cape Camau, ~ 200 km downstream from the river mouth. This, together with the huge downdrift area of the MRD indicates the importance of longshore sediment transport in MRD's evolution over the past 3,000 yrs.

5.2 Longshore sediment transport

The Lower Mekong region is controlled by the Southeast Asian Monsoon and shows two contrasting scenarios annually. During the wet season (May to November), large amounts of sediment are transported toward the river mouth and temporarily deposited there. During the following dry season (December to April), a large part of previously deposited sediment will be resuspended from the seabed by the tidal currents and surface waves. The resuspended sediments are then either pumped upstream (Wolanski et al., 1998), or transported southwestward by coastal current strengthened by strong NE monsoon (Gagliano and McIntire, 1968; Nguyen et al., 2000). Changes in tidal amplitude and location of the salinity front contribute to the formation of the inter-layered sands and muds (Kineke et al., 1996). These processes may explain the limited subaqueous delta front seaward of the river

month with a succession of sub-parallel strata (Zone I). A similar remobilization of temporary deposits during the energetic periods has also been reported on the Amazon shelf (Allison et al., 1995).

A calculation by Geyer et al. (2004) indicates that a surface river plume can only transport flocculated sediments for 5 km while a bottom resuspension can maintain sediment in the water at large distances from the river mouth. Both surface wave and tidal currents contribute to the resuspension of previously deposited Mekong sediments, which are then transported southwestward by coastal currents along the eastern shore of the Camau Peninsula (Zone II).

Cape Camau is located at the intersection of two different tidal systems: to the east, a regular semidiurnal tide with 3.5 m tidal range for the South China Sea, and to the west, an irregular diurnal micro-tide with 0.8-1.0 m tidal range for the Gulf of Thailand. Due to reduced tidal energy, a large amount of longshore transported sediment settles out and accumulates, forming a series of high-gradient clinoforms with high-gradient foresets (Zone III, Fig. 7). Only fine sediment can pass the tip of the cape and reach the western shore of the peninsula, which, combined with the micro-tide from the Gulf of Thailand, explains the low-gradient clinoform structures in Zone IV (low reflectivity and blurred laminae, Fig. 8a).

The organic matter in the sediments of the Mekong continental shelf has two potential sources, which are in situ primary productivity and terrestrial organic matter from fluvial sediments. A significant part of the later source may be from ‘old’ terrestrial soils. For the Mekong subaqueous delta, the average fluvial sediment input may be as high as 160 million tons per year, making the source of the C_{org} in the coastal area inevitably a mixed one. ^{14}C

measurements in this study yield few young ages for bulk organic matter (except at site MKII03) on the subaqueous delta, indicating a contribution of 'old' organic material supplied by fluvial sediments or resuspension of previously deposited sediments. The $\delta^{13}C$ values confirm a mixed terrestrial/marine source (Cores MKII14, MKII09, and MKII07, Table 2).

Although the ^{210}Pb profiles on the subaqueous delta show limited excess activity, a lower limit on the sediment accumulation rate can be estimated from the ^{14}C data, which suggests high rates in cores MKII14 and MKII09 (rates are not available because of rapid accumulation or physical mixing) located around the rapid prograding Cape Camau and slower rates (0.02-0.03 cm/yr) in cores MKII07 and MKII03 located in the Gulf of Thailand with weak hydrodynamics. Compared with the accumulation rate revealed by inland boreholes (0.45 cm/yr for the prodelta facies and 0.29-0.42 for the delta front facies, Ta et al., 2005), accumulation rate estimated from the ^{14}C data of Gulf of Thailand sediments is much lower. This is reasonable as those inland boreholes were retrieved from paleo-river mouths that have a high progradation rate (16 m/yr, this study).

5.3 Late Holocene Sediment Budget

Previous studies show that the paleo-delta front break was around the location of Core BT2, Core TC1 and the center of Camau Peninsula around 3,000 cal yrs BP. The progradation rate of Mekong delta was 20-30 m/yr in the last 2,500 yrs (Nguyen et al 2000; Saito, 2000; Ta et al., 2002b, Fig. 2). However, due to a lack of subaqueous data, the position of the modern delta front break was based on bathymetric estimation. Seismic profiles in this

study successfully delimit the subaqueous delta. The progradation rate of the MRD over the last 3,000 yrs is updated to a value of ~ 16 m/yr around river mouth and ~ 26 m/yr around the tip of Camau Peninsula in the south.

Previous sediment volume estimation in Ta et al. (2002b) used an averaged deltaic sediment thickness of 20±5 m for the study area. Here this value is adjusted to 18±5 m because the thickness of most of the subaqueous deltaic sediment shown in the seismic profiles is between 10 to 20 m. Then there were 17,700 km^2 (area between paleo and modern delta front) × (18±5 m, averaged sediment thickness) × (1.2±0.1 g/cm^3, averaged dry bulk density) = 382±88 billion tons of sediment trapped within the subaerial and subaqueous part of the MRD over the past 3,000 yrs.

The sediment flux of the Mekong River has not changed greatly during the last 3,000 yrs (Ta et al., 2002b). If we further assume the annual 160 million tons of sediment discharge is constant, then every year approximately 80±18% [(382±88 × 10^9 tons) / 3,000 yrs / (160 × 10^6 tons/yr) × 100%] of the sediment delivered by the Mekong River have taken part into the delta's progradation. This is a reasonable result because satellite images show that the sediment plume outside the river mouth can reach areas tens of kilometers seaward of the subaqueous delta front (see Fig. 1, satellite image taken in August 2002 by NASA).

Late Quaternary sediment budget estimates have already been conducted on two other large river systems along the Western Pacific, i.e. the Yangtze and Yellow Rivers. For the Yangtze and Yellow dispersal systems, distal mud wedges / subaqueous delta lobes are found in coastal areas hundreds of kilometers away from the river mouth (Liu et al., 2007a; Liu et al., 2004; Liu et al., 2007b). While for the Mekong, although longshore current has been

carrying away a large amount of fluvial sediment from the river mouth, the majority of these longshore transported sediments are finally trapped within the broad shallow shelf, south of the river mouth, forming the third largest delta plain in the world.

5.4 Incised Valley Fill

Another intriguing discovery in this study is the incised valley fill seaward of the Mekong River mouth shown in Fig. 4. The initial erosion stage for most incised valleys probably occurred immediately after the exposure of the shelf during low sea-level stand. Shelf-wide regressive incisions were formed on the sub-aerial exposed Sunda shelf (Hanebuth et al., 2002; Schimanski and Stattegger, 2005). As for the MRD, the 70 m long borehole BT2 successively penetrated the incised valley fill on the modern delta plain (Ta et al., 2001b, 2002b; Nguyen et al., 2005). This 40-45 m thick record consists of estuarine channel / tidal river sandy silt, muddy tidal flat / salt marsh, estuarine marine sand and finally open bay mud facies in ascending order. This is consistent with the facies architecture shown in Line 2006-3 (Fig. 4).

To fully understand the evolution of the incised valley fill, a schematic cartoon is shown in Fig. 9 drawn after Allen and Posamentier (1993). Like other incised valleys on the Sunda shelf, this incised valley has probably formed since the shelf exposure caused by the regression (Fig. 9a). Holocene sea-level rise initiated around 19,000 cal yrs BP in the South China Sea (Hanebuth et al., 2009). The increased accommodation space was greater than the fluvial sediment flux, thus a transgressive tidal-estuarine facies was formed above the fluvial

facies deposited earlier. At the same time, the alluvial plain was continuously built up downstream (Fig. 9b). As the sea-level continuously rose, the alluvial-tidal-delta complex and estuary mouth sand in the form of a tidal inlet migrated up the estuary (Allen and Posamentier, 1993), deeply cutting into the underlying sediment and forming a "ω" shape bottom (Fig. 9c). The local sea-level reached its maximum height around 5,500 cal yrs BP. Since then, the sea-level has been falling slightly as the MRD began its rapid progradation. The deep cuts formed by tidal inlets were gradually filled with fine materials, which are correlated to the open-bay facies in Core BT2. Here the mud layer, or the open-bay facies, can be treated as a boundary separating an underlying transgressive sequence from the overlying regressive sequence. This is similar to the incised valley fill on the modern Yangtze delta documented by Li et al. (2002). As the delta plain prograded, the estuary gradually moved downstream and formed a thin tidal-estuarine facies shown in Fig.s 4 and 9d.

6. Summary

High resolution seismic profiles reveal 10-20 m thick deltaic sediments within 30 m water depth surrounding the Mekong River Delta (MRD). Based on the differences in clinoform structure and sediment characters, the subaqueous delta is divided into four zones: Zone I. Mekong River mouth, Zone II. East shore of the Camau Peninsula, Zone III. Cape Camau, and Zone IV. West shore of the Camau Peninsula.

In the last 3,000 yrs, the evolution of the MRD shows a morphological asymmetry, which is explained by increased wave influence. After the delta body refilled the former bight,

the delta edge began to be exposed to longshore and coastal currents. Strengthened by the strong NE monsoon, the coastal current transports a large amount of Mekong sediments southwestward. After going through cycles of trapping and resuspension, longshore transported sediments gradually form a large downdrift area and a subaqueous delta. Sediment budget estimation shows that approximately 80±18% of Mekong sediments have been trapped within the delta area and took part in its rapid progradation over the past 3,000 yrs.

An incised valley fill is unveiled by seismic profiling, based on a schematic incised valley fill model, since the low sea level stand is proposed.

Acknowledgement

Financial supports for this joint research come from the International Office of the National Science Foundation (USA), the Office of Naval Research (USA), and the Vietnamese Ministry of Science and Technology. We appreciate the great help from Dr. Elana Leithold and Laurel Childress (NCSU) with the C_{org} and grain size analyses. Two reviewers, Dr. Steven Goodbred Jr. (Vanderbilt University) and one anonymous reviewer, significantly improved the manuscript.

References

Allen, G.P. and Posamentier, H.W., 1993. Sequence stratigraphy and facies model of an incised valley fill: the Gironde Estuary, France. Journal of Sedimentary Research, 63(3): 378-391.

Allison, M.A., Nittrouer, C.A. and Kineke, G.C., 1995. Seasonal sediment storage on mudflats adjacent to the Amazon River. Marine Geology, 125(3-4): 303-328.

Bhattacharya, J.P. and Giosan, L., 2003. Wave-influenced deltas: geomorphological implications for facies reconstruction. Sedimentology, 50: 187-210.

Cattaneo, A., Correggiari, A., Langone, L. and Trincardi, F., 2003. The late-Holocene Gargano subaqueous delta, Adriatic shelf: Sediment pathways and supply fluctuations. Marine Geology, 193(1-2): 61-91.

Chen, Z., Song, B., Wang, Z. and Cai, Y., 2000. Late Quaternary evolution of the sub-aqueous Yangtze Delta, China: Sedimentation, stratigraphy, palynology, and deformation. Marine Geology, 162(2-4): 423-441.

Coleman, J.M. and Roberts, H.H., 1989. Deltaic coastal wetlands. Geologie en Mijnbouw, 68: 1-24.

Correggiari, A., Cattaneo, A. and Trincardi, F., 2005. The modern Po Delta system: Lobe switching and asymmetric prodelta growth. Marine Geology, 222-223: 49-74.

Debenay, J.-P. and Luan, B.T., 2006. Foraminiferal assemblages and the confinement index as tools for assessment of saline intrusion and human impact in the Mekong Delta and neighbouring areas (Vietnam). Revue de Micropaleontologie, 49(2): 74-85.

DeMaster, D.J., Pope, R.H., Levin, L.A. and Blair, N.E., 1994. Biological mixing intensity and rates of organic carbon accumulation in North Carolina slope sediments. Deep-Sea Research II, 41(4-6): 735-753.

Gagliano, S.M. and Mcintire, W.G., 1968. Reports on the Mekong River Delta, Louisiana State University.

Galloway, W.E., 1975. Process framework for describing the morphologic and stratigraphic evolution of deltaic depositional systems. In: M.L. Broussard (Editor), Deltas, Models for Exploration. Houston Geological Society, Houston, pp. 87-98.

Geyer, W.R., Hill, P.S. and Kineke, G.C., 2004. The transport, transformation and dispersal of sediment by buoyant coastal flows. Continental Shelf Research, 24(7-8): 927-949.

Goodbred, S.L. and Kuehl, S.A., 1999. Holocene and modern sediment budgets for the Ganges-Brahmaputra river system; evidence for highstand dispersal to flood-plain, shelf, and deep-sea depocenters. Geology, 27(6): 559-562.

Goodbred, S.L. and Kuehl, S.A., 2000. The significance of large sediment supply, active tectonism, and eustasy on margin sequence development: Late Quaternary stratigraphy and evolution of the Ganges-Brahmaputra delta. Sedimentary Geology, 133(3-4): 227-248.

Hanebuth, T.J.J., Stattegger, K. and Grootes, P.M., 2000. Rapid flooding of the Sunda Shelf: A Late-Glacial sea-level record. Science, 288(5468): 1033-1035.

Hanebuth, T.J.J., Stattegger, K. and Saito, Y., 2002. The stratigraphic architecture of the central Sunda Shelf (SE Asia) recorded by shallow-seismic surveying. Geo-Marine Letters, 22(2): 86-94.

Hanebuth, T.J.J., Stattegger, K., Schimanski, A., Ludmann, T. and Wong, H.K., 2003. Late Pleistocene forced-regressive deposits on the Sunda Shelf (Southeast Asia). Marine Geology, 199(1-2): 139-157.

Hanebuth, T.J.J. and Stattegger, K., 2004. Depositional sequences on a late Pleistocene-Holocene tropical siliciclastic shelf (Sunda Shelf, southeast Asia). Journal of Asian Earth Sciences, 23(1): 113-126.

Hanebuth, T.J.J., Stattegger, K. and Bojanowski, A., 2009. Termination of the Last Glacial Maximum sea-level lowstand: The Sunda-Shelf data revisited. Global and Planetary Change, 66(1-2): 76-84.

Hu, J., Kawamura, H., Hong H and Qi, Y., 2000. A review on the currents in the South China Sea: seasonal circulation, South China Sea Warm Current and Kuroshio Intrusion. Journal of Oceanography, 56: 607-624.

Imamura, F. and To, D.V., 1997. Flood and typhoon disasters in Vietnam in the half century since 1950. Natural Hazards, 15: 71-87.

Kineke, G.C., Sternberg, R.W., Trowbridge, J.H. and Geyer, W.R., 1996. Fluid-mud processes on the Amazon continental shelf. Continental Shelf Research, 16(5-6): 667-696.

Kubicki, A., 2008. Large and very large subaqueous dunes on the continental shelf off southern Vietnam, South China Sea. Geo-Marine Letters, 28: 229-238.

Kuehl, S.A., Levy, B.M., Moore, W.S. and Allison, M.A., 1997. Subaqueous delta of the Ganges-Brahmaputra river system. Marine Geology, 144: 81-96.

Le, T.V.H., Nguyen, H.N., Wolanski, E., Tran, T.C. and Haruyama, S., 2007. The combined impact on the flooding in Vietnam's Mekong River delta of local man-made structures,

sea level rise, and dams upstream in the river catchment. Estuarine, Coastal and Shelf Science, 71(1-2): 110-116.

Leithold, E.L., Blair, N.E. and Perkey, D.W., 2006. Geomorphologic controls on the age of particulate organic carbon from small mountainous and upland rivers. Global Biogeochem. Cycles, 20(GB3022): 1-11.

Li, C. et al., 2002. Late Quaternary incised-valley fill of the Yangtze delta (China): its stratigraphic framework and evolution. Sedimentary Geology, 152(1-2): 133-158.

Liu, J., Saito, Y., Wang, H., Yang, Z. and Nakashima, R., 2007. Sedimentary evolution of the Holocene subaqueous clinoform off the Shandong Peninsula in the Yellow Sea. Marine Geology, 236(3-4): 165-187.

Liu, J.P., Milliman, J.D., Gao, S. and Cheng, P., 2004. Holocene development of the Yellow River's subaqueous delta, North Yellow Sea. Marine Geology, 209(1-4): 45-67.

Liu, J.P. et al., 2007. Flux and fate of Yangtze River sediment delivered to the East China Sea. Geomorphology, 85(3-4): 208-224.

Milliman, J.D. and Meade, R.H., 1983. World-wide delivery of river sediment to the oceans. Journal of Geology, 91: 1-21.

Milliman, J.D. and Syvitski, J.P.M., 1992. Geomorphic/tectonic control of sediment discharge to the ocean: The importance of small mountainous rivers. Journal of Geology, 100(5): 525-544.

Nguyen, L.V., Ta, T.K.O. and Tateishi, M., 2000. Late Holocene depositional environments and coastal evolution of the Mekong River Delta, Southern Vietnam. Journal of Asian Earth Sciences, 18(4): 427-439.

Nguyen, V.L. et al., 2005. Late Quaternary depositional sequences in the Mekong River Delta, Vietnam. In: Z.Y. Chen, Y. Saito and S.L.J. Goodbred (Editors), Mega-Deltas of Asia. China Ocean Press, Beijing, pp. 121-127.

Nittrouer, C.A., Kuehl, S.A., DeMaster, D.J. and Kowsmann, R.O., 1986. The deltaic nature of Amazon shelf sedimentation. GSA Bulletin, 97(4): 444-458.

Nittrouer, C.A. et al., 1996. The geological record preserved by Amazon shelf sedimentation. Continental Shelf Research, 16(5-6): 817-841.

Roberts, H.H., 1997. Dynamic changes of the Holocene Mississippi River delta plain: The delta cycle. Journal of Coastal Research, 13(3): 691-710.

Roberts, H.H., 1998. Delta switching: early responses to the Atchafalaya River diversion. Journal of Coastal Research, 14(3): 882.

Saito, Y., 2000. Deltas in Southeast and East Asia: Their evolution and current problems. In: N. Mimura and H. Yokoki (Editors), APN/SURVAS/LOICZ Joint Conference on Coastal Impact of Climate Change and Adaption in the Asia-Pacific Region, Kobe, Japan, pp. 185-191.

Schimanski, A. and Stattegger, K., 2005. Deglacial and Holocene evolution of the Vietnam shelf: stratigraphy, sediments and sea-level change. Marine Geology, 214(4): 365-387.

Slingerland, R., Driscoll, N.W., Milliman, J.D., Miller, S.R. and Johnstone, E.A., 2008. Anatomy and growth of a Holocene clinothem in the Gulf of Papua. Journal of Geophysical Research, 113(F01S13): doi:10.1029/2006JF000628.

Stanley, D.J. and Warne, A.G., 1994. Worldwide initiation of Holocene marine deltas by deceleration of sea-level rise. Science, 265(5169): 228-231.

Swenson, J.B., 2005. Fluviodeltaic response to sea-level perturbations: amplitude and timing of shoreline translation and coastal onlap. Journal of Geophysical Research, 110: doi:10.1029/2004JF000208.

Ta, T.K.O., Nguyen, V.L., Kobayashi, I., Tateishi, M. and Saito, Y., 2001. Late Pleistocene-Holocene stratigraphy and delta progradation, the Mekong River delta, South Vietnam. Gondwana Research, 4(4): 799-800.

Ta, T.K.O., Nguyen, V.L., Tateishi, M., Kobayashi, I. and Saito, Y., 2001. Sedimentary facies, diatom and foraminifer assemblages in a late Pleistocene-Holocene incised-valley sequence from the Mekong River Delta, Bentre Province, Southern Vietnam: the BT2 core. Journal of Asian Earth Sciences, 20(1): 83-94.

Ta, T.K.O. et al., 2002. Sediment facies and Late Holocene progradation of the Mekong River Delta in Bentre Province, southern Vietnam: an example of evolution from a tide-dominated to a tide- and wave-dominated delta. Sedimentary Geology, 152(3-4): 313-325.

Ta, T.K.O. et al., 2002. Holocene delta evolution and sediment discharge of the Mekong River, southern Vietnam. Quaternary Science Reviews, 21(16-17): 1807-1819.

Ta, T.K.O., Nguyen, V.L., Tateishi, M., Kobayashi, I. and Saito, Y., 2005. Holocene delta evolution and depositional models of the Mekong River Delta, Southern Vietnam, River Deltas-Concepts, Models, and Examples. SEPM (Society for Sedimentary Geology), pp. 453-466.

Tamura, T. et al., 2009. Initiation of the Mekong River delta at 8 ka: evidence from the sedimentary succession in the Cambodian lowland. Quaternary Science Reviews

Special Theme: Modern Analogues in Quaternary Palaeoglaciological Reconstruction (pp.

181-260), 28(3-4): 327-344.

Walsh, J.P. et al., 2004. Clinoform mechanics in the Gulf of Papua, New Guinea. Continental Shelf Research, 24(19): 2487-2510.

Wolanski, E., Ngoc Huan, N., Trong Dao, L., Huu Nhan, N. and Ngoc Thuy, N., 1996. Fine-sediment dynamics in the Mekong River estuary, Vietnam. Estuarine, Coastal and Shelf Science, 43(5): 565-582.

Wolanski, E., Nguyen, H.N. and Spagnol, S., 1998. Sediment dynamics during low flow conditions in the Mekong River Estuary, Vietnam. Journal of Coastal Research, 14: 472-482.

Tables

Table 1. Details of gravity cores used in this study

Core no.	Longitude (º) E	Latitude (º) N	Water Depth (m)	Core Length (cm)	Vertically Averaged Grain Size(µm)*	% of Volume		
						Clay	Silt	Sand
MKI01	106.265	9.347	4.5	15	--	--	--	--
MKI02	105.900	9.243	5.0	27	--	--	--	--
MKII03	104.408	9.841	15.6	57	36.84	14.54	61.99	23.47
MKII07	104.743	9.125	10.0	49	14.79	31.11	66.03	2.86
MKII09	104.561	8.801	10.0	101	11.87	33.81	64.81	1.39
MKII14	105.288	8.512	16.0	50	40.14	24.03	48.26	27.71

* measured with 10 cm interval

Table 2. AMS 14C ages of sedimentary bulk organic matter

Core No.	Water depth (m)	Sample Depth (cm)	^{14}C age (yrs)	$\delta^{13}C$ (per mil)
MKII-3	15.6	0-1	50 ± 25	-21.2
		30-32	495 ± 30	-20.6
		55-57	1570 ± 30	-20.8
MKII-7	10.0	0-1	800 ± 25	-24.3
		14-16	1300± 30	-22.7
		30-32	2930 ± 30	-23.8
		46-48	3120 ± 35	-24.2
MKII-9	10.0	0-4	865 ± 25	-24.2
		39-41	830 ± 25	-24.1
		99-101	845 ± 25	-24.4
MKII-14	16.0	0-1	1840 ± 30	-23.3
		18-20	1350 ± 40	-23.6
		48-50	1800 ± 30	-23.2

* The ^{14}C data are "raw" ages that have been normalized to a constant $\delta^{13}C$ value, but have not been corrected for a reservoir age or atmospheric $^{14}C/^{12}C$ variations.

Table 3. Clinoform and sediment characters along the coastal area in MRD

Zone	Gradient	Seismic Profile Reflectivity	Excess ^{210}Pb Profile	Source of Organic Matter	Grain Size
I	~ 2.5:1000	strong	near surface excess only	--	sand-clay-silt mixing
II	~ 0.8:1000	strong	uniform limited to no excess activity	mixture of terrestrial/marine	sand-clay-silt mixing
III	~ 5.0:1000	moderate	uniform activity with limited excess activity	mixture of terrestrial/marine	clayey silt
IV	~ 1.0:1000	weak	some decrease in excess activity	mostly marine	clayey silt

Figures

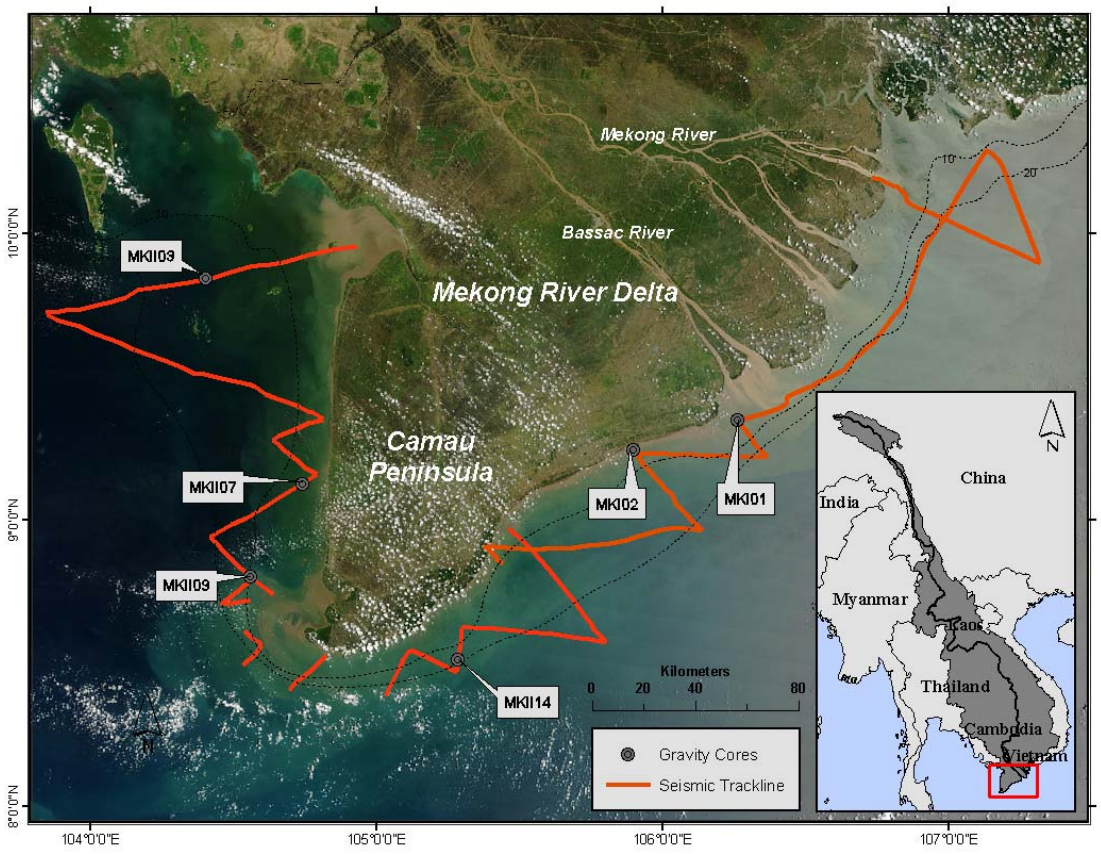

Fig. 1. Location map of the study area, positions of seismic tracklines and gravity cores. Satellite image courtesy of NASA (MODIS, August 2002).

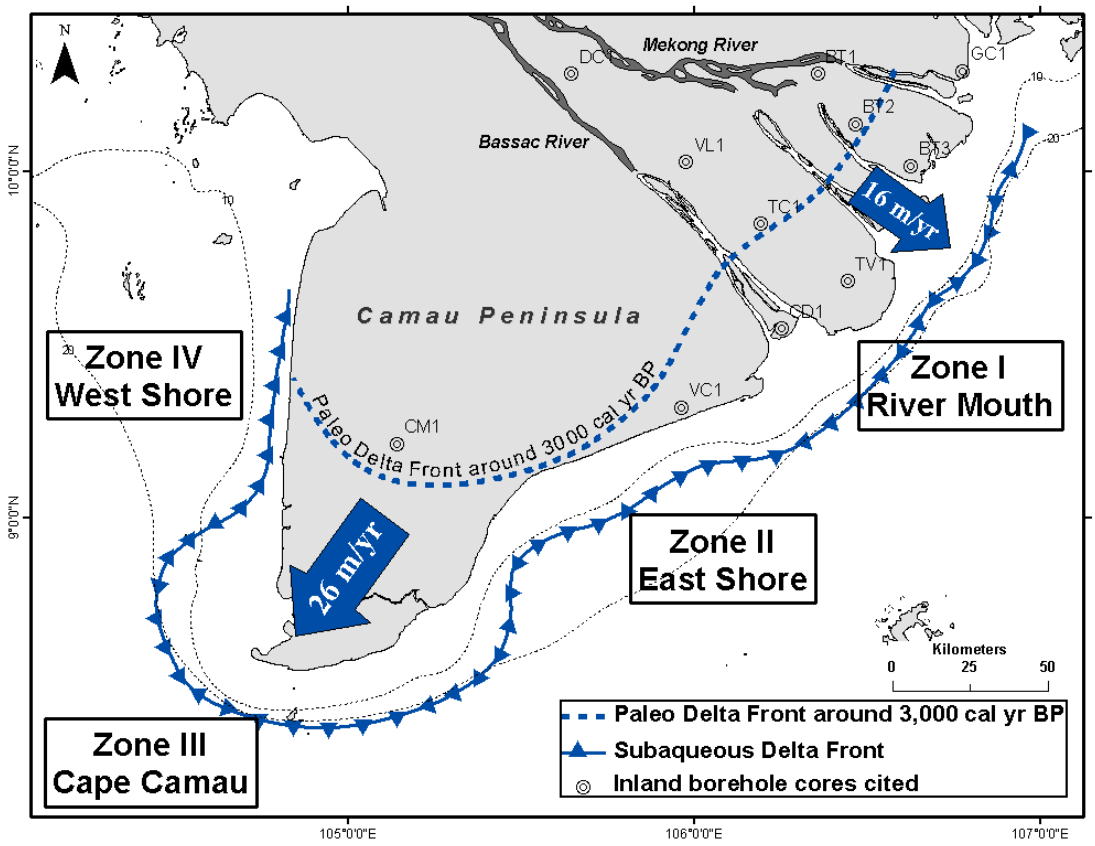

Fig. 2. The zonation of the Mekong River Delta. Zone I. Mekong River mouth, Zone II. East shore of Camau Peninsula, Zone III. Cape Camau, and Zone IV. West shore of Camau Peninsula. The blue dashed line is the paleo delta front around 3000 yr BP after Nguyen et al. (2000) and Ta et al. (2002b).

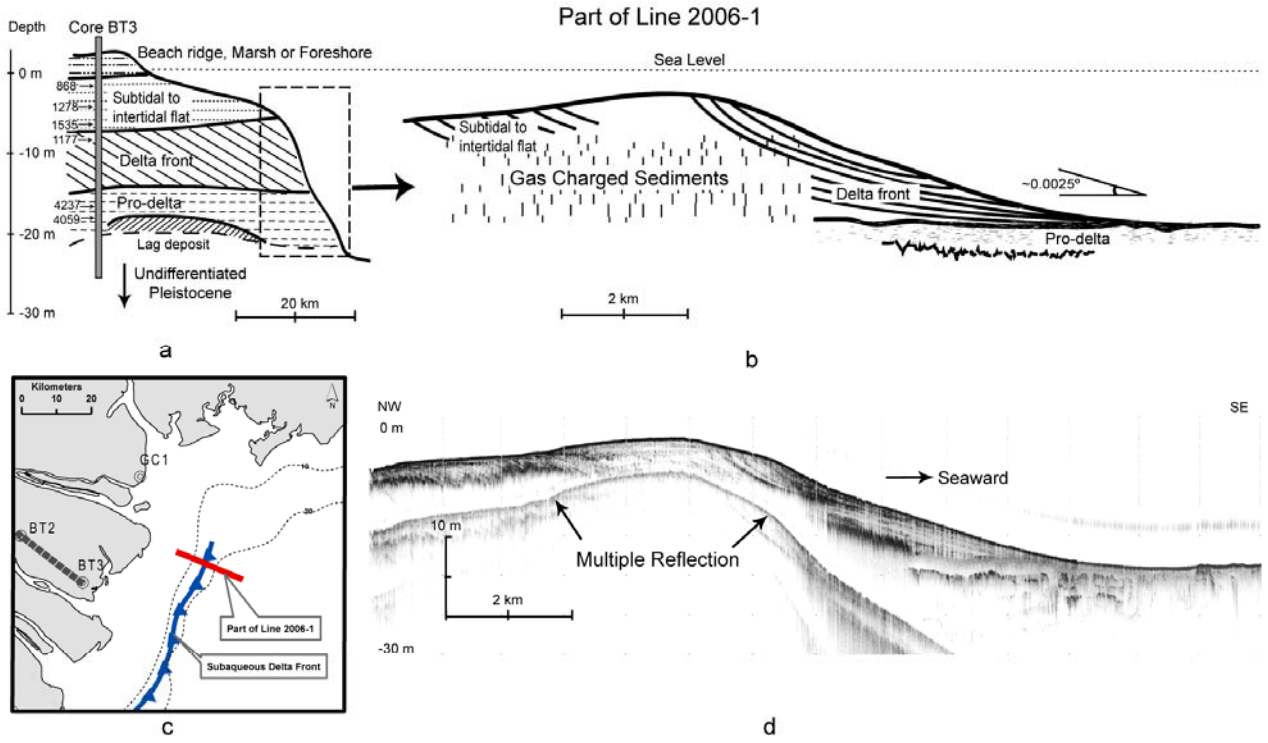

Fig. 3. Seismic trackline 2006-1 seaward of the Mekong River mouth. a. Sedimentation facies based on inland boreholes by Ta et al.(2005); b. Schematic facies architecture; c. Position maps of inland boreholes, cross section and seismic trackline; d. Seismic “Chirp” profile.

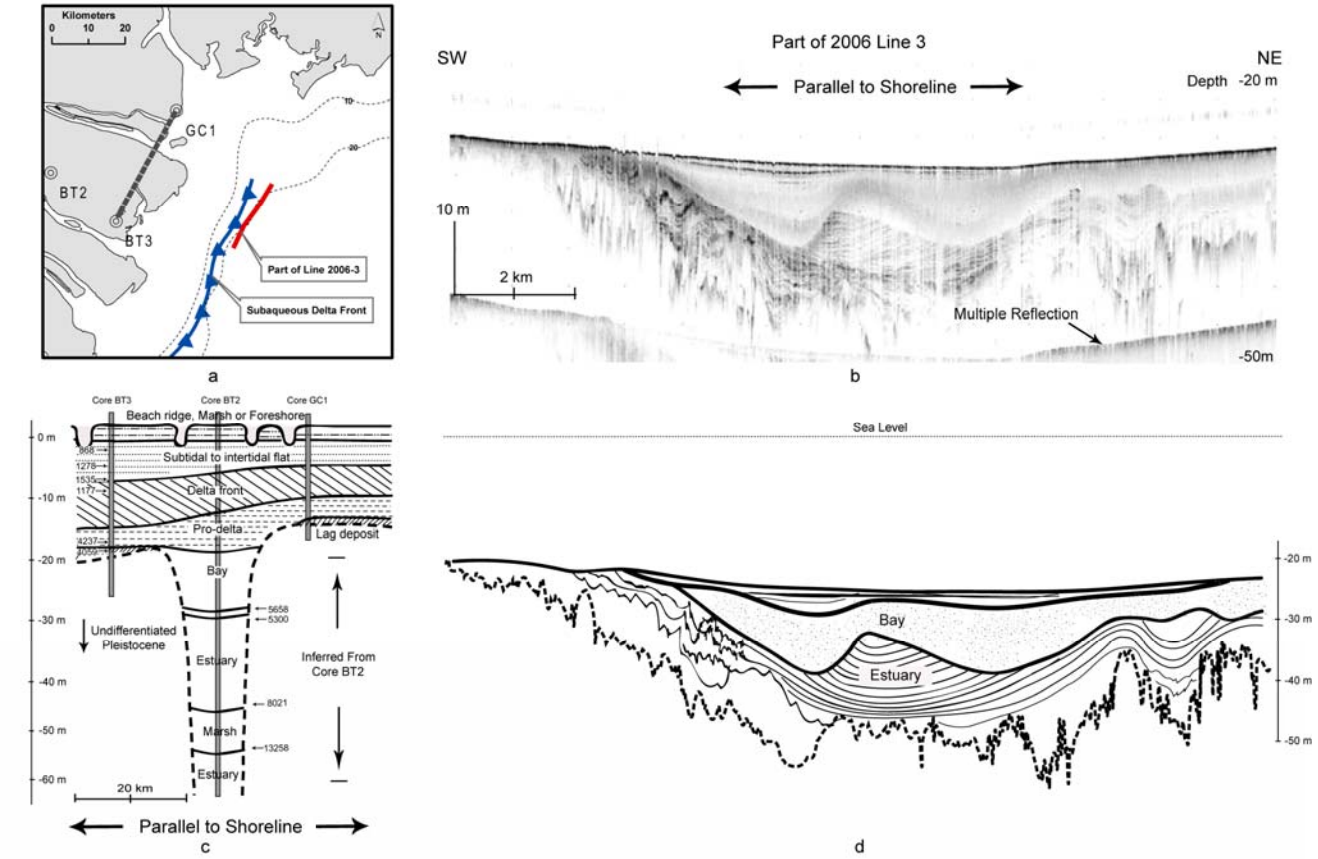

Fig. 4. A filled incised valley seaward of the Mekong River mouth. a. Position maps of inland boreholes, cross section and seismic trackline; b. Seismic "Chirp" profile; c. Sedimentation facies based on inland boreholes by Ta et al. (2002b); d. Schematic facies architecture.

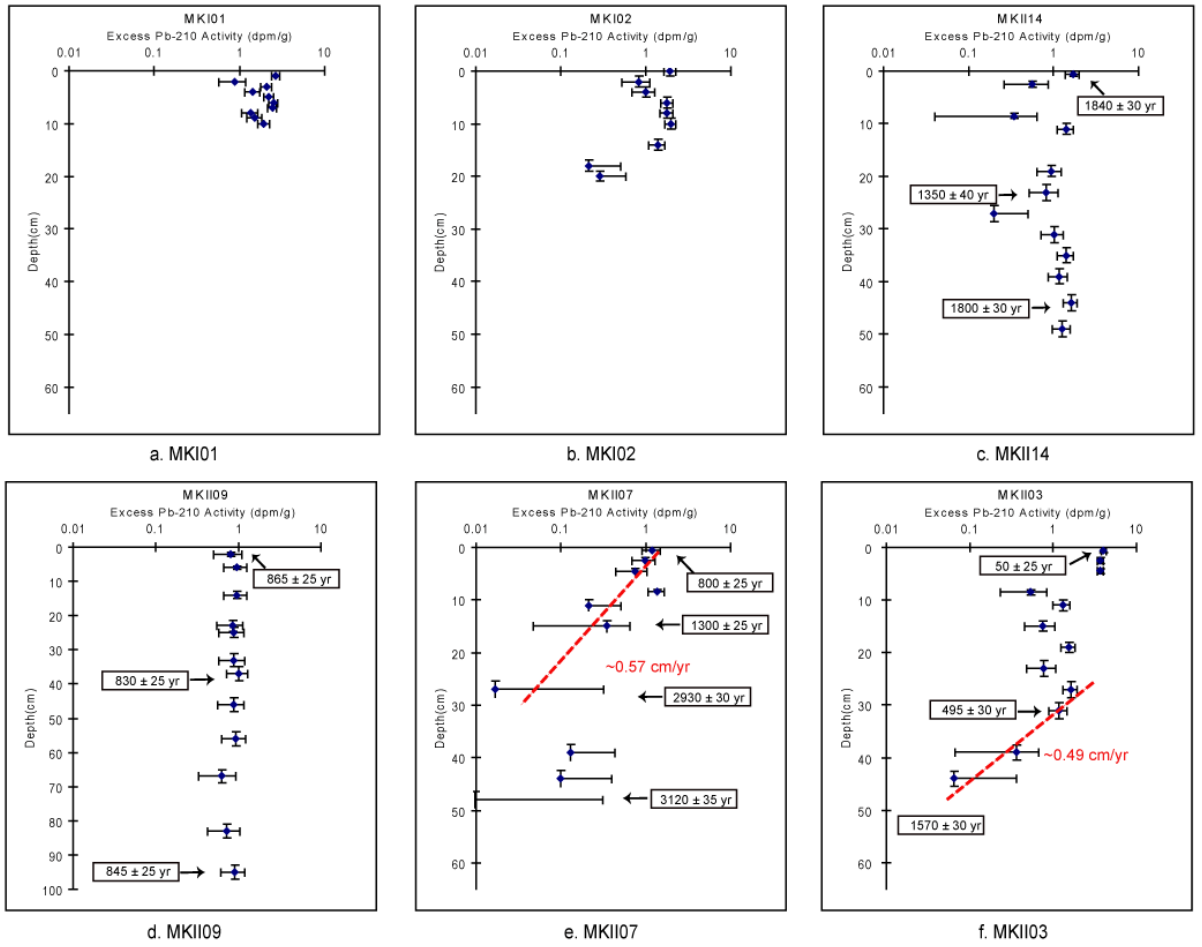

Fig. 5. Excess ^{210}Pb profiles of sediment cores. Zone I (a and b), Zones II (c), Zone III (d) and Zone IV (e and f).

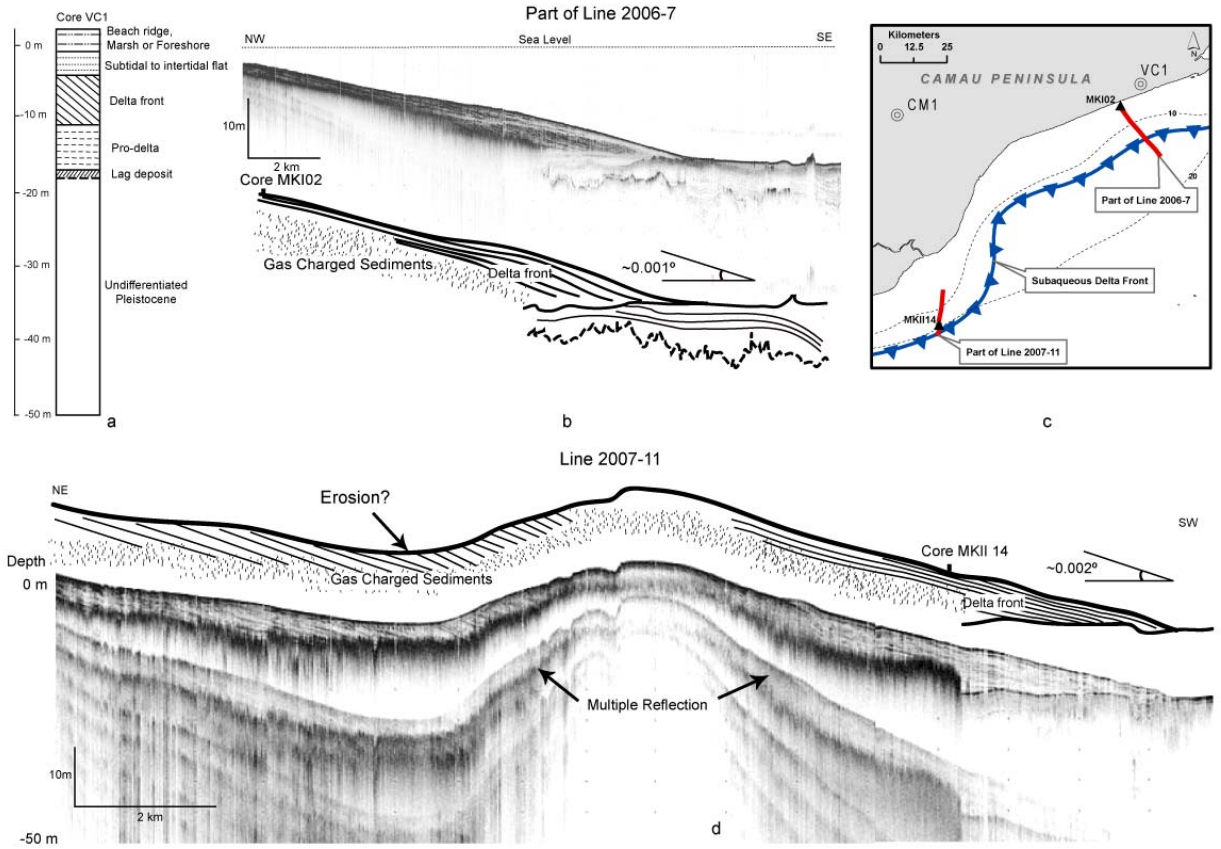

Fig. 6. Seismic profiles from Zone II: 2006-7 and 2007-11. a. Sedimentation facies based on borehole VC1, by Ta et al. (2005); b. Seismic "Chirp" profile with schematic facies architecture of line 2006-7; c. Position maps of inland boreholes, cross section and seismic trackline; d. Seismic "Chirp" profile and schematic facies architecture of line 2007-11.

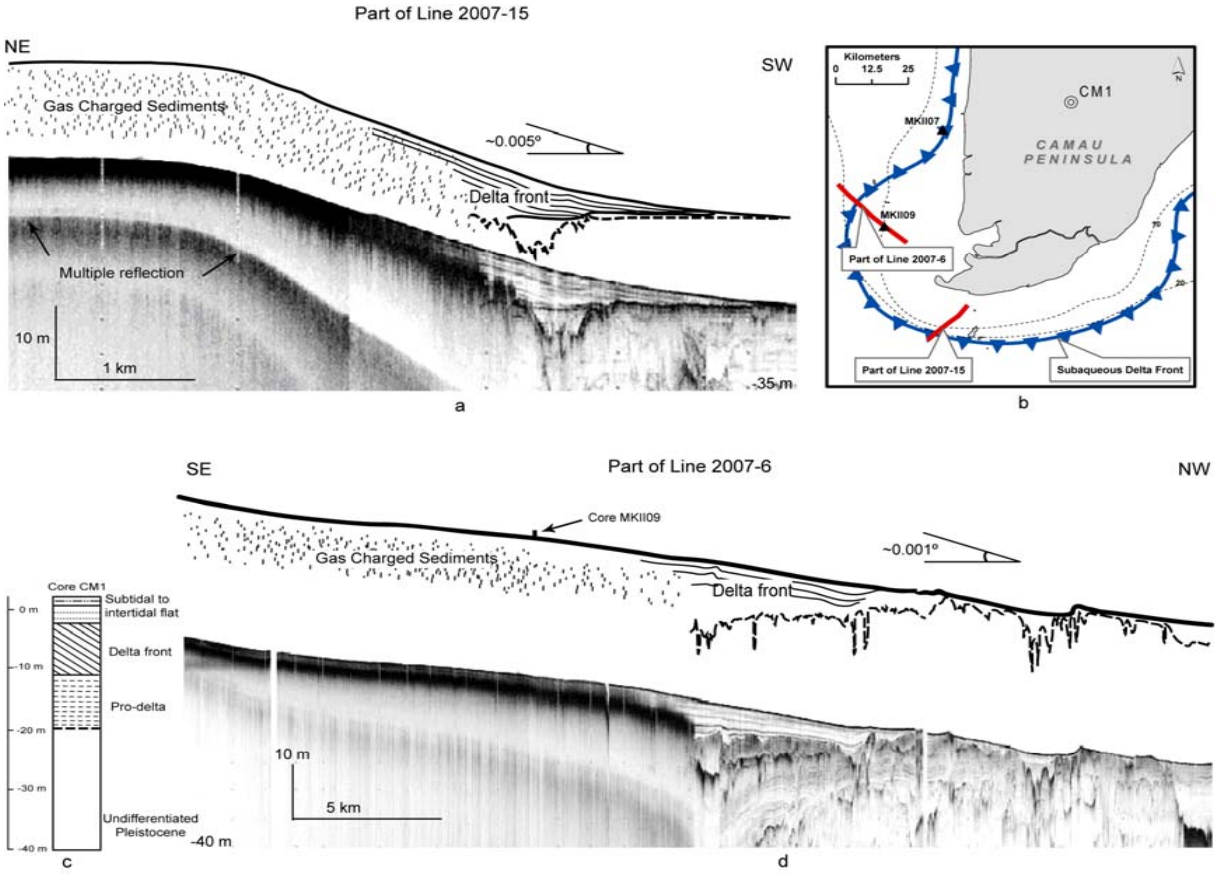

Fig. 7. Seismic profiles in Zone III: 2006-7 and 2007-11. a. Seismic "Chirp" profile and schematic facies architecture of line 2007-15; b. Position maps of inland boreholes and seismic tracklines; c. Sedimentation facies based on borehole CM1, after Nguyen et al., 2005; d. Seismic "Chirp" profile and schematic facies architecture for line 2007-6.

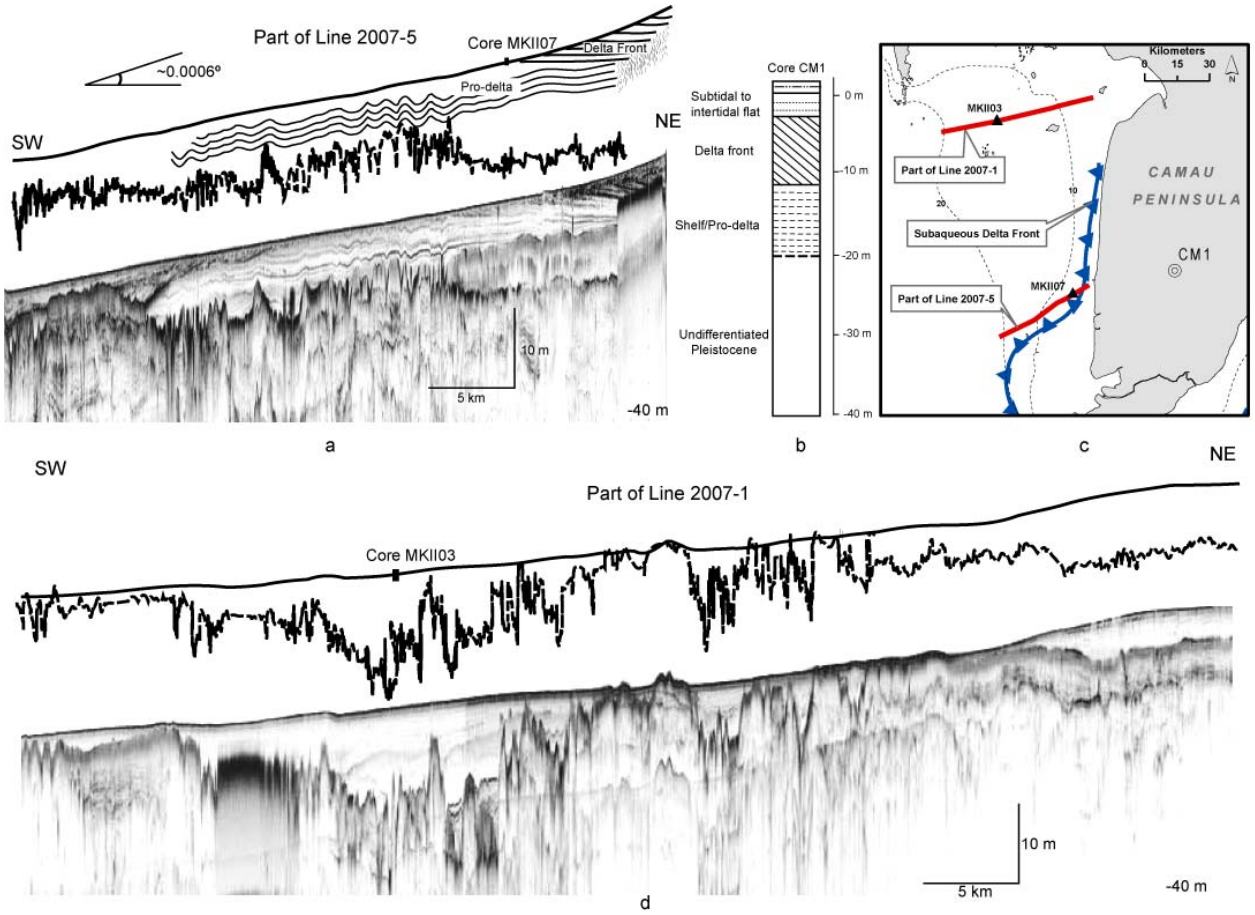

Fig. 8. Seismic profile from Zone IV: 2007-1 and 2007-5. a. Seismic "Chirp" profile and schematic facies architecture of line 2007-5; b. Sedimentation facies based on borehole CM1 by Nguyen et al. (2005); c. Position maps of inland boreholes and seismic tracklines; d. Seismic "Chirp" profile and schematic facies architecture for line 2007-1.

Fig. 9. Schematic cartoon of the development of the incised valley fill. After Allen and Posamentier, 1993: a. The incise valley was formed during low sea-level stand; b. The sea-level rise originated around 19,000 ~ 20,000 cal yrs BP (Hanebuth et al., 2009), a transgressive tidal-estuarine facies was formed. The alluvial plain was continuously built up in the downstream direction; c. Around 5,500 yrs BP the local sea-level reached its maximum. As a result, the flood-tidal-delta complex and estuary–mouth sands in the form of a tidal inlet migrated up the estuary, deeply cutting into the underlying sediment and forming a "ω" shape bottom; d. Sea-level has been slightly lowering since the Holocene high sea-level stand. The deep cutting by tidal inlets was gradually filled with fine materials. As the delta plain prograded, the estuary gradually moved downstream and thus formed a thin tidal-estuary depositional layer; e. Sea level curve for the past 15,000 cal yrs. (A. Mekong River Delta, gray, Ta et al., 2002a and B. Sunda Shelf, blackline, Hanebuth et al., 2000).

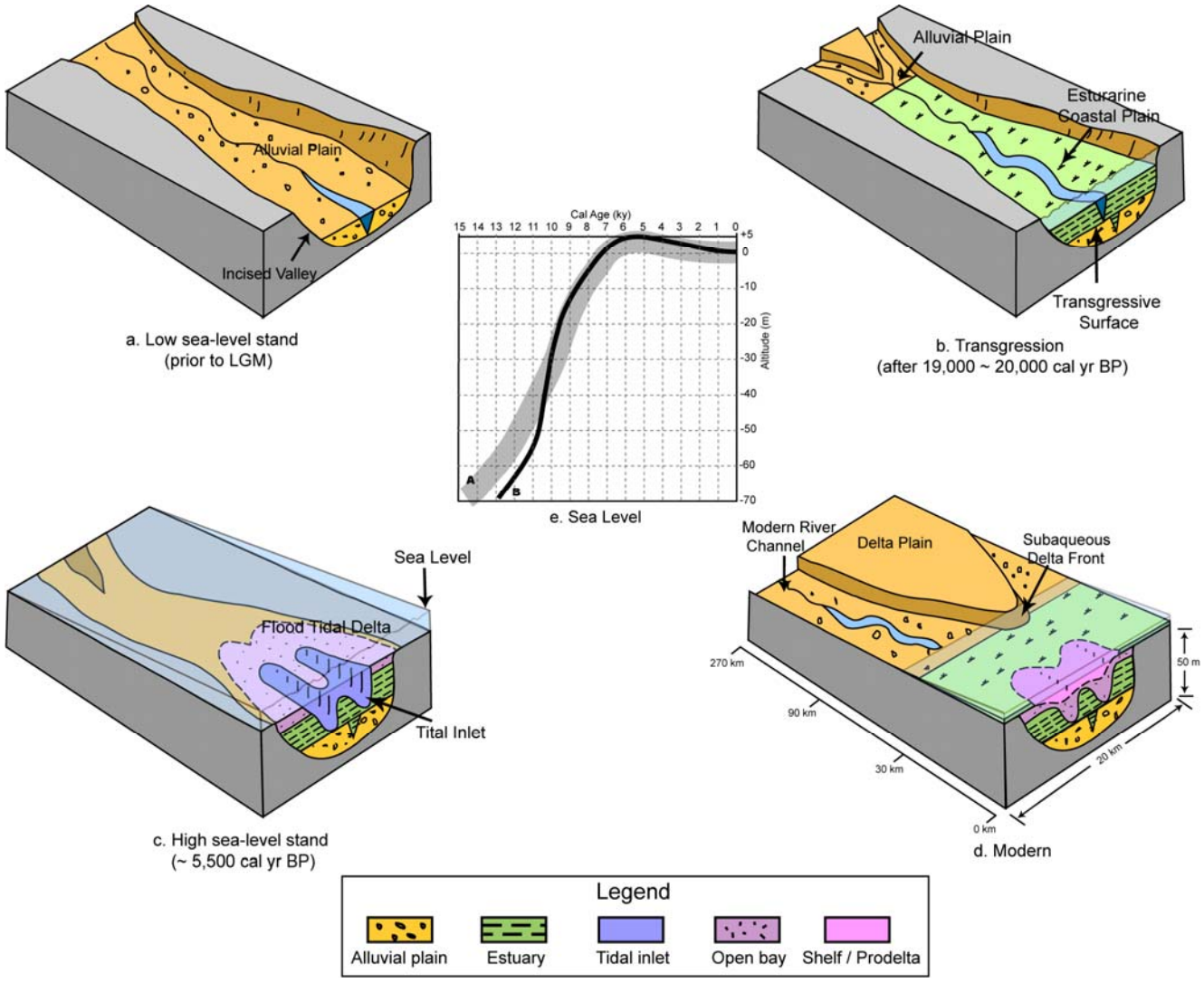
Alluvial Plain
Incised Valley
a. Low sea-level stand
(prior to LGM)
Alluvial Plain
Estuarine
Coastal Plain
Transgressive
Surface
b. Transgression
(after 19,000 ~ 20,000 cal yr BP)
Cal Age (ky)
15 14 13 12 11 10 9 8 7 6 5 4 3 2 1 0
+5
0
-10
-20
-30
-40
-50
-60
-70
Altitude (m)
A
B
e. Sea Level
Sea Level
Flood Tidal Delta
Tital Inlet
c. High sea-level stand
(~ 5,500 cal yr BP)
Modern River
Channel
Delta Plain
Subaqueous
Delta Front
270 km
90 km
30 km
0 km
50 m
20 km
d. Modern
Legend
Alluvial plain
Estuary
Tidal inlet
Open bay
Shelf / Prodelta

CHAPTER 4: TRANSPORT AND DEPOSITION OF THE MEKONG RIVER SEDIMENT: GEOCHEMICAL ANALYSIS AND NUMERICAL MODELING[3]

Zuo Xue, J. Paul Liu, Ruoying He, Shiming Wan, Ke Chen, Yizhen Li

[3] This chapter is based on a manuscript submitted to *Continental Shelf Research*

Abstract

The Mekong River Delta (MRD) has the third largest delta plain in the world. Previous geophysical studies have revealed a limited cross-shelf but elongated subaqueous delta with in 20-30 m water depth inner shelf. In this study we analyzed the clay mineral (XRD) and geochemical characteristics ($\delta^{13}C$, C/N, ^{210}Pb, and AMS ^{14}C) of cored sediments recovered during 2006 and 2007 cruises. Clay mineral analysis indicated that Mekong sediment is the dominant source material for the rapid prograding delta front. $\delta^{13}C$ and AMS ^{14}C values of bulk carbon indicated a mixture of aged terrestrial and fresh marine origin. Excess ^{210}Pb activity profiles showed no steady accumulation on the subaqueous delta.

A numerical model, which couples three-dimensional circulation and sediment transport, was used to simulate the sediment transport and dispersal on the shelf. Based on the weather (wind), river (water and sediment discharge) and ocean (tide, wave, and current) conditions in year 2005, the model calculation showed that 99% of Mekong sediment was retained on the subaqueous delta, which was defined by a previous seismic study. Much of the Mekong sediment that traveled farther along the shelf was fine grained material carried toward the southwest, forming a longshore-tranported mud belt. Sensitivity tests indicated that wind was the most important forcing influencing local sediment transport. The suspended sediment in the turbid water present along the delta plain on MODIS images was composed of fine grained material delivered by the Mekong River and resuspended from the seabed.

Keywords: Mekong, South China Sea, ROMS, Sediment Transport Modeling

1. Introduction

As a connection between land and continental shelves, the fluvial sediments discharged to the ocean bear the characters of both riverine systems and the coastal environment where they are temporally/permanently deposited. A series of 'Source to Sink' studies of the flux and fate of river-derived sediments have been carried out on both large and small river systems. Sedimentary records, such as subaqueous deltas and clinothems, around the river mouths or on the open shelf have been extensively investigated to: (1) interpret the sequence stratigraphy and construct the local sea-level curve; (2) examine interactions between sedimentary processes and hydrodynamics; (3) establish Late Quaternary sediment/carbon budgets; and (4) evaluate the influence of episodic events, such as storms and typhoons, on sediment dynamics.

Rivers also provide a major conduit for the preservation of terrigenous organic matters in marine sediment, most of which will be finally buried on continental shelves and upper slopes (Hedge and Keil, 1995). In passive margin systems, like the Amazon, particulate organic carbon must pass through multiple bioactive reservoirs, such as upland and lowland soils, where prolonged exposure to a range of biogeochemical processes progressively alters chemical compositions. Continued processing on wide energetic shelves incinerates more than half of the terrestrial carbon (Aller et al., 1996). While for active margin river systems like the Eel River, the original upland-generated organic carbon signal is transmitted to the seabed (Blair et al., 2004). Sedimentary organic carbon (kerogen) survives through the fluvial system and deposits on continental shelves. Similar situations have been documented by Leithold at al. (2006) in the small mountainous rivers in Oregon, California, and New

Zealand as well.

The six major fluvial systems on the Western Pacific, i.e. the Yellow (Huanghe), Yangtze (Changjiang), Pearl (Zhujiang), Red (Songhong), Mekong, and Taiwanese Rivers, deliver approximate 2.2 billion tons of sediment to the Bohai Sea, Yellow Sea, East China Sea, and South China Sea (SCS) annually (Table 1). These sediments account for approximately 17% of the terrestrial sediment flux to the global coastal ocean (12.6 billion tons/yr, Syvitski et al., 2005). A number of geophysical, geochemical, and mineralogical studies have been conducted on these dispersal systems targeting the subaerial/subaqueous delta evolution (e.g. Yellow: Liu et al., 2004a; Yang and Liu, 2007; Liu et al. 2007a, Yangtze: Chen et al., 2000; Hori et al., 2001; Liu et al., 2007b, Red: Hori et al., 2004; Tanabe et al., 2006, and Mekong: Nguyen et al., 2000; Ta et al., 2005; Tamura et al., 2009), sedimentary processes (e.g. Yellow: Li et al., 1998, Yangtze: Wei et al., 2007), sediment budget (e.g. Yellow: Liu et al., 2004a, Yangtze: Liu et al., 2007b, and Taiwanese Rivers: Liu et al., 2008), human impacts (e.g. Yellow: Wang et al., 2007, Yangtze: Yang et al., 2003, Pearl: Dai et al., 2008, and Red: Li et al., 2006), and climatic impacts from the El Niño-Southern Oscillation (e.g. Yellow: Wang et al., 2007) and typhoon events (e.g. Milliman and Kao., 2005).

The Mekong River is the third largest river on the Western Pacific in terms of length and sediment inputs (160 million tons/yr, Table 1). Over the past 5,500 yrs the Mekong River Delta (MRD) has prograded 250 km from the Cambodia border toward the SCS (Nguyen et al., 2000), forming the third largest delta plain in the world after the Amazon and Ganges-Brahmaputra deltas. However, so far sedimentation studies of the MRD have been confined within the subaerial part of the MRD based on borehole analyses (Nguyen et al., 2000 and

2005; Ta et al., 2001a, 2001b, 2002a, 2002b, and 2005), leaving the subaqueous part unstudied.

To understand the features and sediment dynamics of the Mekong subaqueous delta, two geophysical and geochemical cruises were conducted by the Sea-level Change and Ocean Margin Evolution Laboratory at North Carolina State University (NCSU) in April 2006 and March 2007. Approximately 1,150 km of high resolution seismic profiles and 19 gravity cores were recovered. While the Late Holocene evolution of the subaqueous delta has been documented in chapter 3, mainly based on geophysical data, the purpose of this chapter is to present the results of mineralogical/geochemical analyses of cored sediments and a coupled three-dimensional circulation and sediment transport model of the sediment dispersal on the Mekong shelf.

2. Geological Setting and Ocean Dynamics

2.1 The Mekong River and Delta

The Mekong River is the largest river on the tropical Western Pacific. It originates in the Tibetan Plateau, runs through China, Myanmar, Thailand, Lao PDR, Cambodia, and enters the SCS in southern Vietnam (Fig. 1). The Mekong River has a length of ~ 4,750 km and a basin area of 832,000 km^2 (HydroSHEDS v2.01, World Wildlife Fund, US). Every year it delivers ~ 495×10^9 m^3 of fresh water and ~ 160 million tons of sediment into the SCS (Milliman and Syvitski, 1992). Clay mineral studies have been conducted on sediment from

the Tibetan Plateau, the MRD plain, and the SCS (Liu et al., 2004b, 2005, and 2007c; Steinke et al., 2008). Samples from the MRD plain have an average content of 28% kaolinite, 35% illite, 26% chlorite, and 11% smectite (Liu et al., 2007c). Clay mineralogy and major element geochemistry analysis of two cores recovered from the southwest SCS (292 m and 1230 m water depth, adjunct to the southern Vietnam shelf) indicate that the Mekong has been a major sedimentary source for this area over the past 190,000 yrs (Liu et al., 2004b). Sediment cores from the Sunda Shelf reveal that clay mineral from the Mekong has limited contribution to this part of the SCS over the past 170,000 yrs (Steinke et al., 2008). Nevertheless, clay mineralogical analysis of sediment on the Mekong shelf was not conducted until this study.

The weather in the Lower Mekong region (from China border to the south) is dominated by the Southeast Asian monsoon system. Approximately 80% of the annual rainfall happens during the rainy season, which is usually between May and October (Debenay and Luan, 2006). Water discharge reaches a maximum in October and a minimum in May at Phnom Penh, Cambodia (the last major gauge station on the Mekong River) (Gagliano and McIntire, 1968; Milliman and Meade, 1983; Wolanski et al., 1998). With ~ 200 new dams to be added to the basin in the next couples of decades, changes are expected in both hydrological regime and delta dynamics (Xue et al., in press).

The MRD has an area of 49,500 km^2 (Le et al., 2007) and it is the third largest delta plain in the world, only exceeded by the Amazon and the Ganges-Brahmaputra Deltas (Coleman and Roberts, 1989). According to Saito (2000), the eastern part of the MRD has been under serious erosion at a rate of 1.1 km^2/yr since 1885, the western part is experiencing

rapid progradation at a rate of 1.2 km^2/ yr. Previous borehole studies showed that the delta plain began its progradation in 8,000 cal yr BP as a result of decelerating sea-level rise (Tamura et al., 2009). Over the past 5,500 yrs, with tremendous Mekong sediment inputs and a slightly lowering sea-level, the MRD has prograded more than 250 km from the Cambodia border toward the SCS (Nguyen et al., 2000). However, this progradation process was not a continuous one: a phase shift from a "tide dominated" delta to a "tide and wave dominated" delta around 3,000 cal yr BP has been proposed based on facies variations along the boreholes recovered from the delta plain (Ta et al., 2002a and b).

The estuarine area of the Mekong has a funnel-like shape and is dominated by macro tides with a maximum range of 3.2 m and average tide of 2.2 m (Wolanski et al., 1996). There are seven distributaries discharging into the SCS, which are, from north to south, Tieu, Dai, Ham Luong, Chen, Hau, Din An, and Tranh De (Fig. 1). The total freshwater discharge reaches its maximum (39,000-40,000 m^3/s in September) during high flow season (from June to December). The minimum freshwater discharge is between 1,700 and 2,800 m^3/s occurring during the low flow season (from January to May) (Wolanski et al., 1998; Hordoir et al., 2006).

Typical suspended sediment concentration (SSC) at Phnom Penh is ~ 250 mg/l during high flow season (Wolanski et al., 1996). Field studies at the Din An river mouth showed that the sediment was made of fine silt and ~ 95% of these sediments were exported to the SCS (Wolanski et al., 1996). Depth-averaged SSC ranged between 160-310 mg/l at the Din An river mouth. During the low flow season, the SSC at Phnom Penh station was 80-100 mg/l. The saline region can extend 50 km up-river. Depth-averaged SSC peaked at 583 mg/l near

the salinity intrusion limit. The maximum near bottom SSC value was 1,400 mg/l during April 14-18, 1996 (Wolanski et al., 1998). The salinity at the river mouth fluctuated between 7 (ebb tides) and 23 psu (spring tides).

In the coastal area, seismic profiling by Xue et al. (2010) revealed a low gradient, subaqueous delta system, up to 20 m thick, surrounding the modern MRD. Although there is a general consensus that wave and currents driven by the strong NE monsoon dominates the net along-shelf sediment transport (Gagliano and McIntire, 1968; Nguyen et al., 2000, Xue et al., 2010), neither the source of the sediment on the Mekong shelf, nor the sediment dynamics has been addressed yet.

2.2 Ocean Dynamics

The coastal area in Southeast Asia is strongly influenced by the NE monsoon (December to February) and the SW monsoon (June to August). The coasts are exposed to seasonal high waves during these monsoon regimes. The NE monsoon influences the eastern margin of the Philippines, Vietnam, and the east coast of the Malaysia Peninsular. The SW monsoons influence the coast of Myanmar, the east coast of southern Thailand, and Indonesia (Wang, 2005). In general, the coastal currents in Southeast Asia are driven by prevailing monsoon winds. The northeasterly winds prevail over the whole region with an average magnitude of ~ 9 m/s in winter. In contrast, relative weak (~ 6 m/s) southwesterly winds dominate over most parts of the SCS in summer (Hu et al., 2000).

Coasts in Southeast Asia experience low to moderate tidal ranges and a variety of

tidal types influenced by conditions in the Pacific and Indian Oceans. Characteristic semi-diurnal tides of the Indian Ocean prevail in the west. Mixed tides of the Pacific occur in the eastern Indonesian archipelago and the Philippine waters. Almost pure diurnal tides predominate in the Gulf of Thailand (GOT) and the Java Sea (Wang, 2005). The coastal area of the MRD is controlled by two tidal sources: one is the regular 3.5 m semidiurnal tides from the SCS to the east of MRD, and the other is an irregular 0.8-1.0 m diurnal tide from the GOT in the west (Le et al., 2007).

The hydrodynamics of the southern Vietnam shelf is strongly influenced by the Southeast Asia monsoon (Hu et al., 2000). The wind field averaged during 1948-2009 shows the study area is dominated by NE wind (Fig.2a). Waves and currents generated by strong NE monsoon dominate the net alongshore sediment transport (Gagliano and McIntire, 1968). Modeled results from northwest of the Mekong River mouth show the currents are up to 0.55 m/s with direction shifting between NE in winter and SW in summer (Kubicki, 2008).

A numerical simulation of the Mekong River plume shows that: (1) the large amount of fresh water brought by the Mekong creates a baroclinic coastal current flowing in the direction of the propagation of the Kelvin wave; (2) the Mekong plume is mostly geostrophic; and (3) the tidal currents generate intensive vertical mixing (Hordori et al., 2006).

3. Data and Methods

3.1 Core Sediments

The research team collected 19 gravity cores during two cruises in April 2006 and March 2007 (core details see Table 2). On board, the sediment cores were subsampled at 1-2 cm intervals and saved in sample bags. During the 2007 cruise, bulk organic sediment samples were collected every 20 cm along the cores and were stored in the refrigerator onboard. In the laboratory at NCSU, grain size analysis (4-5 samples per core with 10 cm intervals) was done using a LS 13 320 Laser Diffraction Particle Size Analyzer (Beckman Coulter©, size range 0.04 μm ~ 2000 μm, Fig. 3). Approximately 12-16 samples from each core were selected for ^{210}Pb analysis. No continuous distribution of any calcareous species occurred down core with sufficient abundance. Consequently, we established the ^{14}C chronologies from the C_{org} content of the bulk-sediment. Methods for the establishment of ^{210}Pb activities, ^{14}C chronologies, and organic carbon (C_{org}) stable isotope ratios ($\delta^{13}C$) are similar to that of DeMaster et al. (1994), Leithold et al. (2006) and Xue et al. (2010).

Clay mineral analysis was carried out at the Institute of Oceanology, Chinese Academy of Sciences, following a procedure similar to Wan et al. (2007). The <2 μm fraction of the sediments were separated based on Stoke's settling velocity principle after removal of carbonate and organic matter by treatment with 0.5 N HCl and 10% hydrogen peroxide. The analysis was performed on oriented mounts with a D8 ADVANCE diffractometer using CUKα (alpha) radiation (40 kV, 40 mA). Each sample was measured three times: (1) under dry air conditions, (2) after ethylene glycol salvation at 100 ºC for 1h; and (3) after ethylene

glycol salvation at 60 ºC for 12 h. The identification of clay minerals was made mainly using the position of the (001) series of basal reflections on the three XRD diagrams of air drying, ethylene glycol salvation and heating conditions XRD identified smectite, illite, kaolinite, chlorite and mixed-layer clays.

3.2 Numerical Modeling

To examine the sedimentary processes over short time scales, we implemented the Coastal Sediment Transport Modeling System (CSTMS, Warner et al., 2008) to the Regional Ocean Modeling System (ROMS, Shchepetkin and McWilliams, 2005) to evaluate the sediment transport and dispersal on the Mekong shelf. A 200 × 150 square configuration was defined with lower left corner around 8.6 ºN and 104.8 ºE (Fig. 4). The grid resolution was approximate 2 km. According to Hordoir et al. (2006), a 2 km resolution is far below the baroclinic Rossby radius of the flow and is an appropriate scale for the width of any of the branches of the Mekong River when it reaches the sea. The 30-second Global Bathymetry and Elevation Data (SRTM30_PLUS, Becker et al., 2009) was smoothed and interpolated to the configuration grid. The water depth of the computational grid ranged between 5.0 and 157.8 m. Vertical resolutions of sigma levels consisted of 20 layers.

To assure the stability and accuracy of the circulation model, the model had three open boundaries (northern, eastern, and southern) and thus the west shore of the MRD was not covered. Initial and boundary conditions were interpolated using salinity and temperature data from HyCOM/NCODA (1/12º equatorial resolution, Hybrid Coordinate Ocean Model

together with NRL Coupled Ocean Data Assimilation scheme, Chassignet et al., 2007). Wind and heat forcing was interpolated using data from NCEP Reanalysis (2.5º resolution, Kalnay et al., 1996). Wavefields were estimated using the Simulating Waves Nearshore model (SWAN version 40.72, Delft University of Technology, 2008). The SWAN model domain was a 50 × 50 square configuration with lower left corner around 6.0 ºN and 104.5 ºE. The grid resolution was approximate 10 km (Fig. 4). Tidal conditions were imposed at the open boundaries and were derived from the OSU TOPEX/Poseidon Global Inverse Solution 7.0 (Egbert and Erofeeva, 2002). A no-gradient condition for sediment was applied at the open boundaries.

Fluvial inputs (freshwater and SSC) were imposed at the western boundary around the branches of the Mekong River. The freshwater discharge was from Hordoir et al. (2006), which was an average of the period 1933-1966. For suspended sediment input, we referred to the results of two in situ observations in the estuarine area during April 1996 (low flow season, Wolanski et al., 1998) and November 1993 (high flow season, Wolanski et al., 1996) (Fig. 5). The amount of sediment input from the Mekong in a 12-month period was 164.4 million tons as to refer to the sediment flux estimated by Milliman and Syvitski (1992) (~ 160 million tons/yr).

The flocculation rate of the Mekong sediment was unavailable. We assumed 90% of Mekong sediment was flocculated. This is a similar setup to that of an Adriatic Sea sediment dispersal study by Harris et al. (2008). The model accounted for four sediment classes: Type 1 and 2 represented the fine grained materials and flocculated materials supplied by the Mekong River; Type 3 and 4 represented the silt/clay and sand resuspended from the seabed.

The hydrodynamic properties of different sediment classes are listed in Table 4. The initial sediment bed was derived by combining the grain size observations in this study with the geophysical data presented in Xue et al. (2010), which shows that the Mekong mud is mainly distributed within the - 20 m isopach.

A 13-month simulation was initialized on December 1st, 2004 to estimate the sediment transport and dispersal in the year of 2005. We choose 2005 as the simulation period because (1) the study area has a similar wind and sea-level pressure pattern in 2005 with that averaged during 1948-2009 (Figs. 2a and 2b), and (2) the HyCOM/NCODA database has an ideal coverage in 2005. As in situ observations were very limited for the study area, model validation was based on water level data from a tidal station, Vung Tau, located at 10.4 ºN and 107.1 ºE (position see Fig. 4; water level validation see Figs. 6a and 6b), sea surface temperature based on the NOAA High-resolution data provided by the NOAA/OAR/ESRL PSD, Boulder, Colorado, USA, from their Web site at http://www.esrl.noaa.gov/psd/ (AVHRR, 0.25 degree resolution, Fig.7), and the Moderate Resolution Imaging Spectroradiometer (MODIS) images (Figs. 8a and 9a).

4. Results

4.1 Sediment Characteristics

The majority of the sediment cores in this study were recovered from the Mekong subaqueous delta, which was delineated based on seismic profiles (position of subaqueous

delta front see Fig.1, from Xue et al., 2010). The sediment cores generally consisted of brown mud with little evidence for bioturbation and few shells Two exceptions were cores MKII02 and MKII03 recovered from relative deep waters (water depth 11.0m for MKII02 and 15.6 m for MKII03) in the GOT, where no deltaic deposit was recorded on seismic profiling. Instead of high-porosity brown mud, these two cores were made up of green to gray colored silts with abundant shell debris. The clay mineralogical and geochemical characters of the sediment cores are described below.

4.1.1 Clay Mineralogy

The grain size and clay mineral composition shows little vertical variation throughout cores in the study area (Figs. 3 and 10). Spatially the surface sediments exhibit a fining trend from a sand-silt-clay mixture dominated by silt on the east coast of the MRD to a clayey silt on the west coast (Table 2). For sediment recovered from the subaqueous delta, illite (13-64%) was the dominant clay mineral, with an average content of 45%; kaolinite (9-32%) and chlorite (6-22%) were less abundant, with an average combined content of 35%. Smectite content increased significantly from 10% (averaged from cores MKI01, MKI02, MKII13) on the east coast to 42% (averaged from cores MKII01, MKII03, MKII05) on the west coast. While the limited smectite content on the east coast is similar with sediment in the Mekong River channel (average smectite content of 11%, Liu et al., 2007c), the high smectite content on the west coast indicates possible source materials from the GOT (average smectite content of 35%, Aoki, 1976; Fig. 10). Chen (1978) proposed that the high smectite content in the GOT sediments was derived mainly from the igneous material of the tropical archipelagoes.

4.1.2 ^{210}Pb, AMS ^{14}C, and δ^{13}C

15 cores were analyzed for ^{210}Pb activities. Supported levels for cores on the east shore and west shore are 1.44±0.3 dpm/g and 1.09±0.3 dpm/g mud (Xue et al., 2010). A supported level of 0.83±0.5 dpm/g mud was used for cores around Cape Camau in this study. The ^{14}C data reported in this study are given as "raw" ^{14}C ages instead of corrected ages (Xue et al., 2010). We assume that the ^{14}C age of the bulk organic matter has remained constant at the sediment-water interface over the duration of the dating interval. Based on excess ^{210}Pb profiles, AMS ^{14}C chronologies, and δ^{13}C values, sediment cores are classified into three basic types as indicated below.

I. Non-steady-state

Cores containing fluctuating ^{210}Pb activities are classified as "non-steady-state" type. The majority of the sediment cores collected in this study are characterized by this type. The "non-steady-state" cores show limited, if any, excess ^{210}Pb activity (for example, cores MKII13, MKII14, and MKII17 shown in Figs. 11a, 11b, and 11c). They are mainly located on the east shore of Camau Peninsula and areas around Cape Camau where the hydrodynamics are strong. Cored sediment consists of a silt-clay-sand mixture with little variation throughout a core. The radiocarbon data from these cores give an uncalibrated, or a "raw", ^{14}C age on the order of 1,100-1,800 yr. This "non-steady-state" ^{14}C activity could be a result of either physical or biological mixing. Nevertheless, considering these cores are mainly made up of homogeneous mud with few worm burrows or shells, these limited excess ^{210}Pb activities can be explained by physical processes such as resuspension or rapid accumulation. The δ^{13}C values of these samples vary between -23 and -25‰ (Table 4, except

for the surface sample of core MKII13, which has a value of -21.7‰), suggesting a mixed terrestrial/marine source for bulk organic carbon.

II. Fluid-mud

Cores containing high-porosity mud with no minimal excess ^{210}Pb activity are classified as "fluid-mud" type. The "fluid-mud" cores are mainly located in the shallow water along the west shore (e.g. Core MKII05 shown in Fig. 11d) and the west end of Cape Camau (e.g. core MKII09 shown in Fig. 11e). Three bulk sediment samples from the top (2 cm), middle (40 cm), and bottom (100 cm) of MKII09 have a ^{14}C age around 850 yr (Table 4, Xue et al., 2010). Both ^{210}Pb and ^{14}C profiles from this core are consistent with rapid accumulation. The δ^{13}C measurements indicate that the C_{org} is a mixture of terrestrial/marine origin (-24.1 to -24. 4‰, Table 4).

III. Steady-state

Although the majority of the cores in this study show either fluctuating or uniform ^{210}Pb activities, cores recovered from areas with no deltaic deposits (e.g. cores MKII02 and MKII03 shown in Figs. 11f and 11g) or seaward of the subaqueous delta limit (e.g. core MKII08 shown in Fig. 11h) exhibit exponentially decreasing ^{210}Pb activities with depth. Calculated apparent accumulation rate is 0.55 cm/yr for MKII02, 0.49 cm/yr for the lower 30 cm of MKII03, and 0.65 cm/yr for MKII08.

Bulk C_{org} ^{14}C measurements from the middle (20-22 cm) and bottom (60-62 cm) of MKII08 yields ages of 195±30 and 865±30 yr. For core MKII03, bulk C_{org} ^{14}C measurements of three samples from the top (0-1 cm), middle (30-32 cm) and bottom (53-55 cm) yielded ages of 50±25, 495±30, and 1570±30 yr, respectively (Xue et al., 2010). These young ^{14}C

ages are consistent with the greater relative abundance of marine planktonic organic matter at these site (as indicated by the $\delta^{13}C$ data, -20.7 ~ -21.5‰ for MKII08 and -20.7 ~ -21.1‰ for MKII03, Table 4).

4.2 Numerical Modeling

4.2.1 Overall Sediment Transport and Dispersal

Time-averaged for the twelve-month calculations in 2005, currents are strongest around the Mekong River mouth (Fig. 12b). Modeled turbidity is highest offshore of the river mouth. Areas of high average sediment concentration do not directly correspond to areas of high average wave orbital velocity (Figs. 12a and 12b). The highest Mekong sediment flux is within 20 km of the distributary mouths (Fig. 12c). Throughout the time modeled, the along-shelf sediment transport is to the southwest except for the SW monsoon season (May to September), discussed in more detail below.

Modeled Mekong sediment is confined to the subaqueous delta front (Fig.13a). More than 99% of Mekong sediment was deposited on the Mekong subaqueous delta delineated in Xue et al. (2010), based on seismic data. The majority of Mekong sediment deposits around the distributary mouths. Much of the Mekong sediment that traveled further is carried toward the southwest. These sediments contribute to a thin deposit parallel to the coast. Nearly all of the along-shelf transported Mekong sediment is characterized with slow settling velocities.

The bed shear stress on the Mekong shelf is mainly induced by current (Fig.14). Significant erosion/accretion is estimated for the area around the Con Son Island, the relative

shallow area around Cape Camau, and the deeper water in the northeast part of the model domain (Figs. 13b and 13c). Most erosion occurred in areas of high current shear stress (Figs. 13c and 14b). Net erosion accounts for 15.9 million tons of bed material (Table 3). Most of the eroded material is from the sand class (Table 3), which has a wider distribution on the initial sediment bed than the flocculated fine class. However, this estimate is sensitive to the initial sediment bed.

To test the influence from different forcings on sediment dynamics, several sensitivity tests were performed with different combinations of wind, wave, and tide. Results of sensitivity tests show that wind is the most important factor affecting local sediment transport. As shown in Fig. 13c, along-shelf sediment transport is significantly decreased once the wind was forced to zero.

4.2.2 NE Monsoon and SW Monsoon Transport

The hydrodynamics of the southern Vietnam shelf are strongly influenced by the Southeast Asian monsoon. This section characterizes transport patterns for January (low flow, NE monsoon season) and August 2005 (high flow, SW monsoon season).

The NE wind dominates the Mekong shelf during January (Fig. 8b). As January is a low flow season (monthly averaged freshwater discharge is 4,000 m^3/s), the presence of Mekong plume is not apparent. Both the MODIS image and model indicates that turbid or high-chlorophyll waters are present around the river mouth and in the coastal areas of the MRD. Figs. 15 and 16 indicate the estimated current speed (along-shelf and cross-shelf) and the SSC of the four different classes averaged for January and August 2005 at cross section

A-A' (position see Figs. 1 and 4). The along-shelf currents, to the southwest, dominate with mean speed of 0.085 m/s during January (Fig. 15b).

August is a typical high flow month (monthly averaged freshwater discharge is 28,000 m^3/s). The Mekong plume is apparent on both MODIS image and model (Fig. 9). The SW monsoon prevails the Mekong shelf. The along-shelf currents, to the northeast, dominate with mean speed of 0.083 m/s (Fig. 16b). The SSC value of both fine grained Mekong sediment and fine particles resuspended from the seabed are lower than those in January. This may explain the relative low turbidity along the coast of the MRD in August (Figs. 9a, 16c, and 16e).

The model reproduces the primary feature of the turbidity visible in MODIS images of the Mekong shelf. Although the direction of the prevailing winds and currents are opposite during the NE monsoon and SW monsoon seasons, the along-shelf transport dominates in both seasons. The high turbidity along the MRD is composed of fine grained Mekong sediment and sediment resuspended from the seabed (Figs. 15c, 15e, 16c, and 16e). Flocculated Mekong sediment is not present on cross section A-A' (Figs. 15d and 16d). Sand is capable of being resuspended from seabed in both monsoon seasons and the bottom boundary layer holds most of the resuspended sand (Figs. 15f and 16f).

5. Discussion

5.1 Source of Sedimentary Organic Matter

Sedimentary organic matter on the Mekong shelf has two potential sources: in situ primary productivity and terrestrial organic matter from fluvial sediment. For the latter one, it may consist of aged/modern soil humus and plant debris/fragments derived from C3 vascular plants (rice and mangrove are dominant plants on the MRD) and recycled sedimentary rock C_{org} (kerogen). ^{14}C measurements yielded few young ages for bulk organic matter on the subaqueous delta, indicating a significant contribution from 'old' organic material supplied by fluvial sediment or from the resuspension of previously deposited sediment. Continuously observations of the bulk organic matter in the Mekong river channel indicated that the $\delta^{13}C$ end-member in the river ranges from -28.0 to -32.0‰ and the C/N ratios range from 7 to12 (personal contact with Erin Ellis and Dr. Jeffrey Richey in the University of Washington). Marine bulk organic matter from surface sediment is usually dominated by algae, and in general has $\delta^{13}C$ values ranging from -19.0 to -22.0‰ (Fontugne and Jouanneau, 1987) and the C/N ratios < 10 (Meyers et al., 1994). Thus, the $\delta^{13}C$ values of cores recovered from the subaqueous delta confirm a mixed terrestrial/marine source (between -21.7 and -25.0‰, Table 4). The grain size is not correlated with water depth, indicating a strong physical reworking on the subaqueous delta (Fig. 17a). C_{org} and N_{org} contents show increasing trend with water depth, however, their correlation is not significant (Figs. 17b and 17c).

Plotting $(C/N)\times C_{org}$, $\delta^{13}C\times C_{org}$, and the (Fraction modern C_{org})$\times C_{org}$ against C_{org} produces a set of linear relationships with slopes indicative of the composition of the added

C_{org} (Blair et al., 2003; Leithold et al., 2006). The atomic C/N value of 8.2 and $\delta^{13}C$ value of -21.2‰ indicates the added C_{org} is primarily of marine-sourced (Figs. 18a and 18b). The ^{14}C-signature of the terrestrial and marine C_{org} added to the shelf sediments is 100%, indicating considerable incorporation of modern or bomb-produced carbon (Fig. 18b). These result indicate an increasing modern marine organic matter input as the sediment being transported into deep waters.

However, considering the different behaviors in the mineralization process between terrigenous and marine organic carbon, caution should be taken when $\delta^{13}C$ is used as the index of paleo-environment. A recent study of Fly River sediment shows that tropical mountainous river margins can sequester significant amount of carbon over decadal to century timescales, most of which appears to be terrigenous in origin and derived from aged soil organic materials (Goni et al., 2008). In other words, the lack of marine carbon and low vascular plant detritus indicates that they are more labile components of the organic materials (Goni et al., 2008; Aller et al., 2008). Meanwhile, segregation during sorting in the marine environment can winnow vascular plant detritus of high C/N ratios, leaving in near-shore regions soil organic matter with C/N ratio similar to marine carbon (Leithold and Blair, 2001).

5.2 Resuspension Processes

Clay mineral analysis in this study shows that Mekong sediment is the major source material for the subaqueous delta. The model result shows that nearly all of the Mekong sediment is trapped on the subaqueous delta (Fig. 13a), substantiating the rapid prograding

delta front revealed by seismic profiling (Xue et al., 2010). However, instead of fine sediment settling out of suspension, the Mekong sediment appears to go through cycles of trapping and resuspension before finally depositing on the subaqueous delta front. Both geochemical analyses of cored sediments and modeled results shed light on resuspension processes over different time scales.

The model result showed that on seasonal to yearly time scales, bottom currents provide the primary energy for resuspension (Figs. 14a and 14b). For both NE monsoon and SW monsoon season, the resuspended sediment along the eastern part of the MRD consist of fine grained delivered by the Mekong river and from the seabed (Figs. 15 and 16). Fig. 19 shows the modeled suspended sediment concentration (averaged over 2005) and the seismic profile recovered at cross section B-B'. The erosional feature on the topset of the clinoform is directly beneath the water of high SSC values. The strong reflection on the surface of the seabed indicates extensive sandy deposits, which is confirmed by grain size data. The sediment from two cores recovered from this area, i.e. MKII13 and MKII14, is a sand-silt-clay mixture and is the coarsest sample in this study. This sandy surface and the grain size data confirm the resuspension process shown by the model result.

On decadal to centennial time scales, the ^{210}Pb profiles of cores from the subaqueous delta show either fluctuating or uniform excess ^{210}Pb activities down core, indicating a rapid accumulation or strong physical mixing process (Figs. 11a to 11e). The C_{org} $\delta^{13}C$ results show that the source of the bulk C_{org} is a marine/terrestrial mix, instead of a terrestrialy-dominated one. The AMS ^{14}C chronology data indicate a considerable contribution from aged C_{org} as a result of either physical weathering of 'old' soil in the basin or, more possible as confirmed

by the model result, the resuspension of previously deposited shelf sediments. A similar resuspension process has been documented on the Amazon Delta (Kineke et al., 1996), which has a comparable marine power/ river power ratio with that of the MRD (Syvitski and Saito, 2007; Table 5).

5.3 Seasonal Transport Patterns

The Mekong plume is mostly geostrophic (Hordoir et al., 2006). Model results from this study show that, on a seasonal scale, the along-shelf transport of Mekong sediment is strongly influenced by the direction and strength of prevailing winds (Figs. 8b, 9b, 15b, and 16b). A river plume will become a coastal current, if strengthened by a downwelling-favorable (southwestward for the Western Pacific) wind or ambient current (Geyer et al., 2004). During the high flow season both monsoon and ambient circulation are northeastward, which weakens the coastal current formed by geotropically balanced Mekong plume. While during the low flow season, strong dry NE monsoonal winds dominate the shelf area. The ambient circulation also shifts its direction southwestward. Thus, the coastal currents are strengthened. Similar seasonal variations in sediment transport patterns have also been documented for the two major dispersal systems on the Western Pacific, i.e. the Yangtze and Yellow (East Asian Monsoon, Yang et al., 1992; Sun et al., 2000), as well as other large rivers around the world such as the Amazon (trade winds, Allison et al., 1995) and Po (Bora and Sirocco Winds, Harris et al., 2008) (comparisons of key parameters see Table 5).

Besides the along-shelf components, a downwelling NE monsoon should also

introduce a cross-shelf transport in the bottom layers toward deep waters. However, both seismic profiles (Xue et al., 2010) and model results show that the Mekong sediment has been mainly trapped within 20 km of the delta plain. This is likely because of: (1) the low-gradient shallow Vietnamese shelf buffers the exchange between coastal waters and deeper waters; and (2) the strength of winter monsoon in the SCS is not comparable with that in the northern Western Pacific and thus the cross-shelf transport is limited.

5.4 Delta Evolution during the Neoglaciation

Like other modern delta systems, the MRD initiated its progradation during last high sea-level stand. A very unique feature of the MRD is the phase shift from a "tide dominated delta" to a "tide and wave dominated delta" around 3,000 yrs BP (Ta et al., 2002a and b). As shown in Fig. 1, over the past 3,000 yrs, the MRD's evolution exhibits a morphological asymmetry with a huge downdrift area. The most rapid progradation has been documented around the river mouth and Cape Camau (Xue et al., 2010). However, progradation along the east shore of the MRD is very limited.

Stalagmite study of the Dongge cave in southern China reveals an abrupt cold event around 3,000 yr BP in Asia, which is coincident with the Bond event 2 recorded in northern Atlantic (Wang et al., 2005; Cosford et al., 2008; and Bond et al., 2001). The Bond event 2, standing for the beginning of Neoglacial period of the Late Holocene, has been associated with intensified winter monsoonal circulation and tropical aridity (Cosford et al., 2008). Ta et al. (2002a) points out that variation in monsoon activities during Late Holocene can be a

possible reason for MRD's phase shift. However, the relationship between the variations in monsoon intensity, alongshore sediment transport, and the delta morphodynamics was not clear until this study.

Numerical modeling facilitates our understanding of monsoon's influence on local sediment transport. Sensitivity tests in this study show that, on seasonal to yearly time scales, wind is a most important forcing influencing local sediment transport. The variations in monsoon activities during the Neoglaciation can affect the along-shelf sediment transport and the delta morphodynamics in two ways: (1) during high flow seasons, tropical aridity limits the rainfall, sediment yield, and thus the SSC along the Mekong channel. Less source materials are delivered to the river mouth; and (2) during the low flow season, wave energy and coastal currents are strengthened by an intensified NE winter monsoon, resuspending and transporting more Mekong sediment toward the GOT. Although model results showed that current-induced bed shear stress dominate the shelf, the coastal area is mainly influenced by wave-induced bed shear stress (Figs. 12a and 14c). This is confirmed by the "coarsening-upward succession" in boreholes (Ta et al., 2002a).

The ratio of the proxy of marine power and river power for the Mekong Delta is comparable with that of Po, however, the MRD develops into a subaqueous-delta-clinoform system instead of a proximal-accumulation-dominated system (Syvitski and Saito, 2007; Walsh and Nittrouer, 2009; Table 5). Instead of being transported hundreds of kilometers along the coast like the Yangtze and Po, the majority of Mekong sediment has been trapped around the delta system. This is mainly because that the MRD is located in the middle of the GOT and the SCS. Due to reduced tidal mixing in the GOT (1.0 m tide compared with the

3.5 m tide in the SCS), a large part of along-shelf transported sediment settles out, forming the rapid prograding Cape Camau (Fig. 1). Along the east shore, limited delta progradation may be explained by strengthened current-induced bed shear stress.

5.5 Limitations of the Model

As pointed by Harris et al. (2008), high resolution numerical modeling is usually limited on seasonal to yearly scales, thus the interannual variability, morphodynamics, or extreme events are not well developed. In this study the year 2005 was selected as the simulation period to represent a general sediment transport and dispersal pattern under normal climatic conditions. No storm or flooding event was included.

The 12-month calculation indicates that 99% of Mekong sediment deposited on the subaqueous delta, however, over a longer time scale, Late Holocene sediment budget estimation shows that only ~ 80±18 % of Mekong sediment was trapped within the delta system over the past 3,000 yrs (Xue et al., 2010). This discrepancy may be explained by variations in sediment flux, bulk bed properties, sea-level, and climate conditions during the Late Holocene.

As in situ observation of the Vietnam shelf is very limited, in this study we had to rely on results of large scale models and observations such as NCEP, HyCOM/NCODA, and TOPEX. Although our model reproduced the general pattern of water level fluctuation, seasonal variations of sea surface temperature, and the turbidity shown by MODIS images, high resolution in situ data are expected to enhance the accuracy of the model.

6. Conclusions

The XRD result shows that Mekong sediment is a dominant source material for the subaqueous delta. The influence from Gulf of Thailand is apparent for sediment along the west shore of the Camau Peninsula, which has a relatively high smectite contents (up to 42%). The majority of bulk carbon has a $\delta^{13}C$ value between -22.7 and -25.0‰ and the AMS ^{14}C yields no young age, indicating a mixture of terrestrial "aged" and fresh marine origin.

$\delta^{13}C$ and AMS ^{14}C values of bulk carbon indicate a mixture of terrestrially "aged" and fresh marine organic matter. Based on excess ^{210}Pb profiles, AMS ^{14}C chronologies, and $\delta^{13}C$ values, sediment cores in this study are classified into three basic types, which are: I. Non-steady-state sedimentation, II. Fluid mud deposits, and III. Steady-state sedimentation. The majority of excess ^{210}Pb profiles have either highly fluctuating or uniform activities down core, indicating strong physical mixing processes or rapid accumulation. Relatively steady accumulation is documented in areas without deltaic deposits or seaward of the subaqueous delta front.

A 13-month numerical model was performed using the Regional Ocean Modeling System (ROMS) and the Community Sediment Transport Model System (CSTMS) to simulate the sediment transport and dispersal in 2005. The modeling system represents the major processes that control sediment dispersal and reproduces turbidity shown by MODIS images. Model calculations indicate that 99% of Mekong sediment has been trapped within 20 km of the delta plain. Depth-integrated sediment flux calculation indicates that the net sediment transport during a 12-month period was to the southwest. Sensitivity tests show that wind is the most important force influencing local sediment transport. Wave orbital velocity

and wave-induced bed shear stress are increasingly important in shallow water.

Along-shelf transport dominates both NE monsoon and SW monsoon seasons. Although the along-shelf current shifts its direction during two monsoon seasons, the turbidity along the delta plain is composed of fine sediment from the Mekong and resuspended from the seabed during both seasons. The sandy sediment is capable of being resuspended mainly by current-induced bed shear stress.

References

Aller, R.C., Blair, N.E. and Brunskill, G.J., 2008. Early diagenetic cycling, incineration, and burial of sedimentary organic carbon in the central Gulf of Papua (Papua New Guinea). Journal of Geophysical Research, 113: F01S09.

Aller, R.C., Blair, N.E., Xia, Q. and Rude, P.D., 1996. Remineralization rates, recycling, and storage of Corg in Amazon Shelf sediments. Continental Shelf Research, 16: 753-786.

Allison, M.A., Nittrouer, C.A. and Kineke, G.C., 1995. Seasonal sediment storage on mudflats adjacent to the Amazon River. Marine Geology, 125(3-4): 303-328.

Aoki, S., 1976. Clay mineral distribution in sediments of the Gulf of Thailand and the South China Sea. Journal of Oceanography, 32(4): 169-174.

Becker, J.J. et al., 2009. Global Bathymetry and Elevation Data at 30 Arc Seconds Resolution: SRTM30_PLUS. Marine Geodesy, 32(4): 355-371.

Blair, N.E., Leithold, E.L. and Aller, R.C., 2004. From bedrock to burial: The evolution of particulate organic carbon across coupled watershed-continental margin systems. Marine Chemistry, 92: 141-156.

Blair, N.E. et al., 2003. The persistence of memory: the fate of ancient sedimentary organic carbon in a modern sedimentary system. Geochimica et Cosmochimica Acta, 67(1): 63-73.

Bond, G. et al., 2001. Persistent solar influence on North Atlantic climate during the Holocene. Science, 294(5549): 2130-2136.

Chassignet, E.P. et al., 2007. The HYCOM (HYbrid Coordinate Ocean Model) data

assimilative system. Journal of Marine Systems, 65(1-4): 60-83.

Chen, P.-Y., 1978. Minerals in bottom sediments of the South China Sea. Geological Society of America Bulletin, 89: 211-222.

Chen, Z., Song, B., Wang, Z. and Cai, Y., 2000. Late Quaternary evolution of the sub-aqueous Yangtze Delta, China: sedimentation, stratigraphy, palynology, and deformation. Marine Geology, 162(2-4): 423-441.

Coleman, J.M. and Roberts, H.H., 1989. Deltaic coastal wetlands. Geologie en Mijnbouw, 68: 1-24.

Cosford, J. et al., 2008. East Asian monsoon variability since the Mid-Holocene recorded in a high-resolution, absolute-dated aragonite speleothem from eastern China. Earth and Planetary Science Letters, 275(3-4): 296-307.

Dai, S.B., Yang, S.L. and Cai, A.M., 2008. Impacts of dams on the sediment flux of the Pearl River, southern China. CATENA, 76(1): 36-43.

Debenay, J.-P. and Luan, B.T., 2006. Foraminiferal assemblages and the confinement index as tools for assessment of saline intrusion and human impact in the Mekong Delta and neighbouring areas (Vietnam). Revue de Micropaleontologie, 49(2): 74-85.

DeMaster, D.J., Pope, R.H., Levin, L.A. and Blair, N.E., 1994. Biological mixing intensity and rates of organic carbon accumulation in North Carolina slope sediments. Deep-Sea Research II, 41(4-6): 735-753.

Egbert, G.D. and Erofeeva, S.Y., 2002. Efficient inverse modeling of barotropic ocean tides. Journal of Atmospheric and Oceanic Technology, 19(2).

Fontugne, M.R. and Jouanneau, J.M., 1987. Modulation of the particulate organic carbon

flux to the ocean by a macrotidal estuary - evidence from measurements of carbon isotopes in organic matter from the Gironde Estuary. Estuarine, Coastal and Shelf Science, 24: 377-387.

Gagliano, S.M. and Mcintire, W.G., 1968. Reports on the Mekong River Delta, Louisiana State University.

Geyer, W.R., Hill, P.S. and Kineke, G.C., 2004. The transport, transformation and dispersal of sediment by buoyant coastal flows. Continental Shelf Research, 24(7-8): 927-949.

Goni, M.A. et al., 2008. Terrigenous organic matter in sediments from the Fly River delta-clinoform system (Papua New Guinea). Journal of Geophysical research, 113.

Harris, C.K., Sherwood, C.R., Signell, R.P., Bever, A.J. and Warner, J.C., 2008. Sediment dispersal in the northwestern Adriatic Sea. Journal of Geophysical Research, 113(C11S03): doi:10.1029/2006JC003868.

Hedges, J.I. and Keil, R.G., 1995. Sedimentary organic matter preservation: an assessment and speculative synthesis. Marine Chemistry, 49(2-3): 81-115.

Hordoir, R., Polcher, J., Brun-Cottan, J.-C. and Madec, G., 2006. Towards a parametrization of river discharges into ocean general circulation models: a closure through energy conservation. Climate Dynamics, 31(7-8): 891-908.

Hori, K. et al., 2001. Sedimentary facies and Holocene progradation rates of the Changjiang (Yangtze) delta, China. Geomorphology, 41(2-3): 233-248.

Hori, K. et al., 2004. Delta initiation and Holocene sea-level change: example from the Song Hong (Red River) delta, Vietnam. Sedimentary Geology, 164(3-4): 237-249.

Hu, J., Kawamura, H., Hong, H. and Qi, Y., 2004. A review on the currents in the South

China Sea: Seasonal circulation, South China Sea warm current and Kuroshio intrusion. Journal of Oceanography, 56(6): 607-624.

Kalnay, E. et al., 1996. The NCEP/NCAR 40-year reanalysis project. Bull. Amer. Meteor. Soc., 77: 437-470.

Kineke, G.C., Sternberg, R.W., Trowbridge, J.H. and Geyer, W.R., 1996. Fluid-mud processes on the Amazon continental shelf. Continental Shelf Research, 16(5-6): 667-696.

Kubicki, A., 2008. Large and very large subaquesous dunes on the continental shelf off southern Vietnam, South China Sea. Geo-Marine Letters, 28: 229-238.

Le, T.V.H., Nguyen, H.N., Wolanski, E., Tran, T.C. and Haruyama, S., 2007. The combined impact on the flooding in Vietnam's Mekong River delta of local man-made structures, sea level rise, and dams upstream in the river catchment. Estuarine, Coastal and Shelf Science, 71(1-2): 110-116.

Leithold, E.L. and Blair, N.E., 2001. Watershed control on the carbon loading of marine sedimentary particles. Geochimica et Cosmochimica Acta, 65(14): 2231-2240.

Leithold, E.L., Blair, N.E. and Perkey, D.W., 2006. Geomorphologic controls on the age of particulate organic carbon from small mountainous and upland rivers. Global Biogeochemical Cycles, 20: GB3022.

Li, G., Wei, H., Yue, S., Cheng, Y. and Han, Y., 1998. Sedimentation in the Yellow River delta, part II: suspended sediment dispersal and deposition on the subaqueous delta. Marine Geology, 149(1-4): 113-131.

Li, Z. et al., 2006. Climate change and human impact on the Song Hong (Red River) Delta, Vietnam, during the Holocene. Quaternary International, 144(1): 4-28.

Liu, J., Saito, Y., Wang, H., Yang, Z. and Nakashima, R., 2007a. Sedimentary evolution of the Holocene subaqueous clinoform off the Shandong Peninsula in the Yellow Sea. Marine Geology, 236(3-4): 165-187.

Liu, J.P. et al., 2008. Flux and fate of small mountainous rivers derived sediments into the Taiwan Strait. Marine Geology, 256(1-4): 65-76.

Liu, J.P., Milliman, J.D., Gao, S. and Cheng, P., 2004a. Holocene development of the Yellow River's subaqueous delta, North Yellow Sea. Marine Geology, 209(1-4): 45-67.

Liu, J.P. et al., 2007b. Flux and fate of Yangtze River sediment delivered to the East China Sea. Geomorphology, 85(3-4): 208-224.

Liu, Z. et al., 2004b. Erosional history of the eastern Tibetan Plateau since 190 kyr ago: clay mineralogical and geochemical investigations from the southwestern South China Sea. Marine Geology, 209(1-4): 1-18.

Liu, Z. et al., 2005. Late Quaternary climatic control on erosion and weathering in the eastern Tibetan Plateau and the Mekong Basin. Quaternary Research, 63(3): 316-328.

Liu, Z., Zhao, Y., Li, J. and Colin, C., 2007c. Late Quaternary clay minerals off Middle Vietnam in the western South China Sea: Implications for source analysis and East Asian monsoon evolution. Science in China, 50(11): 1674-1684.

Lu, X.X. and Siew, R.Y., 2006. Water discharge and sediment flux changes over the past decades in the Lower Mekong River: possible impact of the Chinese dams. Hydrology and Earth System Sciences, 10: 181-195.

Meyers, P.A., 1994. Preservation of elemental and isotopic source identification of sedimentary organic matter. Chemical Geology, 114: 289-302.

Milliman, J.D. and Kao, S.J., 2005. Hyperpycnal discharge of fluvial sediment to the ocean: Impact of super typhoon Herb (1996) on Taiwanese rivers

doi:10.1086/431906. The Journal of Geology, 113(5): 503-516.

Milliman, J.D. and Meade, R.H., 1983. World-wide delivery of river sediment to the oceans. Journal of Geology, 91: 1-21.

Milliman, J.D., Rutkowski, C. and Meybeck, M., 1995. River discharge to the sea: a global rive index. LOICZ Core Project Office, Texel, Netherlands, 125 pp.

Milliman, J.D. and Syvitski, J.P.M., 1992. Geomorphic/tectonic control of sediment discharge to the ocean: The importance of small mountainous rivers. Journal of Geology, 100: 525-544.

Nguyen, L.V., Ta, T.K.O. and Tateishi, M., 2000. Late Holocene depositional environments and coastal evolution of the Mekong River Delta, Southern Vietnam. Journal of Asian Earth Sciences, 18(4): 427-439.

Nguyen, V.L. et al., 2005. Late Quaternary depositional sequences in the Mekong River Delta, Vietnam. In: Z.Y. Chen, Y. Saito and S.L.J. Goodbred (Editors), Mega-Deltas of Asia. China Ocean Press, Beijing, pp. 121-127.

Saito, Y., 2000. Deltas in Southeast and East Asia: Their evolution and current problems. In: N. Mimura and H. Yokoki (Editors), APN/SURVAS/LOICZ Joint Conference on Coastal Impact of Climate Change and Adaption in the Asia-Pacific Region, Kobe, Japan, pp. 185-191.

Shchepetkin, A.F. and McWilliams, J.C., 2005. The Regional Ocean Modeling System (ROMS): a split-explicit, free-surface, topography-following coordinates ocean model.

Ocean Modelling, 9: 347-404.

Steinke, S., Hanebuth, T.J.J., Vogt, C. and Stattegger, K., 2008. Sea level induced variations in clay mineral composition in the southwestern South China Sea over the past 17,000 燰 r. Marine Geology, 250(3-4): 199-210.

Sun, X., Fang, M. and Huang, W., 2000. Spatial and temporal variations in suspended particulate matter transport on the Yellow and East China Sea shelf. Oceanologia et Limnologia Sinica, 31(6): 581-587(in Chinese).

Syvitski, J.P.M. and Saito, Y., 2007. Morphodynamics of deltas under the influence of humans. Global and Planetary Change, 57(3-4): 261-282.

Syvitski, J.P.M., Vorosmarty, C.J., Kettner, A.J. and Green, P., 2005. Impact of humans on the flux of terrestrial sediment to the global coastal ocean. Science, 308(5720): 376-380.

Ta, T.K.O., Nguyen, V.L., Kobayashi, I., Tateishi, M. and Saito, Y., 2001a. Late Pleistocene-Holocene stratigraphy and delta progradation, the Mekong River Delta, South Vietnam. Gondwana Research, 4(4): 799-800.

Ta, T.K.O., Nguyen, V.L., Tateishi, M., Kobayashi, I. and Saito, I., 2005. Holocene delta evolution and depositional models of the Mekong River Delta, Southern Vietnam. In: L. Giosan and J.P. Bhattacharya (Editors), River Deltas-Concepts, Models, and Examples. SEPM, Tulsa.

Ta, T.K.O., Nguyen, V.L., Tateishi, M., Kobayashi, I. and Saito, Y., 2001b. Sedimentary facies, diatom and foraminifer assemblages in a late Pleistocene-Holocene incised-valley sequence from the Mekong River Delta, Bentre Province, Southern Vietnam: the BT2 core. Journal of Asian Earth Sciences, 20(1): 83-94.

Ta, T.K.O. et al., 2002a. Sediment facies and Late Holocene progradation of the Mekong River Delta in Bentre Province, southern Vietnam: an example of evolution from a tide-dominated to a tide- and wave-dominated delta. Sedimentary Geology, 152(3-4): 313-325.

Ta, T.K.O. et al., 2002b. Holocene delta evolution and sediment discharge of the Mekong River, southern Vietnam. Quaternary Science Reviews, 21(16-17): 1807-1819.

Tamura, T. et al., 2009. Initiation of the Mekong River delta at 8 ka: evidence from the sedimentary succession in the Cambodian lowland. Quaternary Science Reviews, 28(3-4): 327-344.

Tanabe, S. et al., 2006. Holocene evolution of the Song Hong (Red River) delta system, northern Vietnam. Sedimentary Geology, 187(1-2): 29-61.

Walsh, J.P. and Nittrouer, C.A., 2009. Understanding fine-grained river-sediment dispersal on continental margins. Marine Geology, 263(1-4): 34-45.

Wan, S., Li, A., Clift, P.D. and Stuut, J.-B.W., 2007. Development of the East Asian monsoon: Mineralogical and sedimentologic records in the northern South China Sea since 20 Ma. Palaeogeography, Palaeoclimatology, Palaeoecology, 254(3-4): 561-582.

Wang, H. et al., 2007. Stepwise decreases of the Huanghe (Yellow River) sediment load (1950-2005): Impacts of climate change and human activities. Global and Planetary Change, 57(3-4): 331-354.

Wang, H., Yang, Z., Wang, Y., Saito, Y. and Liu, J.P., 2008. Reconstruction of sediment flux from the Changjiang (Yangtze River) to the sea since the 1860s. Journal of Hydrology, 349(3-4): 318-332.

Wang, P.P., 2005. The coastal environment of Southeast Asia. In: A. Gupta (Editor), The Physical Geography of Southeast Asia. Oxford, New York, pp. 179-180.

Wang, Y. et al., 2005. The Holocene Asian monsoon: Links to solar changes and North Atlantic climate. Science, 308(5723): 854-857.

Warner, J.C., Sherwood, C.R., Signell, R.P., Harris, C.K. and Arango, H.G., 2008. Development of a three-dimensional, regional, coupled wave, current, and sediment-transport model. Computers & Geosciences, 34(10): 1284-1306.

Wei, T. et al., 2007. Sedimentation rates in relation to sedimentary processes of the Yangtze Estuary, China. Estuarine, Coastal and Shelf Science, 71(1-2): 37-46.

Wolanski, E., Ngoc Huan, N., Trong Dao, L., Huu Nhan, N. and Ngoc Thuy, N., 1996. Fine-sediment dynamics in the Mekong River estuary, Vietnam. Estuarine, Coastal and Shelf Science, 43(5): 565-582.

Wolanski, E., Nguyen, H.N. and Spagnol, S., 1998. Sediment dynamics during low flow conditions in the Mekong River Estuary, Vietnam. Journal of Coastal Research, 14: 472-482.

Xue, Z., Liu, J.P., DeMaster, D., Nguyen, V.L. and Ta, T.K.O., 2010. Late Holocene evolution of the Mekong subaqueous delta, southern Vietnam. Marine Geology, 269(1-2): 46-60.

Xue, Z., Liu, J.P. and Ge, Q., in press. Changes in Hydrology and Sediment Delivery of the Mekong River in the last 50 years: Connection to Damming, Monsoon, and ENSO. Earth Surface Processes and Landforms.

Yang, S.L. et al., 2003. Delta response to decline in sediment supply from the Yangtze River: Evidence of the recent four decades and expectations for the next half-century. Estuarine,

Coastal and Shelf Science, 57(4): 689-699.

Yang, Z.S., Guo, Z. and Wang, Z.X., 1992. The macro pattern of suspended particulate mattter transport to the eastern open ocean on the Yellow and East China Sea Shelf. Acta Oceanologica Sinica, 14(2): 81-90 (in Chinese).

Yang, Z.S. and Liu, J.P., 2007. A unique Yellow River-derived distal subaqueous delta in the Yellow Sea. Marine Geology, 240(1-4): 169-176. Aller, R.C., Blair, N.E. and Brunskill, G.J., 2008. Early diagenetic cycling, incineration, and burial of sedimentary organic carbon in the central Gulf of Papua (Papua New Guinea). Journal of Geophysical Research, 113: F01S09.

Tables

Table 1. Major fluvial sediment inputs to the Western Pacific

River System	Sediment Flux (million ton/ yr)	Reference
Yellow (Huanghe)	1100 (150*)	Milliman and Syvitski, 1992
Yangtze (Changjiang)	480 (189*)	Milliman and Syvitski, 1992
Mekong (Lancang)	160	Milliman and Syvitski, 1992
Red (Songhong)	130	Milliman et al., 1995
Pearl (Zhujiang)	63	Dai et al., 2008
Taiwanese Rivers	300	Liu et al., 2008

* Updated sediment flux of the Yellow and Yangtze Rivers are from Wang et al., 2007 and 2008

Table 2. Details of sediment cores

Core no.	Longitude (º) E	Latitude (º) N	Water Depth (m)	Core Length (cm)	Grain Size (μm, vertically averaged*)	# of Clay Mineral Samples
MKI01	106.265	9.347	4.5	15.0	--	6
MKI02	105.900	9.243	5.0	27.0	--	10
MKI03	105.378	8.905	6.0	32.0	--	--
MKII01	104.984	9.970	2.0	54.0	11.78	3
MKII02	104.689	9.903	11.0	47.0	27.16	--
MKII03	104.408	9.841	15.6	57.0	36.87	--
MKII05	104.800	9.348	3.0	75.0	14.18	3
MKII07	104.743	9.125	10.0	49.0	14.79	--
MKII08	104.496	8.983	25.0	64.0	18.91	--
MKII09	104.561	8.801	10.0	101.0	11.87	3
MKII11	104.506	8.709	19.0	64.0	--	--
MKII12	104.456	8.703	20.0	26.0	--	--
MKII13	105.495	8.942	8.0	65.0	38.92	3
MKII14	105.288	8.512	16.0	50.0	40.14	--
MKII15	105.115	8.544	6.0	26.0	--	--
MKII16	104.827	8.522	5.0	45.0	17.55	--
MKII17	104.715	8.434	15.0	42.0	13.56	--
MKII18	104.532	8.623	22.0	11.0	19.91	--
MKII20	104.565	8.627	1.6	45.0	41.69	--

* grain size values were measured with 10 cm intervals down core.

Table 3. Hydrodynamic properties and model calculated budget of different sediment classes

Sediment Source	Class	Sediment Type	τ_{cr} (Pa)*	W_s (mm/s)*	Fraction of Input*	supplied (million ton)
Mekong River	1	fine grained	0.03	0.1	10% of Mekong	15.4
Mekong River	2	flocculated	0.08	1.0	90% of Mekong	148.9
Seabed	3	flocculated fines	0.10	1.0	spatially variable	1.3
Seabed	4	sand	0.12	10.0	spatially variable	14.6

W_s: settling velocity; τ_{cr}: critical shear stress

*similar setup with that of Harris et al. (2008).

Table 4. Organic matter contents and AMS 14C ages of bulk sediments

Core No.	Sample Depth (cm)	δ^{13} C (per mil)	C%	N%	$(C/N)_{atom}$	^{14}C age* (yrs)
MKII03**	0-1	-21.1	0.99	0.14	8.3	50 ± 25
	30-32	-20.7	0.76	0.10	8.9	495 ± 30
	53-55	-20.8	0.76	0.09	9.7	1570 ± 30
MKII07**	0-1	-23.3	0.91	0.12	8.6	800 ± 25
	14-16	-22.7	0.75	0.10	9.0	1300 ± 25
	30-32	-23.8	0.56	0.06	10.1	2930 ± 30
	45-47	-24.2	0.61	0.07	10.2	3120 ± 35
MKII08	20-22	-21.5	1.42	0.19	8.6	195 ± 30
	60-62	-20.7	1.45	0.20	8.5	865 ± 30
MKII09**	0-1	-24.3	0.92	0.11	9.7	865 ± 25
	40-42	-24.1	0.88	0.11	9.2	830 ± 25
	100-102	-24.4	0.89	0.11	9.6	845 ± 25
MKII11	20-22	-23.9	1.01	0.13	9.3	965 ± 25
	40-42	-23.7	0.92	0.11	9.7	1050 ± 25
	60-62	-23.7	0.94	0.12	9.6	1110 ± 25
MKII13	0-1	-21.7	0.11	0.02	6.4	1520 ± 40
	20-22	-25.0	0.66	0.07	11.0	1550 ± 30
	60-62	-24.7	0.90	0.10	10.7	1530 ± 25
MKII14**	0-1	-23.3	0.55	0.07	9.8	1840 ± 30
	20-22	-23.6	0.58	0.07	10.1	1350 ± 40
	40-42	-23.2	0.52	0.06	10.0	1800 ± 30
MKII16	20-22	-23.8	0.89	0.11	9.7	1780 ± 30
MKII17	0-1	-23.5	0.93	0.12	9.3	1090 ± 30
	20-22	-23.5	0.85	0.11	8.7	1160 ± 30
	40-42	-23.3	0.92	0.13	8.4	1080 ± 25

* These ^{14}C data are "raw" ^{14}C ages that have not been corrected for reservoir age or atmospheric ^{14}C variations, see explanations in Xue et al. (2010);

** Data of cores MKII03, MKII09, MKII07, and MKII14 are partially from Xue et al., (2010).

Table 5. Comparisons of key parameters between the Mekong and other mega deltas (revised after Syvitski and Saito, 2007 and Walsh and Nittrouer, 2009)**.** Q_{av}: average water discharge; D_{grd}: gradient of the delta plain, W_a: maximum wave height, T_i: tidal range, D_{mm}: average grain size, P_m: proxy of marine power ($W_a^2+T_i^2$), Pr: proxy for river power ($11\times Q_{av}\times D_{grd}$), SDC: subaqueous-delta-clinoform systems, PAD: proximal-accumulation-dominated systems.

River	Q_{av} (m^3/s)	D_{grd}	W_a(m)	T_i(m)	D_{mm}(mm)	P_m/P_r	Class
Mekong	17,345	0.00003	1.5	3.5	0.1	2.5	SDC
Yangtze	28,278	0.00006	1.5	4.5	0.05	0.7	SDC
Yellow	1,480	0.00100	1.5	0.8	0.06	0.1	PAD
Po	1,525	0.00004	1.5	0.7	0.4	2.2	PAD
Amazon	198,676	0.0001	2.0	6.0	0.03	1.7	SDC

Figures

Fig. 1. A position map of the study area, gravity cores, and cross section A-A'. The position of paleo and modern delta front is from Nguyen et al., 2000 and Xue et al. 2010, respectively.

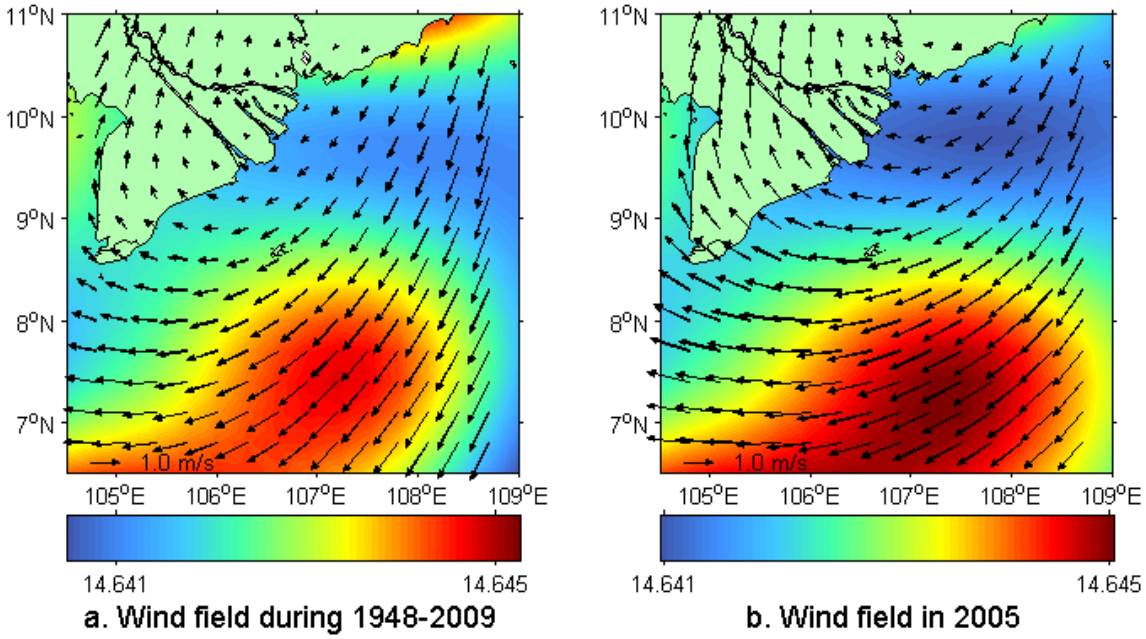

Fig. 2. Wind field and sea level pressure of the study area. Arrows stand for wind, sea level pressure is in color (unit: millibars). Data is based on NCEP reanalysis during a.1948-2009 and b. 2005.

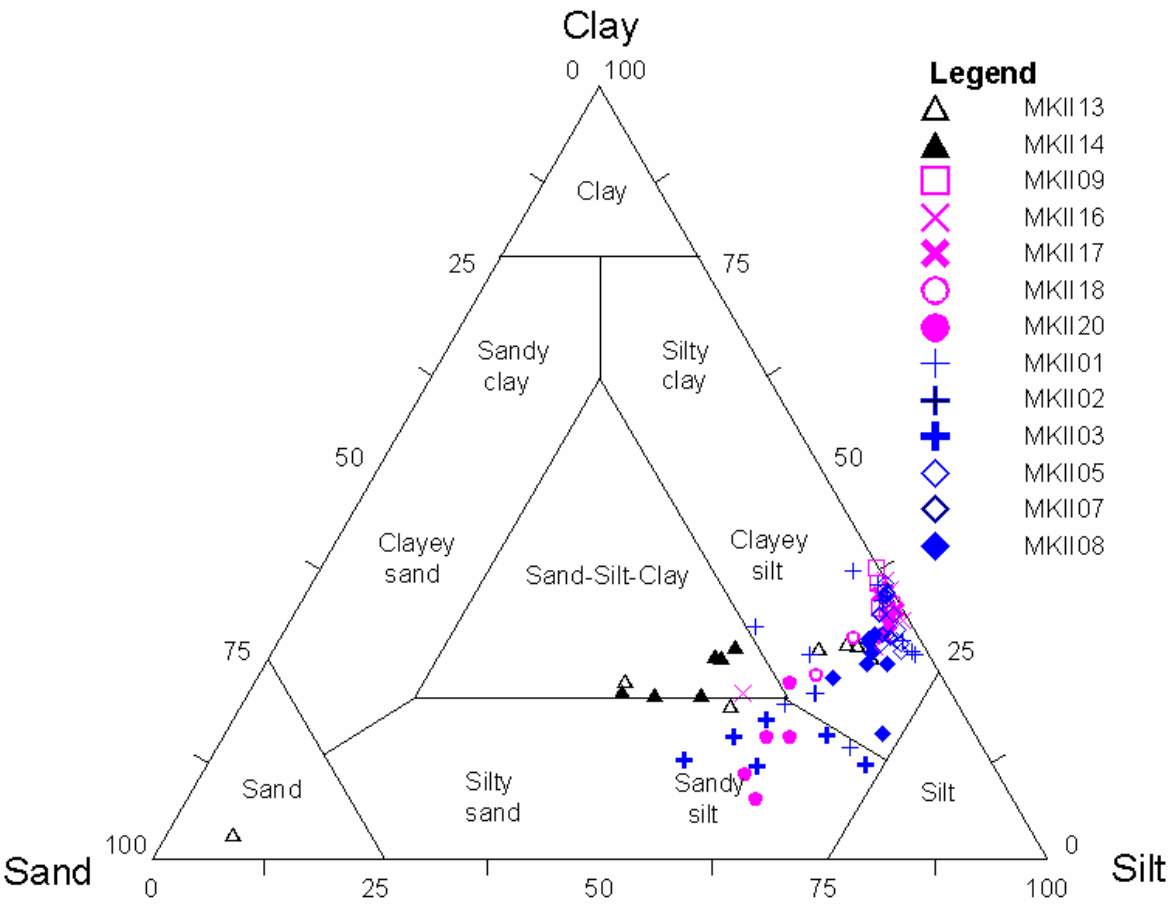

Fig. 3. Ternary plot of sediment grain size. The majority of the sediment is falling into the clayey silt and sandy silt category. The two cores from the east shore of the Camau Penensula, Core MKII13 and MKII14 (triangles), have coarser sediment contents than the rest cores.

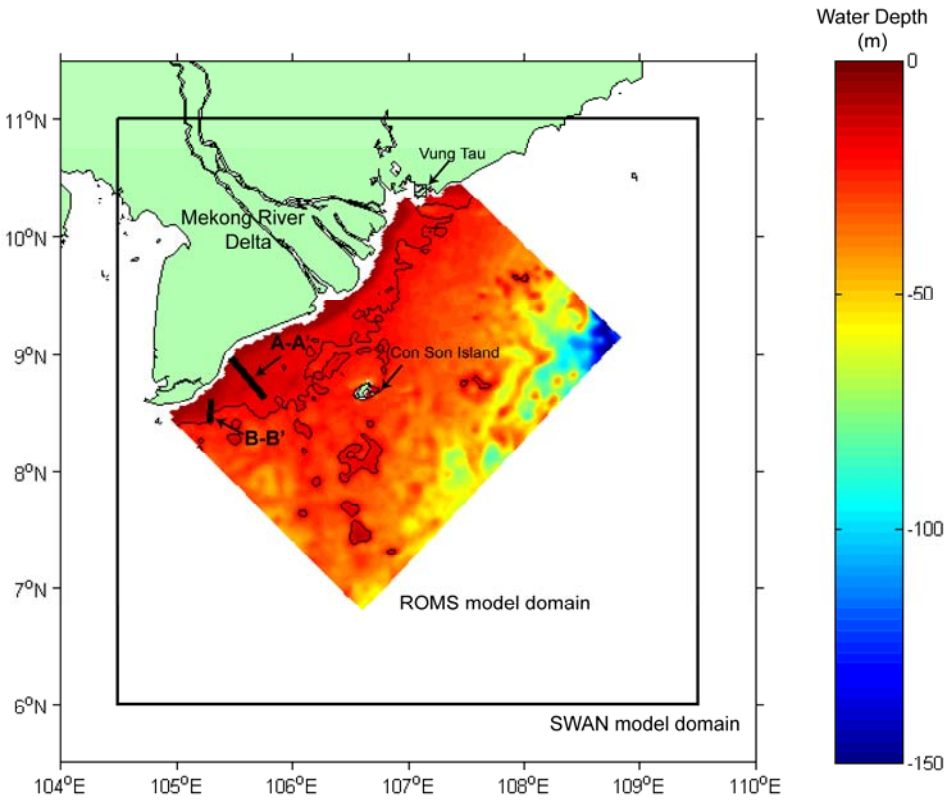

Fig. 4. SWAN and ROMS model domain with water depth and the locations of tidal station and cross section A-A'. Depth contours at 20 m.

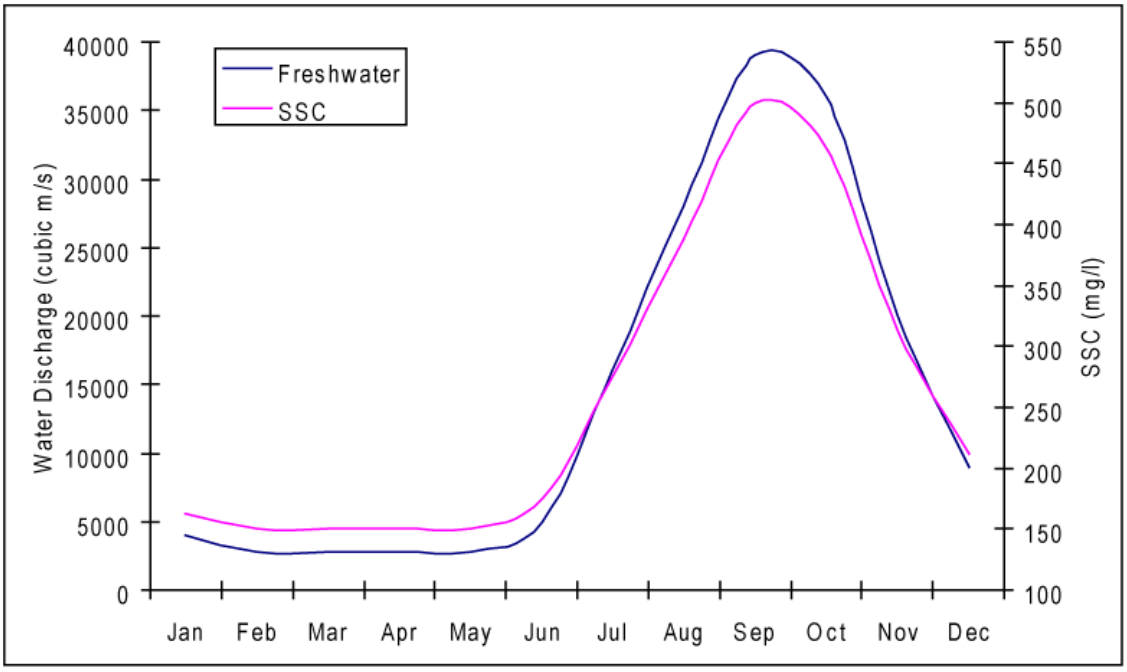

Fig. 5. Water discharge and suspended sediment concentration used in model inputs. Water discharge is from Hordoir et al., 2006, which is averaged over 27 years in the period 1933-1966. suspended sediment concentration is estimated based on Milliman and Syvitski, 1992, Wolanski et al., 1996, and Wolanski et al., 1998.

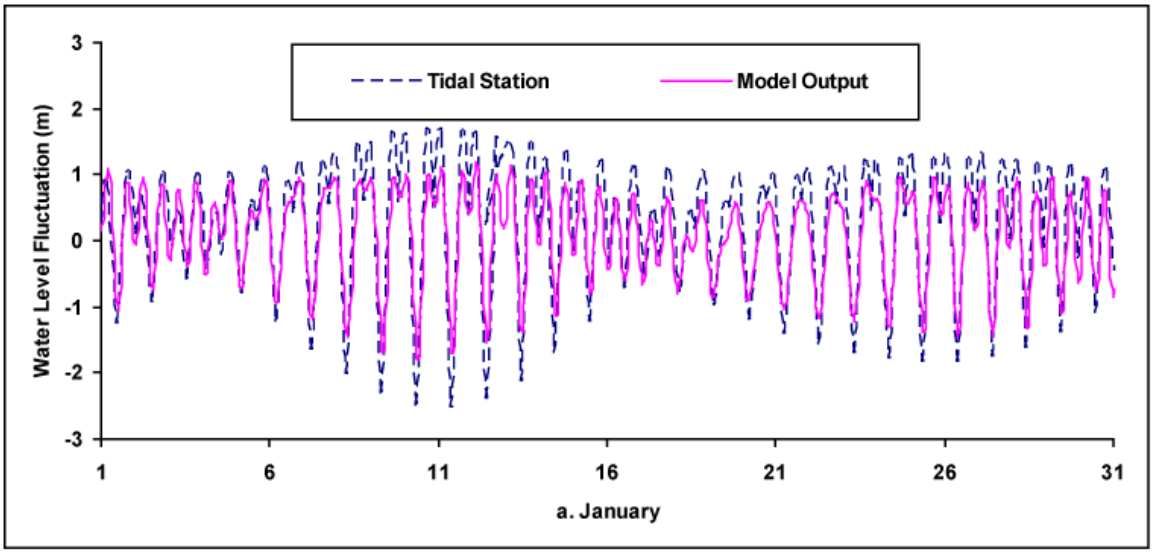

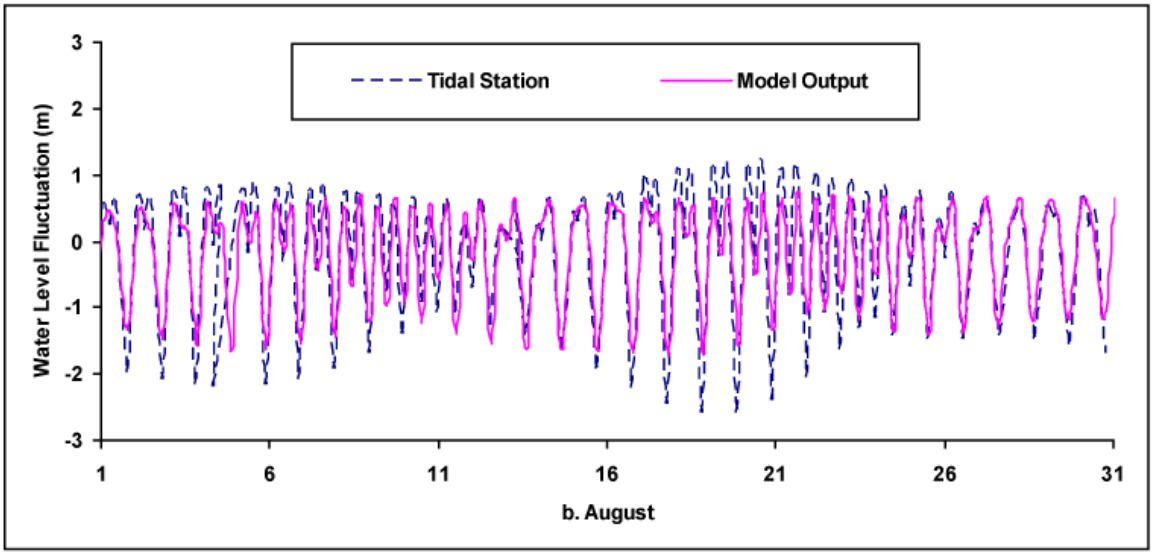

Fig. 6. A comparison between water level flocculation at tidal station Vung Tau and model results. (a) January and (b) August 2005.

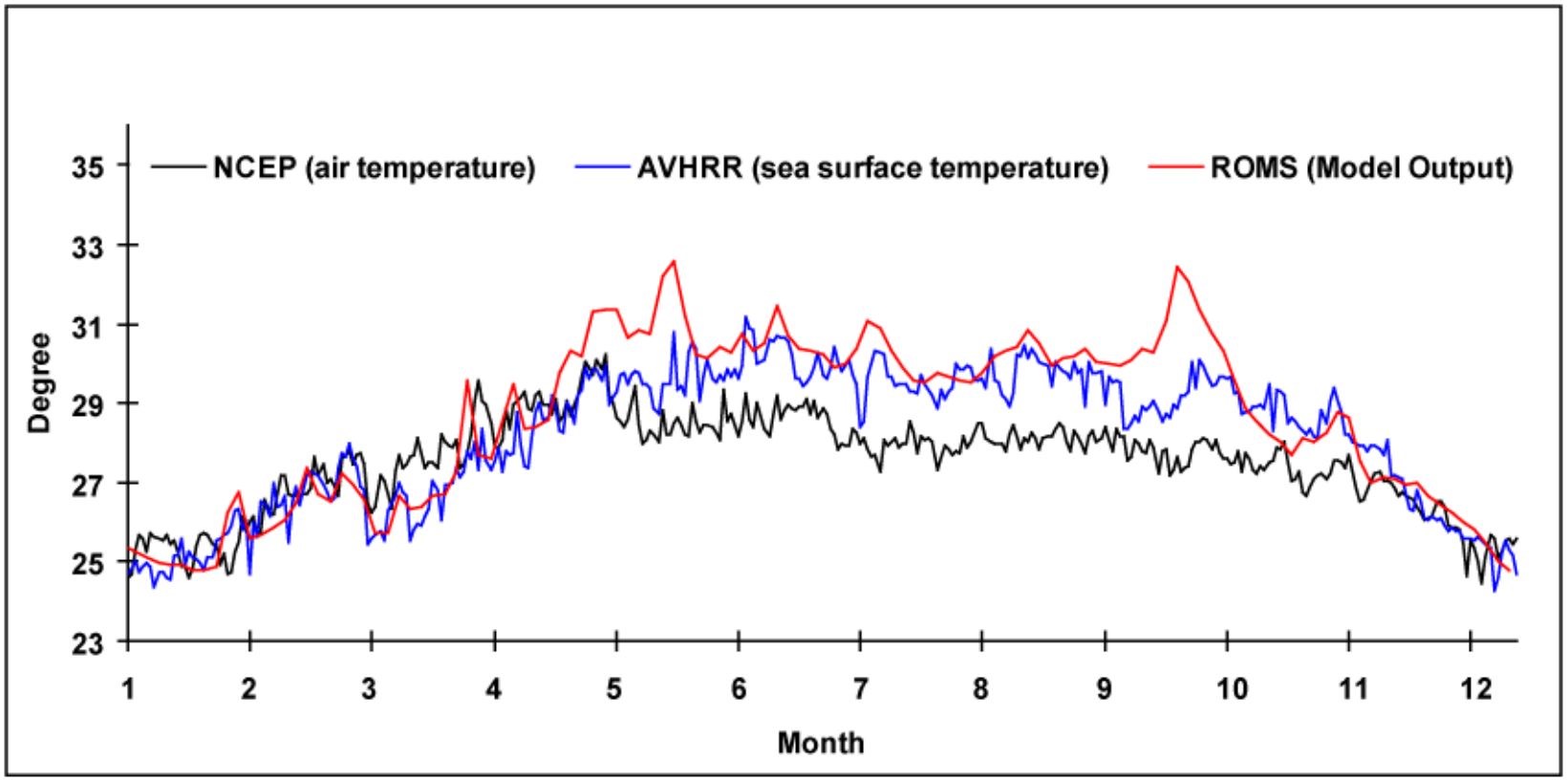

Fig. 7. Time series plot of air temperature (NCEP), observed sea surface temperature by satellite (AVHRR), and sea surface temperature estimated by ROMS model for 2005.

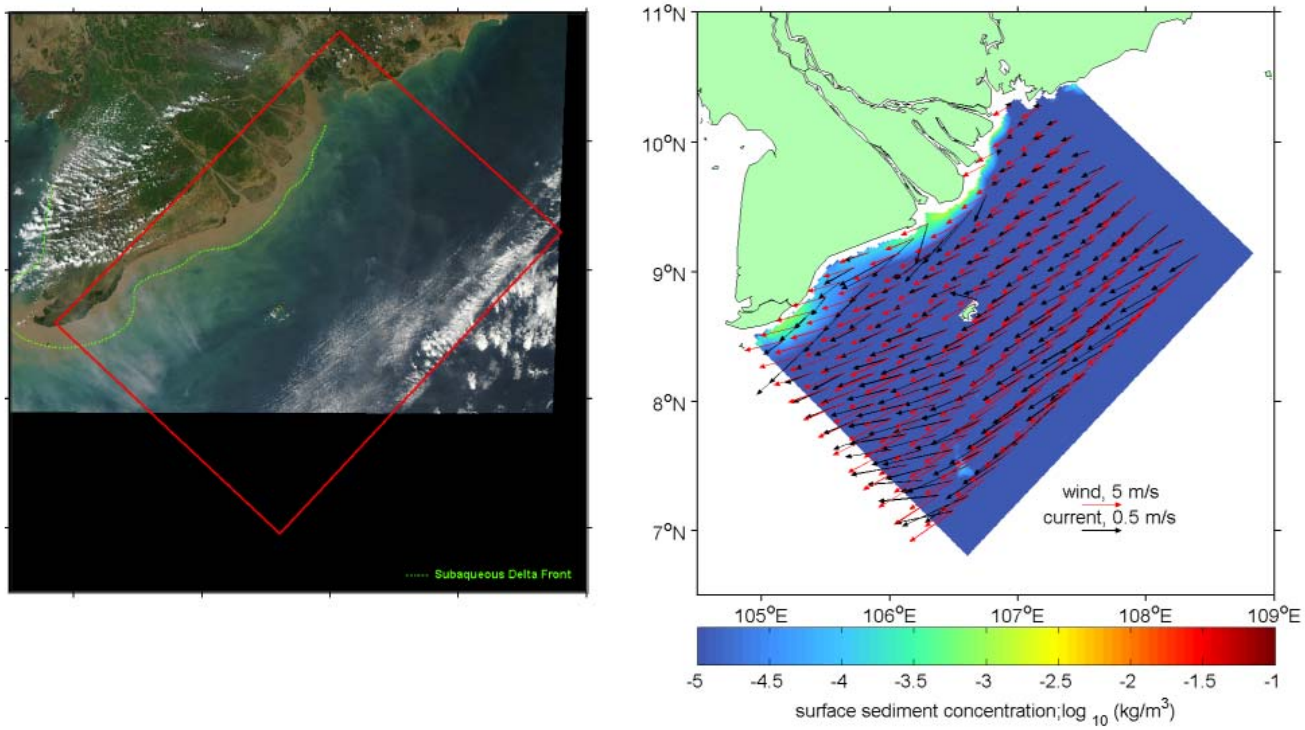

a. MODIS image in January

b. Model Ouput

Fig. 8. Surface sediment concentration in January. (a) Moderate Resolution Imaging Spectroradiometer (MODIS) image from January 2003. (b) Wind velocities (red arrows), and model estimated surface sediment concentration (color) and current velocities (blue arrows), averaged for January 2005. Colors shown in log scale.

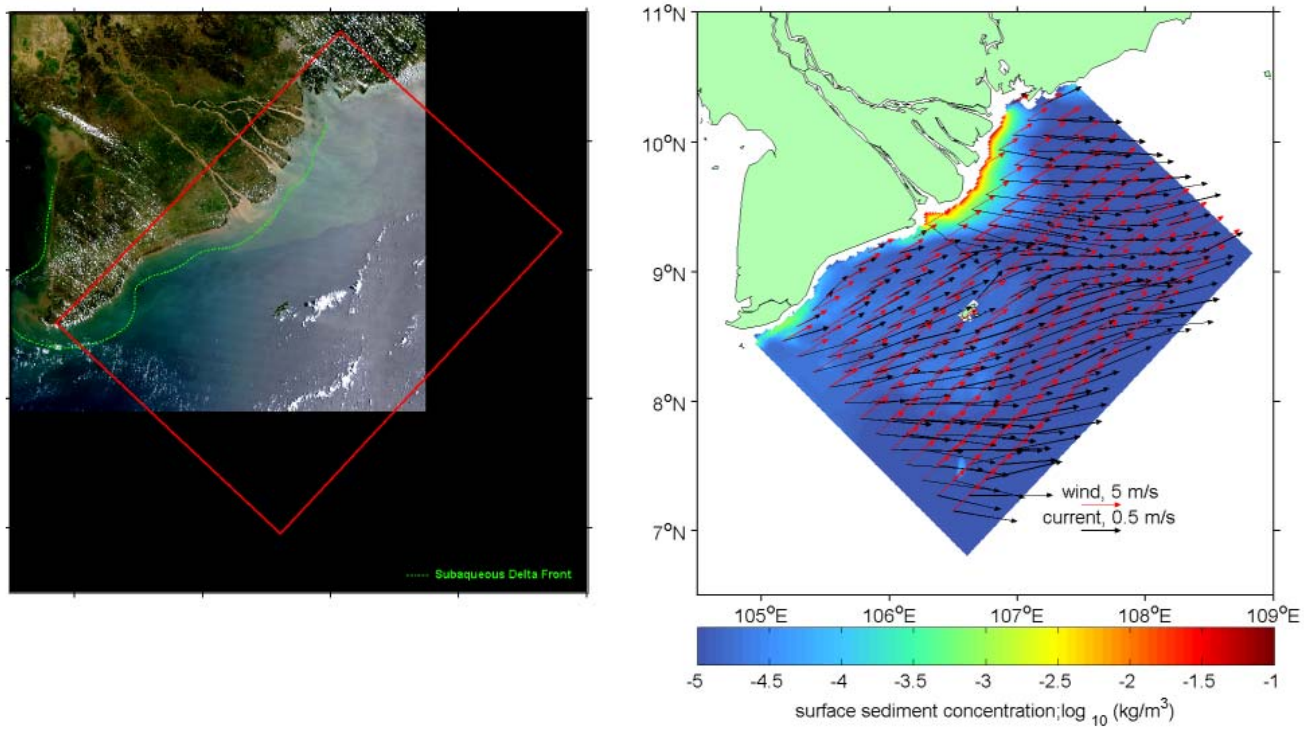

Fig. 9. Surface sediment concentration in August. (a) Moderate Resolution Imaging Spectroradiometer (MODIS) image from August 2002. (b) Wind velocities (red arrows), and model estimated surface sediment concentration (color) and current velocities (blue arrows), averaged for August 2005. Colors shown in log scale.

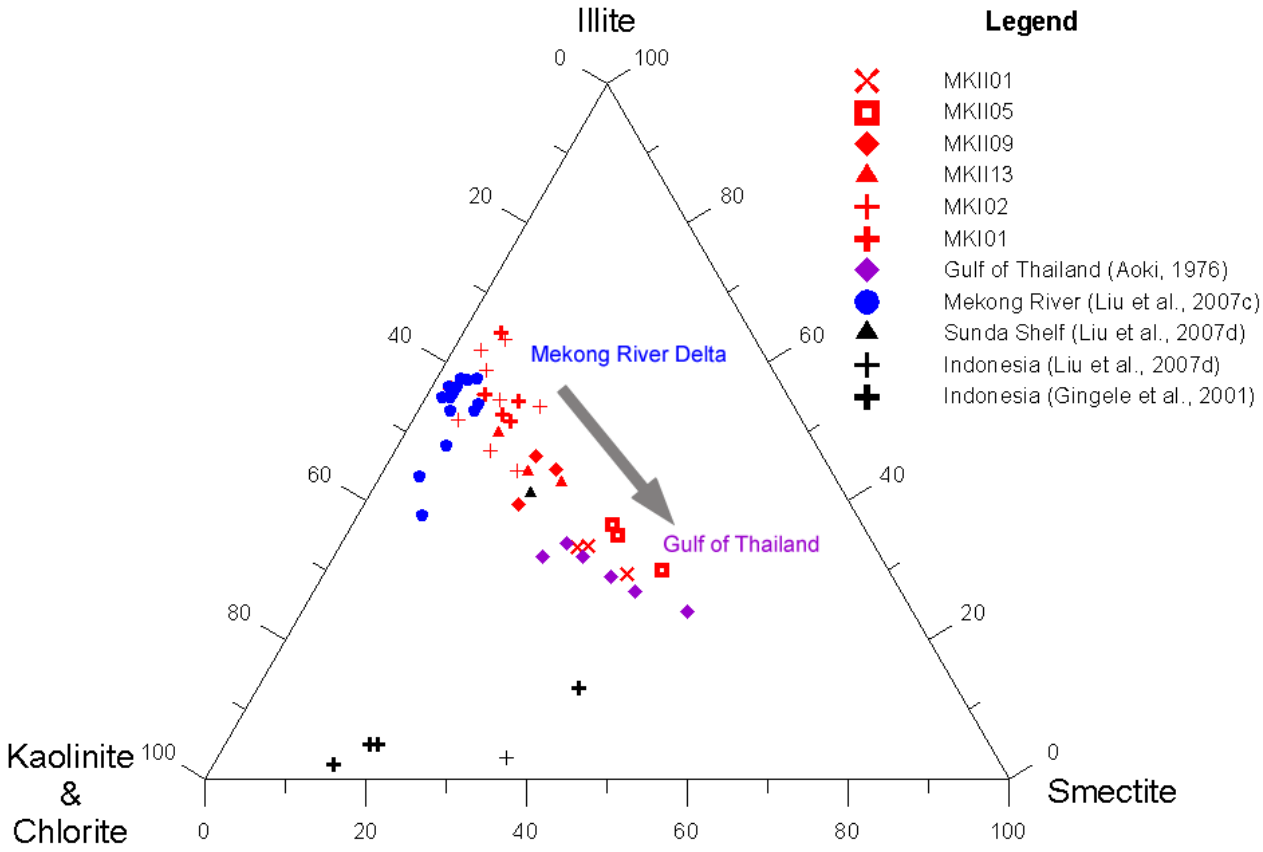

Fig. 10. Ternary plot of clay mineral composition. Mekong shelf (red, this study), Mekong River (blue), Gulf of Thailand (purple), Sunda Shelf (black triangles), and Indonesia (black cross).

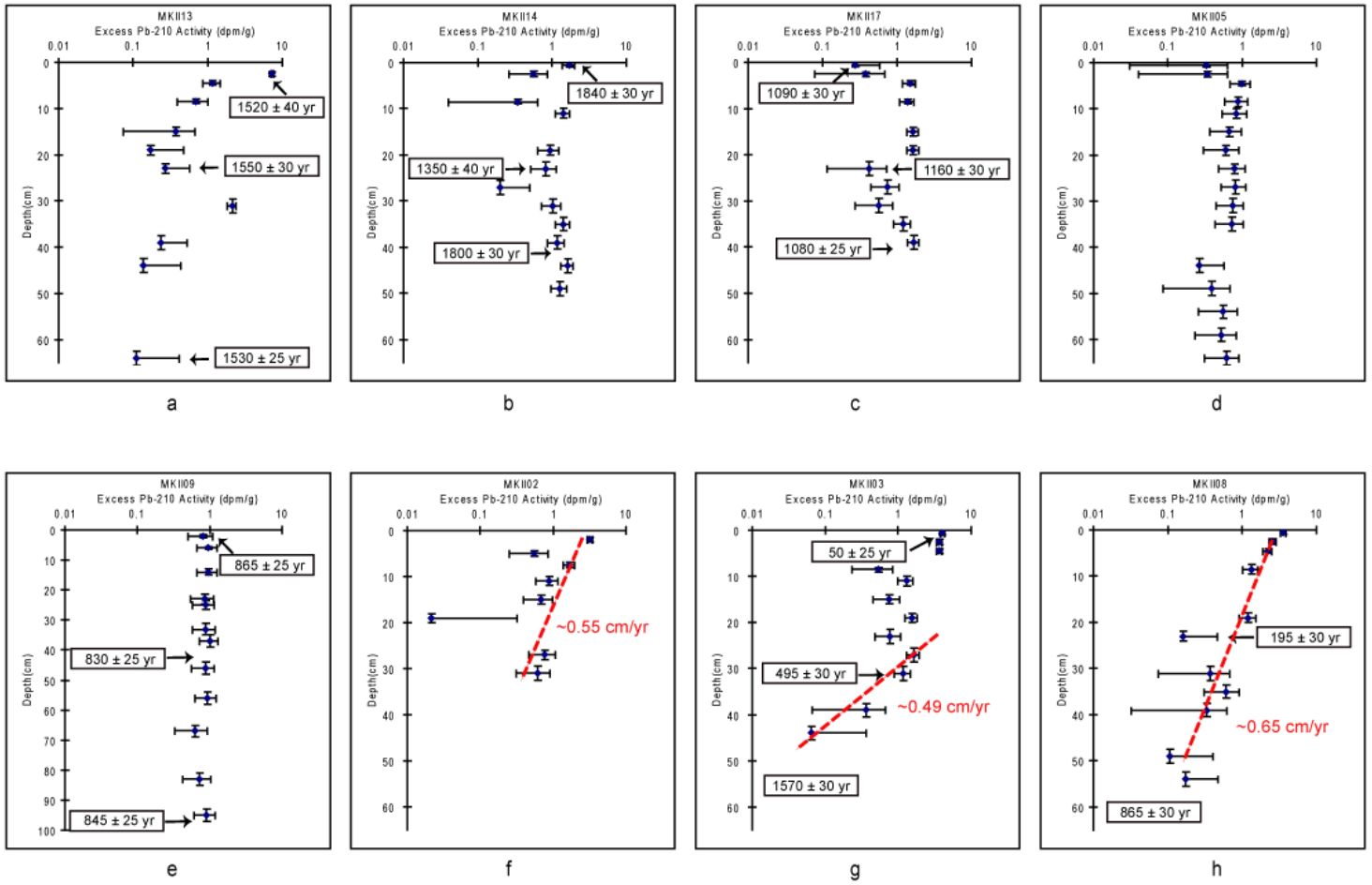

Fig. 11. Excess ^{210}Pb profiles of sediment cores.

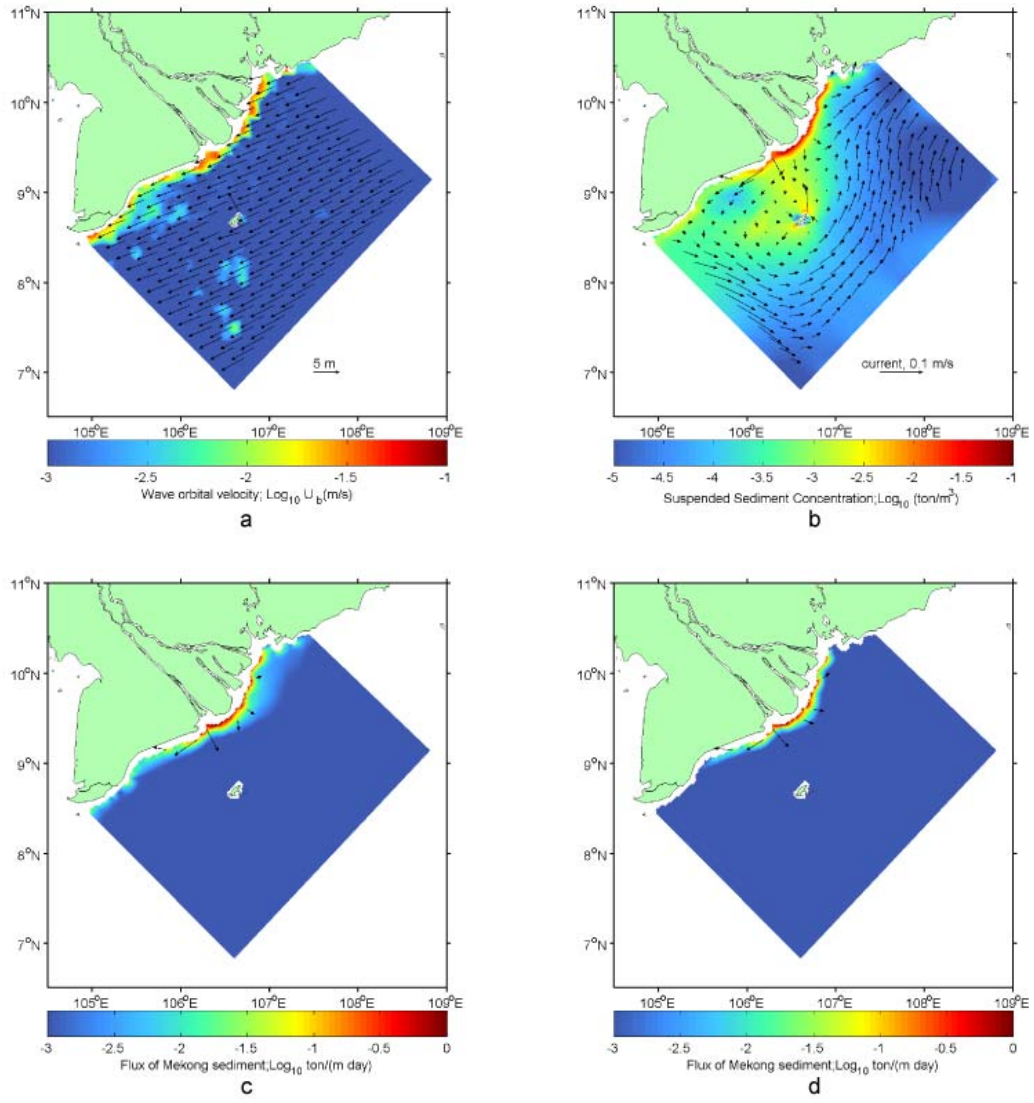

Fig. 12. Time averaged wave, suspended sediment concentration, and sediment flux. (a) wave direction (arrows) and wave orbital velocity (color), (b) depth averaged suspended sediment concentration (color) and current velocity (arrows), (c) depth-integrated daily averaged sediment flux (ton m^{-1} day^{-1}), and (d) depth-integrated daily averaged sediment flux without wind forcing (ton m^{-1} day^{-1}). Flux direction shown as arrows where flux exceeds 0.01 ton m^{-1} day^{-1}. Colors shown in log scale.

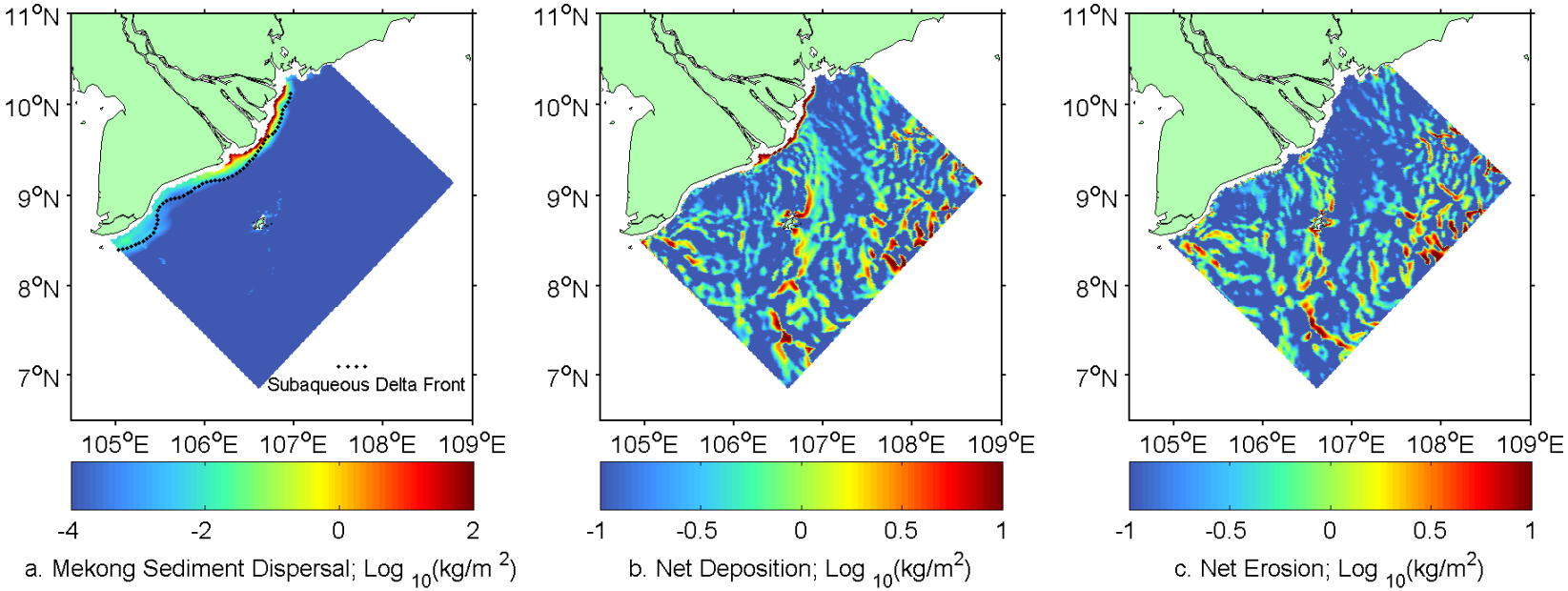

Fig. 13. Modeled deposition of fluvial sediment. (a) Final deposition of fluvial sediment estimated for the Mekong River. (b) Net deposition at the end of 2005. (c) Net erosion at the end of 2005. Colors shown in log scale.

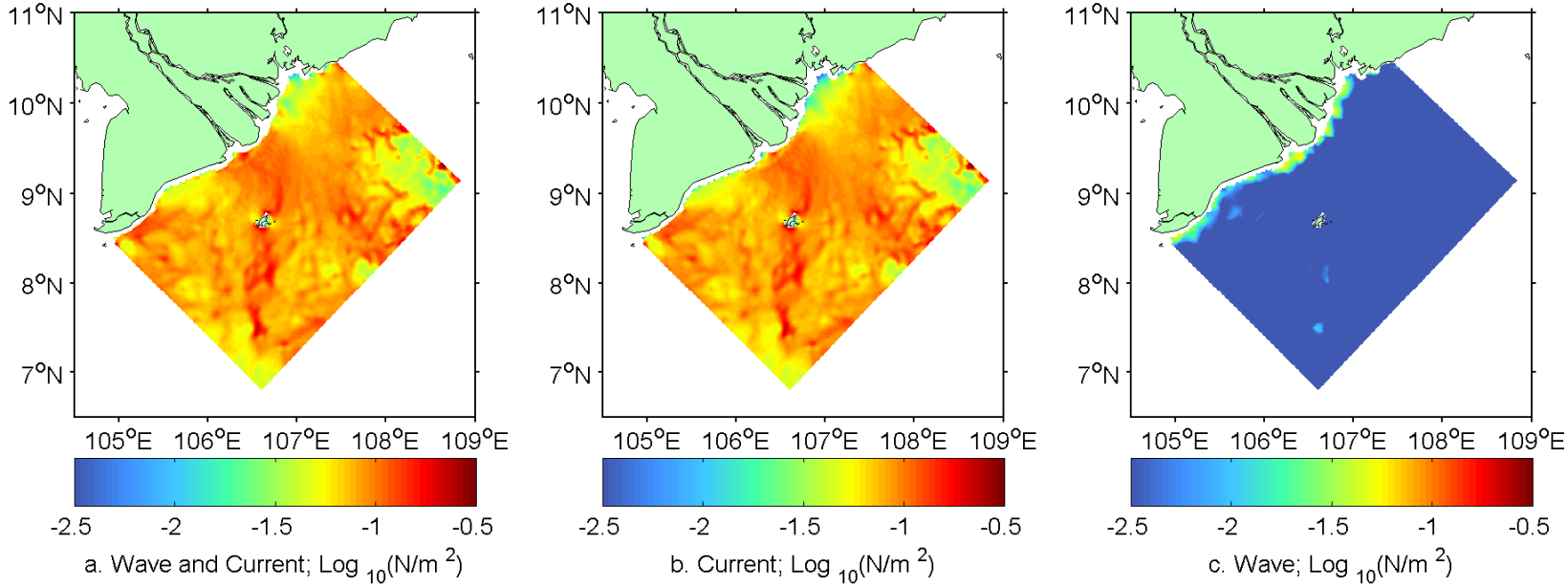

Fig. 14. Bed shear stresses averaged during 2005. (a) Combined wave-current skin friction shear stress averaged during 2005. (b) Current component of shear stress. (c) Wave component of shear stress. Colors shown in log scale.

Fig. 15. Current velocity and suspended sediment concentration during January. (a) cross-shelf component of current (+, offshore; -, onshore), (b) along-shelf component of current (+, parallel to the shore to the northeast ; -, parallel to the shore to the southwest), (c) suspended sediment concentration of fine grained Mekong sediment, (d) suspended sediment concentration of flocculated Mekong sediment, (e) suspended sediment concentration of flocculated fines resuspended from seabed, and (f) suspended sediment concentration of sand resuspended from seabed. Time averaged for January 2005. Colors shown in log scale. X-axis stands for cross-shelf distance (km).

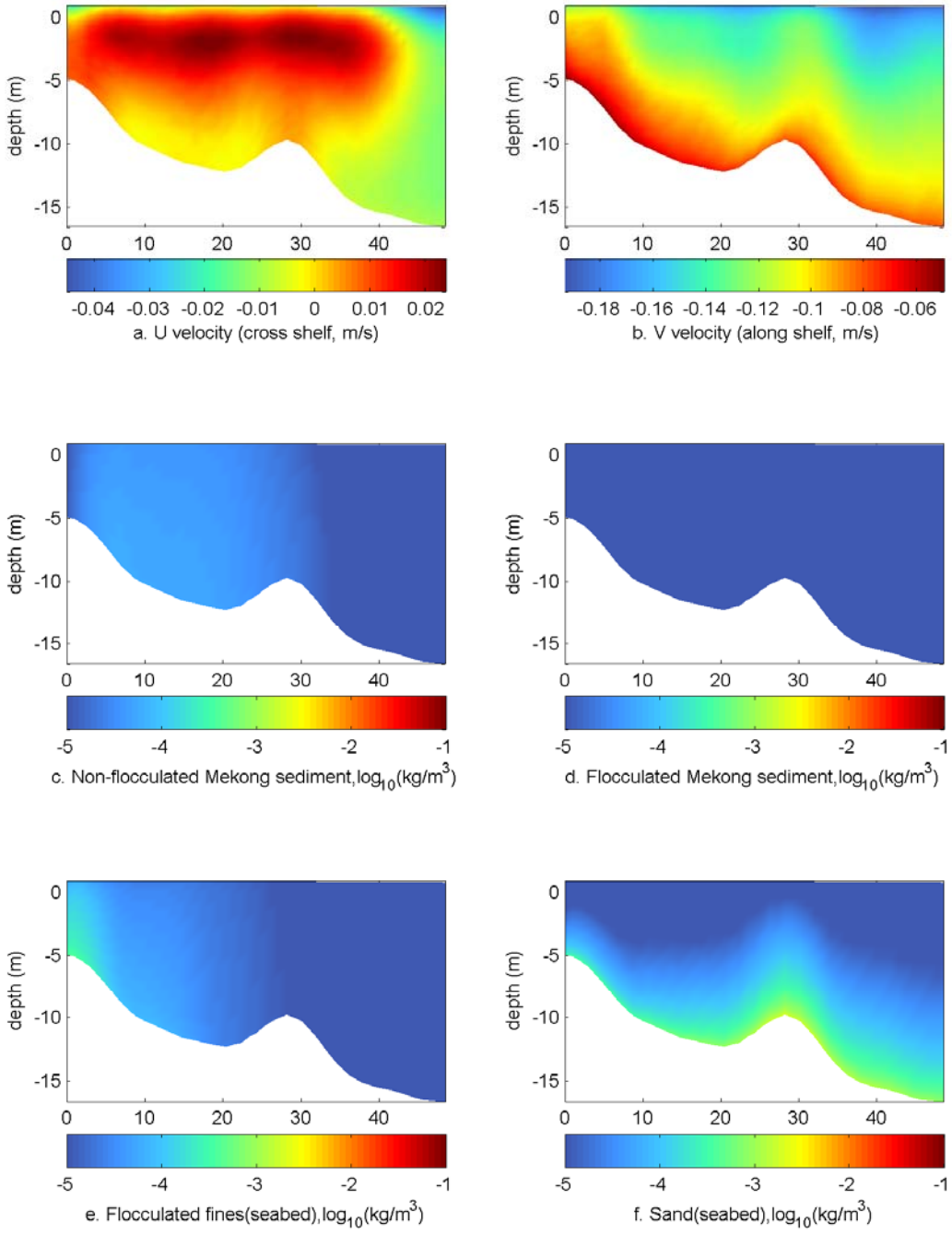
depth (m)
0
-5
-10
-15
0 10 20 30 40
-0.04 -0.03 -0.02 -0.01 0 0.01 0.02
a. U velocity (cross shelf, m/s)
-0.18 -0.16 -0.14 -0.12 -0.1 -0.08 -0.06
b. V velocity (along shelf, m/s)
-5 -4 -3 -2 -1
c. Non-flocculated Mekong sediment, log10(kg/m3)
d. Flocculated Mekong sediment, log10(kg/m3)
e. Flocculated fines(seabed), log10(kg/m3)
f. Sand(seabed), log10(kg/m3)

Fig. 16. Current velocity and suspended sediment concentration during August. (a) cross-shelf component of current (+, offshore; -, onshore), (b) along-shelf component of current (+, parallel to the shore to the northeast ; -, parallel to the shore to the southwest), (c) suspended sediment concentration of fine grained Mekong sediment, (d) suspended sediment concentration of flocculated Mekong sediment, (e) suspended sediment concentration of flocculated fines resuspended from seabed, and (f) suspended sediment concentration of sand resuspended from seabed. Time averaged for August 2005. Colors shown in log scale. X-axis stands for cross-shelf distance (km).

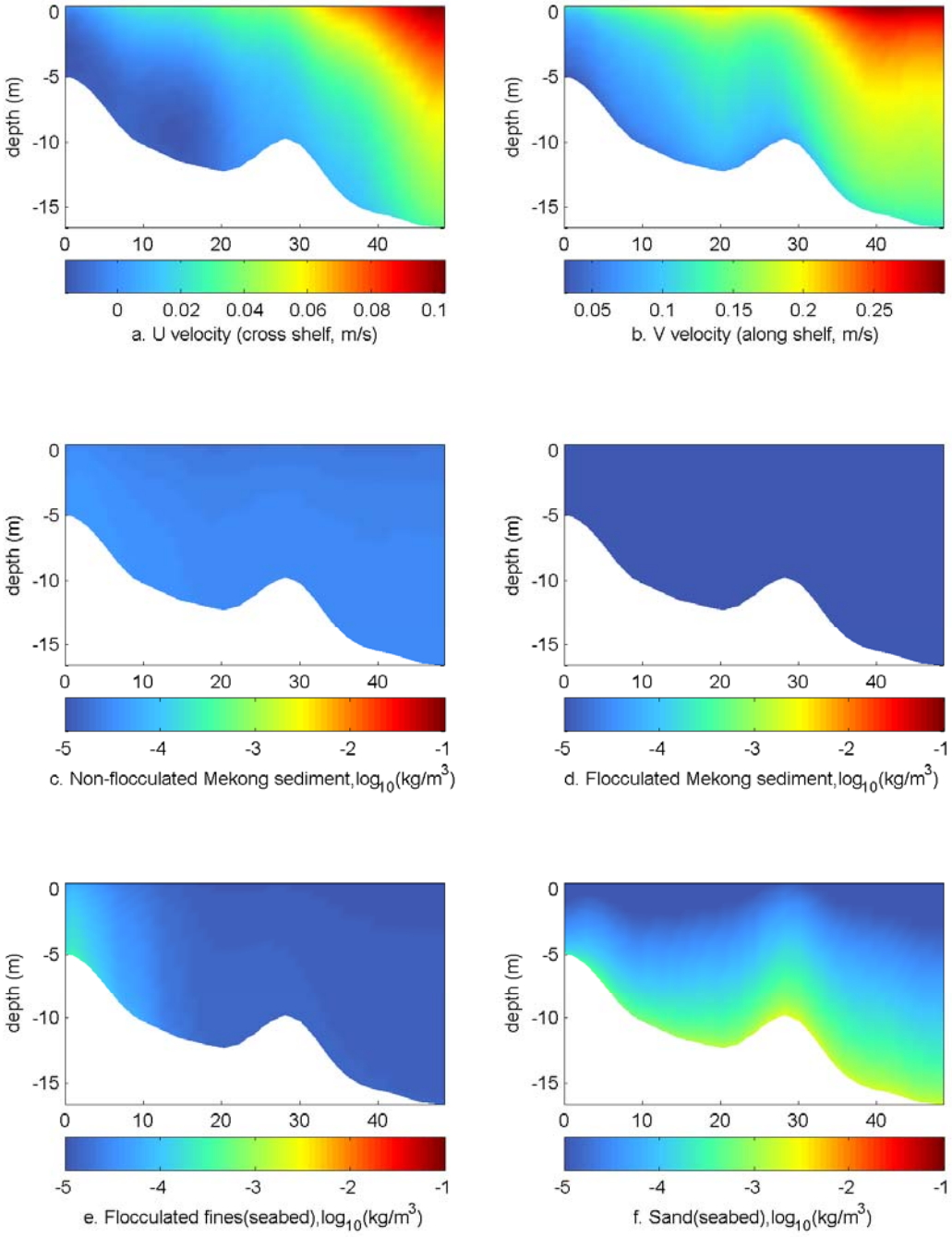
depth (m)
0
-5
-10
-15
0 10 20 30 40
0 0.02 0.04 0.06 0.08 0.1
a. U velocity (cross shelf, m/s)
0.05 0.1 0.15 0.2 0.25
b. V velocity (along shelf, m/s)
-5 -4 -3 -2 -1
c. Non-flocculated Mekong sediment, log10(kg/m3)
d. Flocculated Mekong sediment, log10(kg/m3)
e. Flocculated fines(seabed), log10(kg/m3)
f. Sand(seabed), log10(kg/m3)

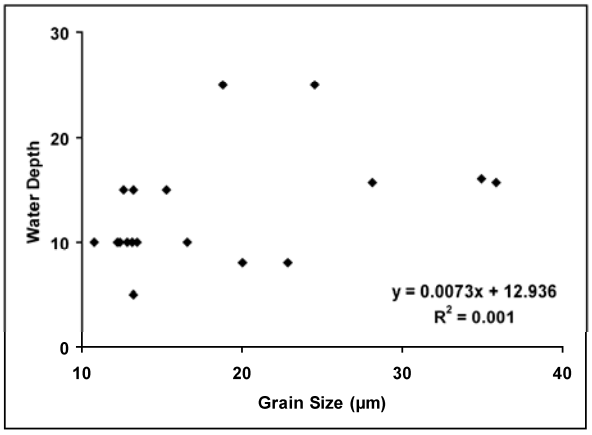

a

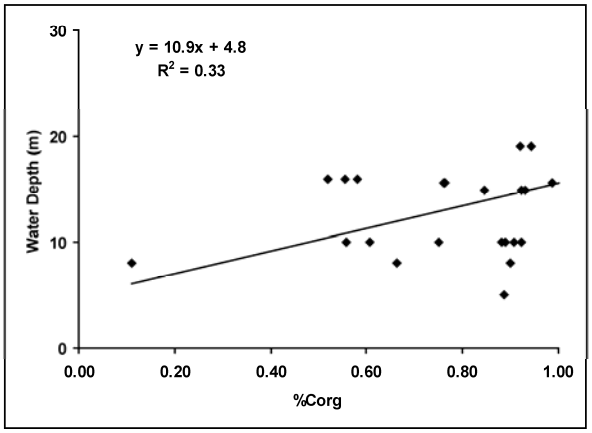

b

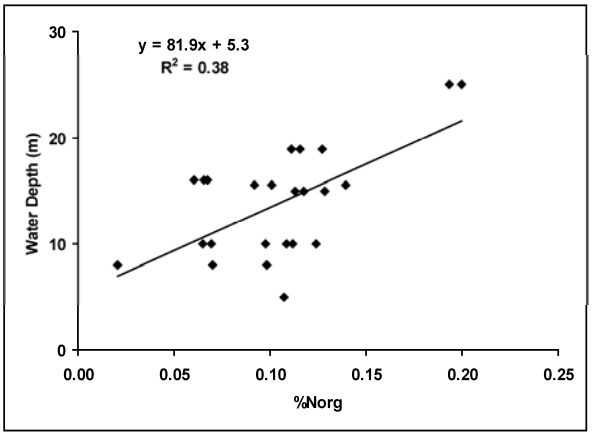

c

Fig. 17. Correlation between water depth, grain size, % C_{org}, and % N_{org}.

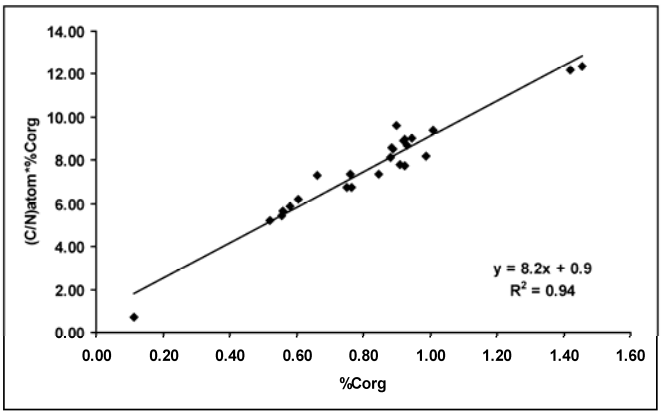

a

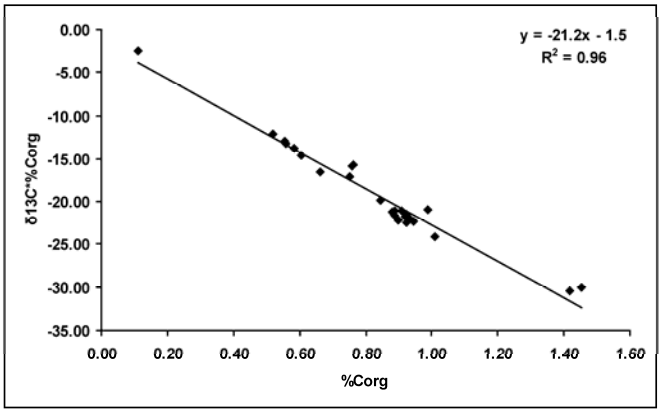

b

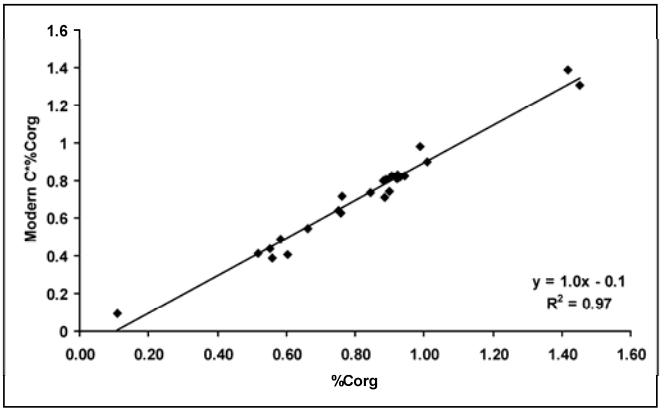

c

Fig. 18. The isotopic signature of C_{org} added to the shelf sediments. The slopes of the best-fit lines correspond to the average $(C/N)_{atom}$ (a), $\delta^{13}C$ (b), and % modern ^{14}C content (c) of the C_{org} responsible for the change in C_{org}.

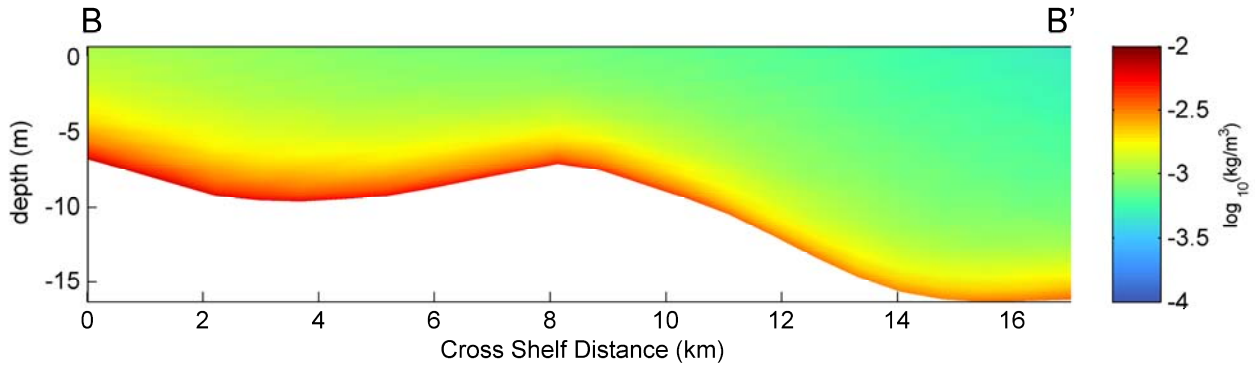

a. Suspended Sediment Concentration (model result)

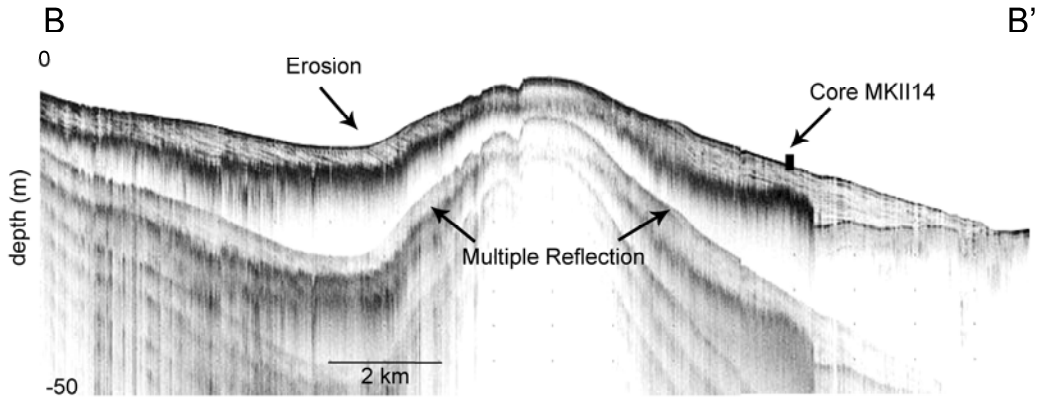

b. Subaqueous Delta on Seismic Profile

Fig. 19. Suspended sediment concentration and seismic profile at cross section B-B'. (a) Modeled suspended sediment concentration and (b) seismic profile by "Chirp" sub-bottom profiler.

CHAPTER 5: CONCLUSIONS AND FUTURE WORK

1. Conclusions

This dissertation research was a "Source-to-Sink" study focusing on both the Mekong River's water and sediment discharge and its derived sediment transport and dispersal on the continental shelf of the South China Sea (SCS). Both the land and subaqueous part of the Mekong system was investigated through a number of approaches, including statistics, geophysics, geochemistry, and numerical modeling. Research of the land part mainly addressed the climatic (e.g., precipitation) and anthropogenic (e.g., damming) impacts on the hydrology and sediment delivery of the Mekong River and the possible response of its delta. Research of the subaqueous part of the dispersal system involved (a) acquisition and interpretation of ~ 1150 km high-resolution CHIRP seismic profiles; (b) collection and analyses of cored sediments (accumulation rate, sediment dating, organic carbon source, and clay mineral); and (c) numerical modeling of the sediment transport and dispersal on the Mekong shelf. The main findings of this study included:

1) Mann-Kendall trend analysis showed no significant change in precipitation and runoff over a 50-yr period at eight gauge stations in the Lower Mekong. Correlation between runoff and precipitation significantly changed after the impoundment of Manwan Dam in 1993. However, the dam doesn't show apparent influence on the runoff-SSC relationship. River runoff showed a smoother periodogram, which is closely related with ENSO after the impoundment of the dam. In the next couple of decades, approximate 200 new dams are likely to be built in the Mekong basin. River runoff will have an even closer connection with

local precipitation, and thus become more sensitive to ENSO impacts.

2) High resolution seismic profiles revealed 10-20 m thick deltaic sediments within 30 m water depth surrounding the Mekong River Delta (MRD). Over the past 3,000 yr, the evolution of the MRD has shown a morphological asymmetry, which may be explained by increased wave influence. The highest delta progradation rate (~ 26 m/yr) was found around Cape Camau, ~ 200 km downstream from the river mouth. Sediment budget estimation showed that approximately 80±18% of Mekong sediments have been trapped within the delta area, as part of the rapid progradation over the past 3,000 yr. A schematic incised valley fill model, since the low sea level stand was proposed.

3) Clay mineral analysis showed that Mekong sediment was the major source material for the subaqueous delta. The ^{210}Pb profiles of cores from the subaqueous delta showed either fluctuating or uniform excess ^{210}Pb activities, indicating a rapid accumulation or strong physical mixing process. ^{14}C measurements yielded few young ages for bulk organic matter on the subaqueous delta, indicating a contribution of 'old' organic material supplied by fluvial sediments or resuspension of previously deposited sediments. The δ^{13}C values confirmed a mixed terrestrial/marine source. A lower limit on the sediment accumulation rate can be estimated from the ^{14}C data, which suggested high rates around the rapidly prograding Cape Camau and slower rates in the Gulf of Thailand. .

4) Numerical modeling of the sediment transport and dispersal on the Mekong shelf represented conditions in year 2005. Model calculation showed that 99% of Mekong sediment was retained within 20 km of the delta plain. Much of the Mekong sediment that traveled further was fine grained particles carried toward the southwest. Wave orbital

velocity and wave-induced bed shear stress were higher in the shallow water. Sensitivity tests indicated that wind was the most important forcing influencing local sediment transport. Along-shelf transport dominated during both NE monsoon and SW monsoon seasons. Although the along-shelf current shifts its direction during two monsoon seasons, the turbidity along the delta plain was composed of fine sediment from the Mekong and resuspended from the seabed during both seasons. The current-induced bed shear stresses dominated the Mekong shelf.

2. Future work

This dissertation represented a comprehensive analysis of hydrological data, seismic profiles, sediment cores, and application of numerical modeling tools to examine the flux and fate of water discharge, sediment transport and dispersal process of the Mekong dispersal system. Although great efforts were made to complete the 2006 and 2007 cruises, further field data, including hydrological, geophysical, vibercores, and continuous observations, are expected to enhance our understanding of such a large dispersal system. To be more specific:

(1) Hydrological analyses did not cover the gauge stations on the delta plains. The source of the hydrological data used in this study is from the Mekong River Commission (MRC). The hydrological dataset at MRC is very sporadic, continuous water level and suspended sediment concentration (SSC) observations were not available for channels on the delta plain. This prevented a comprehensive analysis of changes in sediment delivery from the Mekong River to the SCS.

(2) More geophysical surveys should be carried out on the Mekong shelf. The seismic profiles in this study mainly covered the subaqueous delta, which only explained the fate of approximate 80% of the Mekong derived sediment over the past 3,000 yr. Further geophysical surveys are needed in deep waters to discover possible distal depo-centers of the Mekong sediment.

(3) Vibracores are needed to substantiate the current explanation of the stratigraphic architecture of the subaqueous delta. Both 2006 and 2007 cruises were conducted using a small fishery administration vessel (Fig.1), which was not capable of performing vibracoring. Recovered gravity cores were less than 2 m in length and could not penetrate the delta front facies. Although the facies correlation between seismic profiling and inland boreholes was successful, a detailed examination of vibracores will facilitate our understanding of the sedimentary processes on the subaqueous delta.

(4) Continuous observations of in situ hydrodynamics and SSC are needed to enhance the accuracy of numerical modeling. As in situ observation of the study area is very limited, I have had to rely on results from large scale models and databases in this study. Although the numerical modeling reproduced the general pattern of water level flocculation, seasonal variations of sea surface temperature, and the turbidity shown by MODIS images, high resolution in situ data, including fluvial inputs, circulation, temperature, salinity, and SSC, would be expected to enhance the accuracy of the model. Meanwhile, to assure model stability, current model domain only covered the relative deep waters (water depth > 5 m) along the eastern part of the MRD, sediment dynamics of the shallow areas as well as the western part of the MRD need to be explored.

Fig. 1. Vessel BT-0707-KN used during 2006 and 2007 cruises